

UNIVERSITY OF MALTA  
Institute for Sustainable Energy

M.Sc. Dissertation

DESIGN AND PROTOTYPING OF A THERMAL  
ENERGY METER FOR SOLAR APPLICATIONS

by

Joseph Vella

A dissertation submitted in partial fulfilment of the requirements of  
the award of Master of Science in Sustainable Energy

June 2021



L-Università  
ta' Malta

## **University of Malta Library – Electronic Thesis & Dissertations (ETD) Repository**

The copyright of this thesis/dissertation belongs to the author. The author's rights in respect of this work are as defined by the Copyright Act (Chapter 415) of the Laws of Malta or as modified by any successive legislation.

Users may access this full-text thesis/dissertation and can make use of the information contained in accordance with the Copyright Act provided that the author must be properly acknowledged. Further distribution or reproduction in any format is prohibited without the prior permission of the copyright holder.

## **Copyright Notice**

- 1) Copyright in text of this dissertation rests with the Author. Copies (by any process) either in full, or of extracts may be made only in accordance with regulations held by the Library of the University of Malta. Details may be obtained from the Librarian. This page must form part of any such copies made. Further copies (by any process) made in accordance with such instructions may not be made without the permission (in writing) of the Author.
  
- 2) Ownership of the right over any original intellectual property which may be contained in or derived from this dissertation is vested in the University of Malta and may not be made available for use by third parties without the written permission of the University, which will prescribe the terms and conditions of any such agreement.

## Abstract

In 2009, the EU Renewable Energy Directive 2009/28/EC had for the first time recognised solar thermal systems as contributing towards the renewable energy target of EU Member States, rather than just saving energy. This was a major step change in its perception towards this technology, which was consolidated by the updated directive (EU) 2018/2001 that specifically requested Member States to promote the use of renewable heating systems in buildings. However, quite often, solar heating systems do not come with an accompanying thermal energy meter. This implies that the user is not able to quantify or report the thermal energy savings. Consequently, Member States often resort to estimates when it comes to reporting their annual thermal renewable energy generation to the EU.

This project aims at addressing these challenges by designing, building and testing a low-cost, reliable, versatile, and accurate thermal energy meter that can easily fit to any solar heating system with the scope of monitoring and storing performance data, as well as controlling the use of backup electric heaters with the intention of optimising the use of solar energy, without compromising the availability of hot water. Moreover, the device shall include features to alert the user of any potential malfunctions of the SWH, which can all be accessed through a user-friendly web-based interface.

The requirements and means to monitor the performance of a SWH to a high degree of accuracy were explored, and using appropriate hardware and software configurations, a prototype was produced, calibrated and tested on a typical domestic thermosiphon solar heating system. After extensive testing and fine-tuning, it was confirmed that the monitoring device functioned as intended with stable operation. By the end of the project, the prototype has passed all tests and fulfilled all the aims of the project, for monitoring the system, storing and presenting data, controlling solar heater operation, reporting malfunctions and making it all accessible through any network-connected device.

Given that the market does not offer a similar device at a reasonable price, the product has the potential of being further developed to make it market ready. To that end, future endeavours will be made to patent it and to apply for seed funding for further development towards commercialisation.

## **Acknowledgements**

This dissertation could not have been possible without the assistance of numerous individuals towards whom I would like to extend my heart-felt thanks, for their constant help and support throughout the entire project.

First and foremost, I wish to express my sincere gratitude towards my supervisor, Dr. Ing Charles Yousif, and my co-supervisor, Dr. Cedric Caruana, whose assistance was invaluable. I am deeply grateful for their counsel and encouragement, and for the knowledge, techniques, and skills I have gained with their help throughout the course.

I would also like to acknowledge the staff at the Institute for Sustainable Energy, for always being willing to help in spite of their busy schedule, namely Mr Aaron Grech and Mr Terence Cilia. I take this opportunity to also thank Mr Julian Gambin from the University of Malta IT Services Department for his guidance in networking.

I am grateful to my siblings and parents for their moral and emotional support shown to me throughout this lengthy project. In addition, I would also like to thank my friends for their constant encouragement and enthusiasm along the way.

And finally, last but by no means least, I am also indebted to my fellow colleague, Mr Daniel Frendo, for his constant encouragement and support throughout the project.

# Table of Contents

<b>Copyright Notice .....</b>	<b>I</b>
<b>Abstract.....</b>	<b>II</b>
<b>Acknowledgements.....</b>	<b>III</b>
<b>Table of Contents .....</b>	<b>IV</b>
<b>List of Figures.....</b>	<b>VII</b>
<b>List of Tables .....</b>	<b>XI</b>
<b>List of Abbreviations and Symbols.....</b>	<b>XIII</b>
<b>Chapter 1 Introduction and objectives.....</b>	<b>1</b>
1.1 Background .....	1
1.2 Scope of the work .....	3
1.3 Structure of the thesis.....	4
<b>Chapter 2 Literature Review.....</b>	<b>5</b>
2.1 Introduction.....	5
2.1.1 About renewable energy sources and technologies (RES and RET).....	6
2.1.2 European Renewable Energy Directive 2009/28/EC.....	6
2.1.3 Solar thermal systems deployment .....	7
2.2 SWH energy-metering and monitoring systems .....	9
2.2.1 Cost effectiveness of monitoring solar energy systems.....	11
2.2.2 Monitoring systems case studies.....	11
2.3 Attitudes and behaviours for renewable energies .....	17
2.3.1 The intentions to adopt renewable energy harvesting technologies: Economic, Social or Environmental?.....	17
2.3.2 The role of monitoring devices .....	18
2.4 Summary of a SWH monitoring device requirements .....	20
2.5 Thermal analysis of solar collectors .....	20
2.6 Performance analysis of solar collectors.....	22

2.6.1	Collector thermal efficiency .....	22
2.6.2	FPC incidence angle modifier.....	25
2.6.3	Collector time constant .....	25
2.7	Collector selection process .....	26
2.7.1	Computer modelling and Performance Analysis Tools .....	27
2.7.2	Limitations of simulation.....	28
2.8	Performance analysis of Solar Water Heater (SWH) systems.....	29
2.8.1	Overall system Efficiency.....	29
2.8.2	Solar Energy Utilisation Factor (SEUF).....	30
2.8.3	Solar Fraction.....	31
2.8.4	Surplus Hot Water Fraction .....	31
<b>Chapter 3</b>	<b>Methodology .....</b>	<b>33</b>
3.1	Monitoring Parameters.....	33
3.2	Hardware and software configurations .....	34
3.2.1	Solar Thermal Water Heater .....	37
3.2.2	Microcontroller .....	38
3.2.3	Water Flowmeters .....	41
3.2.4	Temperature Sensors.....	43
3.2.5	Solar Irradiance Meter (Photovoltaic panel).....	45
3.2.6	AC voltage sensor .....	50
3.2.7	Hall Effect Current Transformer.....	53
3.2.8	Custom PCB (Printed Circuit Board) .....	54
3.3	Internet of Things (IoT) / Data-Logging.....	55
3.3.1	Data uploads and downloads / Data-logging feature .....	57
3.3.2	Internet disconnections and upload failures.....	57
3.4	Design of a User-Interface (UI) .....	58
3.4.1	Data requests/ UI parameter value updates.....	58
3.4.2	Parameter/ Settings updating .....	59
3.4.3	UI walkthrough .....	59

3.5	Prototype installation and development timeline.....	70
3.6	Design of experiments .....	72
3.6.1	Control of water consumptions.....	73
3.6.2	Control of backup heater.....	73
<b>Chapter 4</b>	<b>Results and Observations .....</b>	<b>75</b>
4.1	Solar Water Heater functionality check.....	76
4.2	Software and UI functionality check .....	77
4.2.1	Changes in <i>Settings</i> and offline saving .....	79
4.2.2	Autonomous control feature functionality test .....	79
4.2.3	Internet Disconnection Timeouts.....	82
4.3	Parameter accuracies, precisions, and calibration requirements (long-term stability).....	83
4.4	Solar shading instances .....	86
4.5	Water draw-offs .....	87
4.6	<i>Primary efficiencies</i> results section with different weather conditions .....	89
4.6.1	Cold and clear weather.....	89
4.6.2	Warm and clear weather .....	92
4.6.3	Cold and cloudy weather .....	93
4.6.4	Warm and cloudy weather .....	94
4.7	Long duration tests and <i>Energy Utilisation Efficiencies</i> results.....	95
4.7.1	Few backup heater uses .....	95
4.7.2	No backup heater use .....	96
4.7.3	Heavy backup heater use .....	97
4.8	Investigating an ideal consumption using the monitoring device.....	98
4.9	Determining the stagnation point using the monitoring device .....	99
<b>Chapter 5</b>	<b>Conclusion &amp; Future Works .....</b>	<b>101</b>
5.1	Conclusions.....	101
5.2	Future works .....	103
<b>References</b> .....		<b>105</b>



## List of Figures

Figure 1.1: Number of new SWHs installed in Malta throughout the years 2008-2014 and the projected installations for the years 2015-2020 [8].....	2
Figure 2.1: Share of energy from renewable sources for heating and cooling for the year 2019 [15].....	7
Figure 2.2: Production of direct use solar thermal energy in the EU-28 zone [17].....	8
Figure 2.3: Growths in solar thermal collectors' surface and solar PV electricity production for the EU-28 zone [18], [19]. .....	9
Figure 2.4: Current setup of the solar process heater and location of sensors [28] .....	14
Figure 2.5: Monthly in-operation solar irradiation, primary energy savings and fractional energy savings for the period September 2013 to August 2014 [28]. .....	14
Figure 2.7: The HOBO® U30 Remote Monitoring System by Onset Computer Corporation [29].....	15
Figure 2.8: Simplified system layout highlighting the locations of the measuring instruments and sensors [24].....	16
Figure 2.9: Energy transfers within a solar thermal system [24].....	17
Figure 2.10: Comparison of efficiencies of various collectors, at irradiation levels of $500\text{W}/\text{m}^2$ (hollow) and $1000\text{W}/\text{m}^2$ (solid). In the case of PTCs, irradiation is considered as beam radiation [11]. .....	24
Figure 2.11: Efficiencies of various common liquid collectors and comparisons with various applications [11].....	27
Figure 3.1: The hardware and software development stages for the SWH monitoring device. ....	35

Figure 3.2: Monitoring system schematic for a common collector-storage type SWH. Dataflows through and from the microcontroller are also shown.....	36
Figure 3.3: Heltec Automation WiFi Kit 32 module [51]. .....	38
Figure 3.4: Heltec ESP32 WiFi kit module pinout diagram [50]. .....	40
Figure 3.5: 3D render of the solar panel fixture to be installed for irradiance monitoring.....	46
Figure 3.6: Circuit schematic for obtaining the IV curve of the panel. ....	47
Figure 3.7: IV curve of a generic PV panel at global solar irradiance levels of ~1000W/m <sup>2</sup> . .....	47
Figure 3.8: Solar Irradiance meter schematic .....	48
Figure 3.9: Solar Irradiance calibration setup.....	49
Figure 3.10: Raw waveforms from the AC voltage module for a (a) incorrect mid- value and (b) correct mid-value. ....	51
Figure 3.11: RMS signal of a ~240Vac source using a (a) 5,000 sample reading with no in-between delays; (b) 50,000 sample reading with no in-between delays; and (c) 500 sample readings with a 500us in-between delay.....	52
Figure 3.12: The second version PCB designed to fit the Heltec WiFi kit 32 module ( ①). .....	55
Figure 3.13: Data flows to and from the monitoring device.....	56
Figure 3.14: User-interface heading showing the 5 main tabs upon page loading. ....	59
Figure 3.15: The Current Readings tab as presented on the first page of the UI.....	60
Figure 3.16: <i>Highcharts</i> [63] chart presenting all gathered parameter data viewed in the <i>View Charts</i> tab. Also displayed is the additional menu accessed by clicking the menu icon on the right. ....	61

Figure 3.17 (a) Hierarchal order of control options and (b) User-interface control options showing instance where <i>Autonomous Control</i> is disabled (left) and instance where <i>Autonomous Control</i> is enabled (right). .....	62
Figure 3.18: Flowchart showing the execution flow of the <i>autonomous control</i> process. ....	63
Figure 3.19: Blank SWH Primary Efficiencies report. ....	65
Figure 3.20: Blank Energy Unitisation Efficiencies report. ....	68
Figure 3.21: Blank <i>Settings</i> page showing all updatable parameters.....	69
Figure 3.22: Monitoring system prototype installation on a common thermosyphon type SWH, located at the Institute for Sustainable Energy in Marsaxlokk, Malta. ....	70
Figure 3.23: Combination of tests to be performed to test the capabilities of the monitoring system. Warm weather signifies ambient temperature highs > 25°C and lows > 18°C; Cold weather signifies ambient temperature highs < 15°C and lows < 5°C. Clear signifies total daily solar irradiance > 8kWh; Cloudy signifies total daily solar irradiance < 5kWh. ....	72
Figure 4.1: Real-time monitored parameter values displayed on the homepage of the UI during a water draw-off instance. ....	78
Figure 4.2: Embedded data-validation in the UI.....	78
Figure 4.3: UI alert confirming that the changed parameters from the <i>Settings</i> tab is accepted.....	79
Figure 4.4: UI displaying an 'ON' status for the backup heater (left), and the indicator lights showing 'closed position' status on the relay module (right) .....	79
Figure 4.5: <i>Storage temperature</i> (black) and <i>consumed electrical energy</i> (blue) chart for the 5 <sup>th</sup> (17:00) till the 6 <sup>th</sup> (09:00) of May 2021 with <i>Autonomous Control</i> feature enabled with only the storage temperature as the controlling factor. ....	80

Figure 4.6: Storage temperature (black), electrical consumption (teal) and solar irradiance (purple) chart for 12 <sup>th</sup> -15 <sup>th</sup> of May with Autonomous Control feature turned on with all control features enabled. ....	81
Figure 4.7: Reconnection to the internet after rebooting due to a disconnection timeout. ....	82
Figure 4.8: Solar shading effect on solar irradiance readings. Charts showing solar irradiance (in kWh/m <sup>2</sup> ) for the 25 <sup>th</sup> and 26 <sup>th</sup> of April 2021. ....	86
Figure 4.9: Solar shading occurrence due to a metal structure surrounding the installation area. ....	87
Figure 4.10: <i>Qo Solar Tank Consumption</i> trend showing instances of hot water consumptions for the 24 <sup>th</sup> of April 2021. ....	88
Figure 4.11: <i>Storage temperature</i> rise and <i>current solar flux</i> trend between 07:00 and 19:00 for the 17 <sup>th</sup> of March 2021. ....	92
Figure 4.12: <i>Storage temperature</i> rise and <i>current solar flux</i> trend between 06:00 and 18:00 the 18 <sup>th</sup> of May 2021. ....	100

# List of Tables

Table 2.1: Examples of commercially available thermal monitoring systems and controllers .....	12
Table 2.2: Series of quality tests for solar collectors [42]. .....	26
Table 3.1: Specifications of the thermosiphon flat-plate solar heating system. ....	37
Table 3.2: Heltec ESP32 WiFi kit module specifications [50]. .....	39
Table 3.3: Pin allocation of sensors and modules .....	40
Table 3.4: <i>YFS-201</i> Hall Type Flow Sensor specifications .....	42
Table 3.5: <i>DS18B20</i> temperature sensors specifications [56] .....	44
Table 3.6: Generic PV panel specifications. ....	45
Table 3.7: ZMPT101B Voltage transformer specifications [57] .....	50
Table 3.8: <i>HSTS016L</i> specifications [58] .....	53
Table 3.9: Field numbers and corresponding parameters stored on the ThingSpeak™ database. ....	56
Table 3.10: Prototypes developed showing progress timeline. All prototypes were installed on the same SWH located at the Institute for Sustainable Energy in Marsaxlokk, Malta. ....	71
Table 4.1: Description of the contents of this chapter. ....	75
Table 4.2: Functionality check of SWH, displaying alerts due to the obtained low efficiencies. ....	77
Table 4.3: Parameter accuracies and precision calculations for 19/04/2021 (top/ blue) and 03/05/2021 (bottom/ green). Also presented are the % changes in accuracies and precisions after 21 days of consecutive monitoring. ....	85
Table 4.4: Energy Utilisation Efficiencies results for the 24th of April 2021. ....	88

Table 4.5: SWH primary efficiencies report for the 16th of February 2021. ....	90
Table 4.6: SWH Primary Efficiencies for the 17 <sup>th</sup> of March 2021. ....	91
Table 4.7: SWH primary efficiencies report for the 17th of May 2021.....	93
Table 4.8: SWH primary efficiencies report for the 16th of March 2021. ....	94
Table 4.9: SWH primary efficiencies report for the 1 <sup>st</sup> of May 2021.....	94
Table 4.10: Energy Utilisation Efficiency results for the 20 <sup>th</sup> (00:00) till the 23 <sup>rd</sup> of May (23:59) 2021. ....	96
Table 4.11: Energy Utilisation Efficiency results for the 16 <sup>th</sup> (00:00) till the 19 <sup>th</sup> of May (23:59) 2021. ....	97
Table 4.12: Energy Utilisation Efficiencies report for the 10th till 17th of February 2021.....	98
Table 4.13: Energy Utilisation Efficiency report for the 1 <sup>st</sup> (00:00) till the 4 <sup>th</sup> of May (23:59) 2021.....	99

# List of Abbreviations and Symbols

## Abbreviations

AC	Alternate Current
ADC	Analog-to-Digital Convertor
AFPC	Advanced Flat Plate Collectors
API	Application Programming Interface
ASHRAE	American Society of Heating, Refrigerating and Air-Conditioning Engineers
CO <sub>2</sub>	Carbon Dioxide
COP	Coefficient of Performance
CPC	Compound Parabolic Collector
CSS	Cascading Style Sheets
DC	Direct Current
DHC	District Heating and Cooling
DWSH	Domestic Solar Water Heater
EDA	Electronic Design Automation
ETC	Evacuated Tube Collector
FPC	Flat-Plate Collector
GND	Ground
GPIO	General Purpose Input Output
GSHP	Ground Source Heat Pump
GSM	Global System for Mobile Communications
HTTP	Hypertext Transfer Protocol
IDE	Integrated Development Environment
IoT	Internet of Things
IP	Internet Protocol
ISO	International Organization for Standardization
ISR	Interrupt Service Routine
IV	Current-Voltage
JSON	JavaScript Object Notation

OLED	Organic Light-Emitting Diode
PCB	Printed Circuit Board
PET-G	Polyethylene Terephthalate - Glycol
PTC	Parabolic Trough Collector
PV	Photovoltaic
RE	Renewable Energy
RES	Renewable Energy Sources
RET	Renewable Energy Technologies
RMS	Root Mean Square
ROM	Read-Only Memory
SEUF	Solar Energy Utilisation Factor
SF	Solar Fraction
STC	Standard Testing Conditions
SWH	Solar Water Heater
URL	Uniform Resource Locator
VPN	Virtual Private Network



## Symbols

$\dot{m}_{HW}$	Instantaneous mass flow rate of the hot water outlet (kg/s)
$\dot{m}_c$	Instantaneous mass flow rate of the transfer fluid in contact with the collector (kg)
$\Delta T_c$	Temperature difference between the outlet temperature, $T_{co}$ , and the inlet temperature, $T_{ci}$ , of the collector (K)
$A_a$	Collector absorber area (m <sup>2</sup> )
$A_c$	Collector total aperture area (m <sup>2</sup> )
$b_0$	Angle modifier constant
$b_1$	Angle modifier constant
$c_1$	Collector thermal efficiency constant
$c_2$	Collector thermal efficiency constant
$c_p$	Specific heat capacity of the fluid at constant pressure (J/kg. K)
$E_{Solar}$	Period solar irradiance yield on the collector (kWh)
$E_p$	Electrical energy used by circulation pumps (kWh)
$F_R$	Collector correction factor
$G'_{day}$	Daily solar irradiance incident on the panel (J)
$G'_{period}$	Period solar irradiance incident on the panel (J)
$G_c$	Total instantaneous solar intensity (direct and diffuse) (W/m <sup>2</sup> )
$I_{RMS}$	Root mean square current draw (A)
$I_a$	Current drawn by the backup heater (A)
$k_{\tau\alpha}$	Incident angle modifier
$P_{RMS}$	Root mean square instantaneous power (W)
$Q_{demand}$	Period energy consumed as hot water (J) or (kwh)
$Q_{Elec}$	Period electrical energy consumption of the overall system (kWh)
$Q_i$	Storage tank water inlet flowrate (L/min)
$Q_o$	Storage tank outlet water flowrate (L/min)
$Q_{swh}$	Solar contribution to hot water (kWh)
$q_u$	Heat gain by the transfer fluid (J)
$Q_{Z-swh}$	Solar contribution to tap water (kWh)

$T_a$	Ambient temperature ( $^{\circ}\text{C}$ )
$T_i$	Storage tank inlet water temperature ( $^{\circ}\text{C}$ )
$T_o$	SWH outlet water temperature ( $^{\circ}\text{C}$ )
$T_{oi}$	Collector's initial inlet water temperature ( $^{\circ}\text{C}$ )
$T_{ot}$	Collector outlet water temperature after time $t$ ( $^{\circ}\text{C}$ )
$T_p$	Average (stagnation) temperature of the absorber/ plate ( $^{\circ}\text{C}$ )
$T_s$	Storage tank water temperature ( $^{\circ}\text{C}$ )
$T_{s-\max}$	Maximum storage tank water temperature ( $^{\circ}\text{C}$ )
$T_{s-\min}$	Minimum storage tank water temperature ( $^{\circ}\text{C}$ )
$U_L$	Heat transfer loss coefficient of the collector ( $\text{W}/\text{M}^2 \cdot ^{\circ}\text{C}$ )
$V_{\text{RMS}}$	Root mean square voltage source (V)
$V_a$	Outlet/ mains AC voltage (V)
$W_a$	Power rating of the backup heater (kw)
$\eta_0$	Maximum efficiency of a collector
$\eta_{\text{combined}}$	Period overall system (primary) efficiency
$\eta_{\text{day}}$	SWH's collector efficiency during the day
$\eta_{\text{night}}$	SWH's storage tank efficiency during the night
$\eta_{\text{sys}}$	Overall efficiency of a SWH system (revised)
$\eta_{Z-\text{sys}}$	Overall efficiency of a SWH system
$\eta_{\text{FPC}}$	Efficiency of a collector
$\Delta H_{\text{night losses}}$	Heat losses during the night (J)
$\Delta T_s$	Storage tank temperature rise/ fall (K)
$\Delta T$	Temperature difference between the outlet temperature, $T_o$ , and the inlet temperature, $T_i$ , of the storage tank (K)
$F'$	Collector efficiency factor
$P$	Instantaneous electrical power (kw)
$t$	Total time per instance of detected water flow or solar irradiance (s)
$\theta$	Solar irradiance incident angle
$\tau\alpha$	Collector's absorber transmittance-absorptance product
$c$	Specific heat capacity of water (J/kg. K)
$m$	Storage tank capacity (kg)

# Chapter 1 Introduction and objectives

## 1.1 Background

The key environmental challenge that is dominating worldwide is that of mitigating the impacts of greenhouse gas (GHG) emissions, particularly that of the rising global temperature and the resulting observable effects on the environment. Effects of climate change predicted by scientists in the past are now occurring at alarming rates, such as prolonged and intensified heatwaves (and in other areas, tropical storms), accelerated sea-level rise and shrinking glaciers. It is highly likely that the causes of global warming and its effects are the result of human activity since the 1850s, which proceeded at unprecedented rates over recent years. Carbon Dioxide (CO<sub>2</sub>), a GHG released through human-driven and natural (although marginal) activities, has had atmospheric concentration levels almost doubling since pre-industrial times, resulting in the global average temperature to rise. In fact, nineteen of the recorded warmest years have occurred since 2000, with no signs of abating [1].

Many countries are now working collectively to mitigate the effects of climate change by emitting less GHG emissions. The drive to switch to Renewable Energy Sources (RESs) has been more persistent in recent years, especially following the 2015 Paris Agreement, which saw 196 state parties signing a legally binding international treaty on Climate Change. The agreement commits all countries to a target of keeping the global temperature rise to well below 2°C, with efforts to limit change to below 1.5°C [2]. Moreover, EU member states explicitly set a goal to reduce GHG emissions by 40% (recently proposed to be raised to 55%) compared to 1990 levels and increase renewable energy share to at least 32%, by 2030 [3]. As a result, the importance of Renewable Energy Technologies (RETs) is ever-increasing.

One of the largest sources of GHG emissions from human activities is the electricity and thermal energy production sector, which as of 2019, accounted for 31.9% of the global GHG emissions [4]. A considerable portion of this energy is used for water heating purposes which is an essential part of everyday life, especially in homes where it is used for showering, laundry, space-heating, pool-heating among other functions, but also in industrial applications such as chemical production [5]. The U.S. Energy Information Administration (EIA)'s Residential Energy Consumption Survey (RECS) reported that

in 2015, an estimated 19% of the total energy delivered to a household was used for water-heating purposes [6]. In Malta, the dominant water heating means in the domestic sector is the electric water boiler, which as of 2009, was present in 90.5% of all occupied households, summing up to 23.88% of the total electrical energy consumption of a typical household. On the other hand, by the same year, only 9.28% of Maltese households were equipped with a solar domestic water heater (SDWH), the majority found in households of three persons or more [7].

Nowadays, it is becoming crucial that energy savings and efficiencies are reliably measured and quantified, as countries are being required to report the annual contribution of RETs at a national level, and this includes solar water heaters (SWHs). Unlike other RETs such as solar photovoltaic systems (PVs) and micro wind electric systems that are mostly equipped with an energy metering system, SWHs are not, and this has had a detrimental effect on their popularity. In fact, in Malta, a downward trend (refer to Figure 1.1) for SWH installations was observed over the years despite the consistent grants being offered [8]. One main attribution towards this negative trend is the consumer shift towards PV systems, which all offer some form of energy performance reporting. The public is in turn discouraged in investing in such technologies [9] due to a general perception that the payback period for SWHs is longer than it actually is.

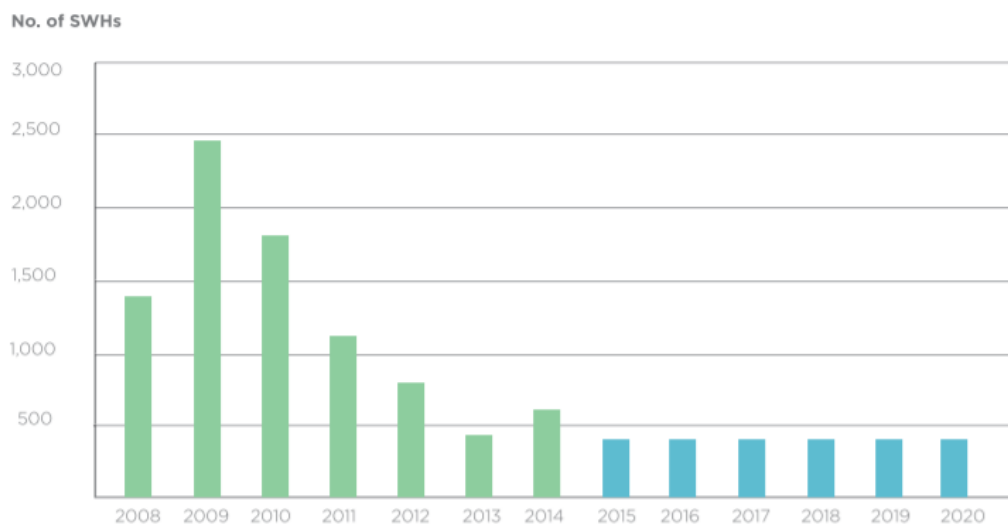


Figure 1.1: Number of new SWHs installed in Malta throughout the years 2008-2014 and the projected installations for the years 2015-2020 [8]

Most manufacturers of SWHs do not provide thermal metering systems because current available products are relatively expensive, have limited functionalities, and often require substantial modification on SWH setups.

## 1.2 Scope of the work

This project aims at designing, prototyping and testing a low-cost, reliable, user-friendly and versatile SWH monitoring device and controller. The device will log key parameters and will integrate a multitude of features for optimising the SWH performance including the control of its backup electric heater. The collected data will be presented through a web-based user-friendly interface, which may be accessed from any network-connected device.

The objectives of the dissertation are:

1. Carry out a detailed market analysis on any available thermal energy meters, including their costs, functionality and versatility;
2. Understand the performance characteristics of SWHs and determine the necessary parameters that need to be monitored;
3. Explore the options of available sensors and modules and choose the best combination that fits the specific requirements for the thermal energy meter design setup, such as size, accuracy, cost, and compatibility;
4. Design a printed circuit board (PCB) with all components and build a prototype to be tested with a real solar water heating system operating under typical hot water consumption.

The research questions for this study are:

- What does the current market offer with regards to thermal monitoring systems and controllers?
- What are the key parameters of a SWH system and what techniques should be followed to monitor them?
- How is the performance of a SWH quantified and how should it be presented to general users in a well-interpretable manner?
- Can a low-cost SWH monitoring system and controller be accurate and reliable?

### 1.3 Structure of the thesis

The thesis is made up of 5 main chapters, as follows:

**Chapter 1** gives a brief introduction on the negative effects of GHGs and the need to switch to RESs. The limitations of current solar heating energy metering systems and the objectives of the project to address these limitations are also highlighted in this chapter.

**Chapter 2** goes into further detail about the current energy mix and the share of renewables. The different types of SWH collectors and the requirements and methods to evaluate SWH performance are reviewed. Existing thermal metering systems are also explored in this chapter, presenting their features, availability, and price levels. In addition, this chapter describes the importance of metering systems by evaluating the behaviour of RET users with and without compatible monitoring systems.

**Chapter 3** deals with the hardware selection for the monitoring system and the firmware developed to provide users with accurate and easily interpreted energy results. An overview of the user-interface (UI) is also provided in this chapter, highlighting the features and customisability offered within the unified interface including the control of the backup heater. At the end of this chapter, the design of experiments is developed, which shall serve as a functionality check for all features of the monitoring system.

**Chapter 4** presents the results obtained from the monitoring system, including sample performance results for the main weather conditions encountered in Malta. The different control levels of the backup heater are extensively tested for periods of three consecutive days or more, to verify correct feature functionality, including the quantifying of electrical energy consumption. In this chapter, the UI is also tested for data-validation checks, data presentation and responsiveness. Finally, the chapter gives an overview of the attainable accuracies and precisions from the monitoring system.

**Chapter 5** lists the conclusions drawn from this dissertation, also giving recommendations for further works to improve on security, reliability and accuracy in preparation towards making the monitoring device market ready.

## Chapter 2 Literature Review

### 2.1 Introduction

The sun's effective blackbody temperature is that of 5762K, emitting a total power of  $3.8 \times 10^{20}$  MW, or 63 MW/m<sup>2</sup> of the sun's surface. Out of all this power, which is emitted in all directions, only a tiny fraction of it reaches the earth. In fact, just  $1.7 \times 10^{14}$  kW is intercepted on Earth [10]. Despite of this mere fraction, just 30 minutes of solar irradiation on Earth is enough to exceed the energy demand for an entire year.

All forms of stored energies found on Earth are solar in origin. This includes fossil fuels such as coal, oil, and natural gas, all originating from photosynthesis processes and turned into energy dense fuels through a combination of prolonged high temperature and pressure conditions. Even clean energy sources such as wind, hydro and tidal energies are solar in origin, and are caused by imbalance in temperatures at different locations.

Compared to other sources of clean energy, direct solar energy is the most abundant and versatile form of energy, recognised throughout the entire history of mankind. In addition to the endless ways of how the sun's energy has been utilised by both humans and nature for basic tasks through time, it is now possible to harness the sun's energy to perform intricate tasks, including heating and cooling of buildings, domestic and industrial water heating, electrical power generation, water desalination, amongst others [10]-[12].

Despite of this, fossil fuels have been, and still are, the main sources of energy due to their relatively cheap prices, high energy density, and convenience of storage and accessibility. These factors, along with the fact that environmental damage by fossil fuels was of little concern until recently, has made them the dominant source of energy worldwide. Unfortunately, however, the implications of using fossil fuels extensively have now shown and will keep showing their degrading environmental and health effects. The undeniable degradation of the environment due to fossil fuels has become more apparent due to the ever-increasing population, industrial activities, energy availability and use. Coming up with solutions which would solve the environmental crisis is no easy task and requires long-term sustainable actions and developments. RESs thus appear to be the most viable and effective solution, which open endless potentials

for green-energy generation. Many alternative energy sources have the potential of replacing fossil fuels however, the verdict to which energy source/s should be utilised boils down to the basic principles of sustainable development; being social, economic, and environmental considerations.

With economic development and human population on the rise, demand and consumption of energy will also certainly grow, posing a threat to our planet and future generations if degradation on our planet persists. Thus, a switch to carbon neutral (and negative) sources of energy is necessary, and the push from governmental entities concerning energy and developments will certainly play a role in how energy is created and consumed.

### **2.1.1 About renewable energy sources and technologies (RES and RET)**

RESs can be defined as naturally occurring phenomena which through appropriate technologies (RETs), may be converted into useful energy with the ability to compete in the energy share market. RESs arise from the sun's energy through indirect or direct effects on the Earth and include anything from wind energy to biomass. Renewable energies (REs) have great potential, however, are generally linked to many concerns including intermittency, geographical characteristics, seasonal variances, accessibility, technical complications, and cost-effectiveness. As technologies progress, we are seeing efficiency improvements in RETs with lower capital and maintenance costs and improved reliability and lifetime. Moreover, RE implementations are generating numerous green job opportunities leading to nationwide economic benefits, such as research and development, manufacturing, marketing and promotions, installations, operations, and maintenance.

### **2.1.2 European Renewable Energy Directive 2009/28/EC**

In 2009, the European Renewable Energy Directive 2009/28/EC (recast directive 2018/2001/EU [13]) has recognised for the first-time solar heating, aerothermal, geothermal and hydrothermal for heating purposes as a renewable energy resource. Moreover, the recent Energy Performance of Buildings Directive (EU) 2018/844 calls for a larger share of solar heating in buildings and prominently places it as an important tool to enhance the proposed new smartness indicator for buildings, given its ease of energy storage and cost effectiveness [14]. Increase in RES share for thermal



applications has been on the rise ever since [13]. In 2019, 22.1% of the gross final energy used for heating and cooling purposes in the EU-27 zone was derived from RES. As can be observed in Figure 2.1, the best performing country from the EU-27 zone was Sweden with 66.1% of energy for heating and cooling derived from RES, while the worst performing was Ireland with 6.3% [15]. One important consideration is that much of Sweden's RES share for heating and cooling was derived from shallow geothermal heat energy systems, which are not possible in other countries. In fact, around a fifth of all buildings in Sweden make use of a ground source heat pump (GSHP), making them the world leading country in the shallow geothermal application [16].

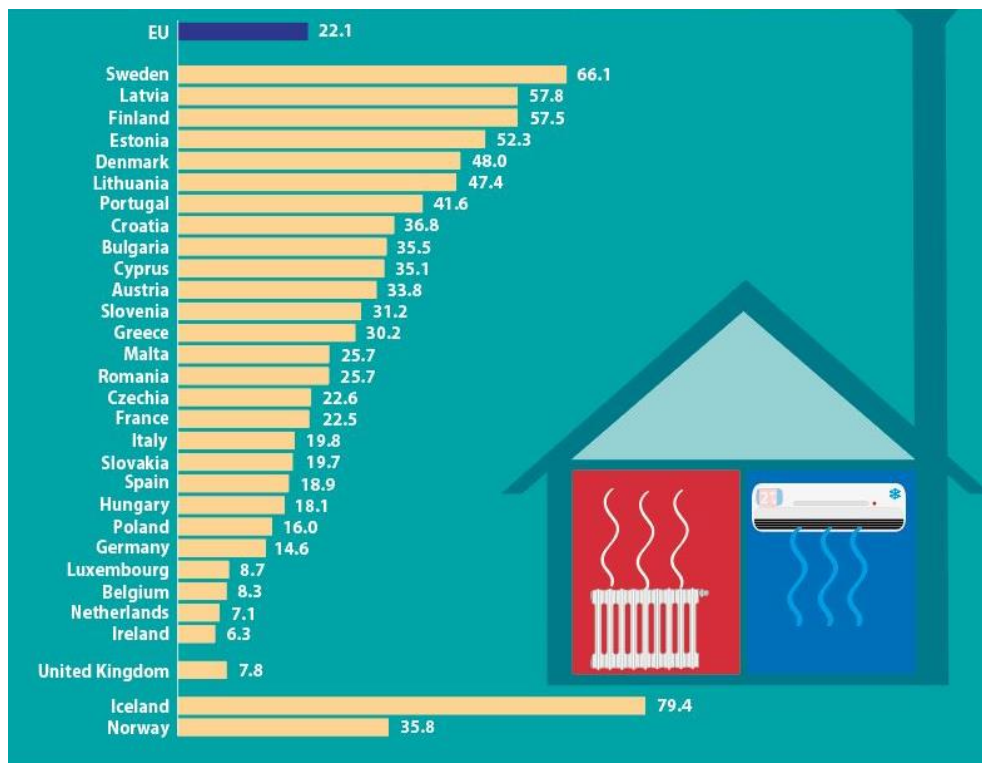


Figure 2.1: Share of energy from renewable sources for heating and cooling for the year 2019 [15].

### 2.1.3 Solar thermal systems deployment

One of the most prominent RET is solar heating, which has been around for centuries due to its operational simplicity and adaptability. Presently, most solar heating technologies take the form of the common solar water heater (SWH), generally composed of a collector, heat storage and a fluid transfer system. The main use of solar water heating is for domestic water heating (DWH) in residential households. In fact, by

2014, the domestic sector accounted for approximately 63% of the total installed collector coverage area of solar thermal. Despite being of significant contribution towards renewable energy generation, solar thermal technologies have faced great competition in recent years. In small scale heating systems, particularly for small apartments and detached houses, heat pumps coupled with solar PV systems dominated, especially in European and Chinese markets. On the other hand, solar thermal technologies were the leading market for the industrial sector and large-scale solar-assisted district heating and cooling (DHC) systems, although the contribution to the overall market was still very low relative to domestic installations [17].

By the end of 2017, the total global solar thermal collector coverage was that of 675 million m<sup>2</sup>, providing a 472 GW<sub>thermal</sub> capacity. The estimated total yield reached 388 TWh<sub>thermal</sub>, a 7.6 factor increase compared to 2000 figures. The largest share was China, with 68.8% of the total capacity, followed by Europe and North America with 11% and 4% respectively. In 2016, the overall solar thermal energy yield (including solar energy used to generate other forms of energy) reached 50.1 TWh for the EU-28 zone, equalling to 2% of the total RES share [17]. On the other hand, the production of direct use solar thermal energy (thermal energy available to final users) for the EU-28 zone was of 24.2 TWh<sub>thermal</sub> for the same year. This is about three times as much as the direct use solar thermal energy production in 2006, as can be observed in Figure 2.2.

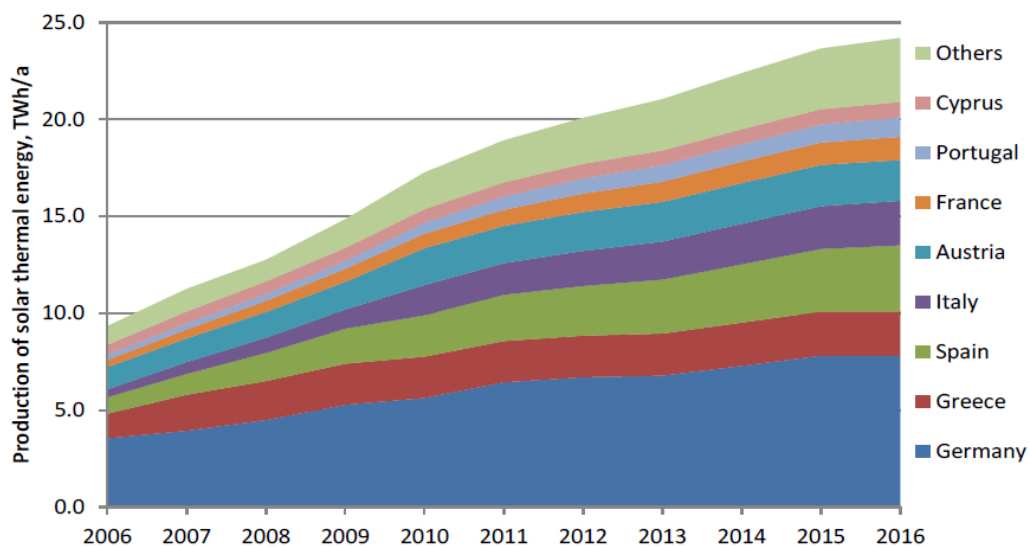


Figure 2.2: Production of direct use solar thermal energy in the EU-28 zone [17].

However, growth in solar thermal technology sales greatly slowed down globally in recent years. For instance, growth in new solar thermal collectors' surface declined by 1.02% in the EU-28 zone from 2018 to 2019 [18]. In contrast, during the same year, growth in solar PV electricity production capacity increased by 6.86% [19]. The growths in solar thermal collectors' surface and solar PV electricity production capacities over recent years are presented in Figure 2.3 [18], [19], which also reveals the much higher overall deployment rates of solar PV technologies compared to solar thermal technologies.

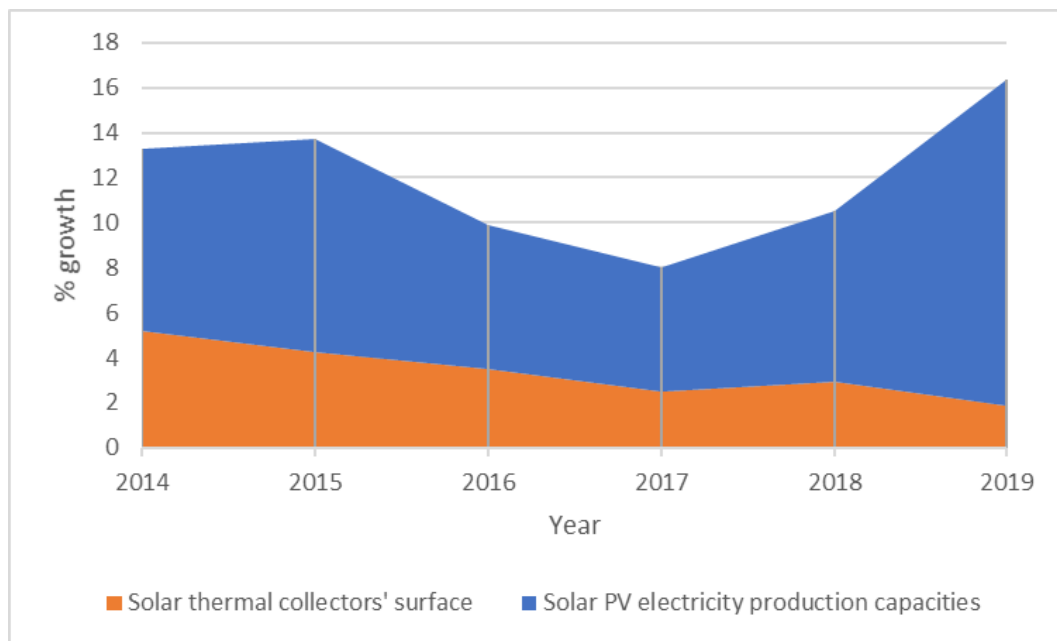


Figure 2.3: Growths in solar thermal collectors' surface and solar PV electricity production for the EU-28 zone [18], [19].

## 2.2 SWH energy-metering and monitoring systems

Unfortunately, policy makers and market promoters often disregard solar thermal technologies and applications, due to solar thermal energy mostly not reliably quantified and reported. Unlike in the case of PV systems, owners of solar heating systems are generally unaware of the energy production figures of their installed systems, especially in small-scale applications such as in the domestic sector. Consequently, statistical agencies resort to estimates on solar thermal energy yields. This is proving to hinder SWH technology deployment, and making photovoltaic systems appear more attractive to potential customers, especially due to the difficulty in prediction of amortisation time for solar thermal systems [20]-[22].

For years, medium to large solar thermal systems (mainly industrial and DHC applications) have had their direct solar generated thermal energy measured and displayed reliably and transparently. Most of these systems include continuous metering (data-logging), remote monitoring and controlling, and often include underperformance and malfunctioning detection features. This results in faults being spotted early-on, possibly preventing failures and downtimes while also helping in achieving optimal solar yields all year round. The reasoning for justifying the acquisition of such advanced monitoring systems on medium-large solar thermal systems is that failures, downtime, and underperformance can result in very high expenses, hence the price paid for the monitoring system is often rewarding. For smaller systems however, this is different. Nowadays, a basic domestic thermosyphon SWH can be purchased for less than €1000, and an energy metering and performance monitoring device could add an additional 10% to 50% to the expense, depending on the level of control and metering. Consequently, most small SWHs (especially the basic thermosyphon type) presently do not include any energy metering or performance displaying device whatsoever. Furthermore, an internet connection feature is even more rare in small SWHs, limiting energy metering and performance information (if available) to only onsite personnel and not to manufacturers, energy auditors, technicians etc. [22]

In some cases, a controller is provided with small SWHs however, has limited functionality, typically for simple control of the backup heater by means of a timer and/or a temperature controller, utilising a single temperature sensor in the tank. In this case, the controller is not equipped with adequate sensors to perform energy metering tasks.

Some manufacturers of modern SWH systems offer heat metering as an option. In such cases, since the temperature sensors and the flowmeter are already catered for by the manufacturer, additional costs for heat metering can be lower, ranging from 10% to 30% to the costs (higher prices for an online system). If retrofitting a SWH system with no energy metering design considerations however, total costs including installation typically add 30 – 50% to the total costs. As it stands, solar thermal metering and controller systems offered as retrofitting kits do not include a feature to monitor and control the SWH through an online portal or an app, although some manufacturers offer this option as an upgrade at a higher asking price [20]-[22].

A European market survey conducted by the German research institute Fraunhofer ISE [23], showed that only 35% of basic domestic SWH controllers offered data logging features. The share rises to 70% to more complex systems involving space heating. Less than 30% of these controllers are equipped with smart features giving owners the ability to control their system remotely [23]. The survey [23], conducted on 132 controllers, showed that features vary significantly from one controller to another, and manufacturers often offer users features (and sensors) as optional add-ons, rather than having the features pre-configured.

### **2.2.1 Cost effectiveness of monitoring solar energy systems**

Economic studies of energy conversion systems are typically complex, in addition to being very expensive to implement. Zukowski et al. [24], during their implementation of a tailor-made monitoring system on a medium scale existing solar thermal system, deduced that the cost for monitoring and data collection/ reporting reached two-thirds of the material and installation costs of the actual solar system [24]. However, as previously mentioned, the costs benefits outweigh the costs for medium to large systems, as expenses due to failures, malfunctioning and underperformance are greatly reduced. For small systems however, the extra costs generally are not justified.

An ideal small SWH monitoring system should be low-cost, easy to install, adaptable, and reliable for long term-studies. Thermal energy metering should be a standard feature, with easy presentation of energy (and possibly cost) savings, while also providing mechanisms for identification of mechanical failures, malfunctioning and system underperformance. Lastly, data collection should be transparent and available for proper energy reporting [21], [22].

### **2.2.2 Monitoring systems case studies**

As previously mentioned in Section 2.1.3, monitoring devices may be included in modern systems or retrofitted on SWH systems to perform certain energy metering or control tasks. These devices may be categorized in 3 main groups:

- Basic electronic displays targeted at small SWH installations with no data-logging facility that only show instantaneous hot water temperature and status of the backup heater. Some also include a temperature and/ or timer controller to control the backup heater switching times;

- Featureful energy-metering systems and controllers with a middle price tag, usually targeted at small and medium sized SWH installations; and
- Tailored smart monitoring systems with enhanced features and detailed energy metering intended for large (industrial and DHC) SWH installations. Such systems are expensive, and often require development and custom fitting.

Table 2.1 lists some commercially available SWH monitoring systems and controllers targeted at small and medium SWH installations, along with their features and price tag (if available):

Table 2.1: Examples of commercially available thermal monitoring systems and controllers

<b>Brand</b>	<b>Model</b>	<b>Features</b>	<b>Price</b>
<b>Jiaxing Passion New Energy Technology [25]</b>	SR1535	3-point temperature sensing, water flow sensing, backup heater control, circulation pump control, error handling.	On Request
<b>Hitsan Incorporation BESFUL</b>	BF-160AW	3-point temperature sensing, water level sensing.	~€85
<b>SunReports [26]</b>	Apollo1 Energy Monitor	3-point temperature sensing, backup heater status sensing, circulation pump status sensing, flow sensing, energy metering, optional PV monitoring.	On Request
<b>Stiebel Eltron Renewables [27]</b>	SOM 6 Plus	4-point temperature sensing, flow sensing, circulation pump control, energy metering, antifreeze function.	~€145
<b>Stiebel Eltron Renewables [27]</b>	SOM 10	10-point temperature sensing, 3-point flow sensing, 10 relay controls (for pumps and backup heaters), energy metering, antifreeze control, pump speed control.	~€1000

From what was observed, SWH thermal metering devices are available for purchasing, some providing beyond satisfactory monitoring features. However, it was noted that setup of the devices is not straightforward, often requiring replacement of parts and modification on the system. Additionally, only a very few can log data and report thermal energy performances, and even less can do it remotely. As reliability and functionality are improved, so does the price tag, up to a point where it would not be justifiable to install the monitoring system, especially for the average domestic SWH user. It was also noted that proprietary sensors that are required by some monitoring and control system are often sold separately, hence apart from increasing costs considerably, would be of even more inconvenience to the consumers. Without these sensors, the controllers/ monitoring systems would still work, but will offer limited functionality.

The following are three case studies describing tailor-made monitoring systems fitted on medium and large SWH installations. Case studies are useful as they provide indications of what a customer would require in an end-product or service, or in this case, the hardware and feature requirements which provide satisfactory performance analysis.

#### **2.2.2.1 Soltex: textile company in south of Germany**

One method for on-site real-time monitoring solar process heat systems is outlined by Frey et al. [28], a method developed and utilised within the project named *Soltex* (Solar process heat for a medium-sized textile industry). The monitoring system was installed to provide detailed feedback of hot water production using a solar process heat system in the south of Germany. The collector type is that of a parabolic solar concentrator, rated at  $70\text{kW}_{\text{thermal}}$  [28]. The manufacturing process of the textile company requires a large hot water heat store, which typically varies from  $10\text{m}^3$  to  $70\text{m}^3$  depending on current capacity. The process of heating is done through a water/ glycol mixture which is circulated through the collectors till it reaches  $60^\circ\text{C}$ , which is then redirected to the storage via a 3-way temperature-controlled valve, where it heats the heat-store through a heat exchanger. The measurement sensors utilised in this project consist of five temperature sensors, two flowmeters, and two irradiance meters. Figure 2.4 is the solar process heating setup employed at the textile company, also highlighting the sensor locations.

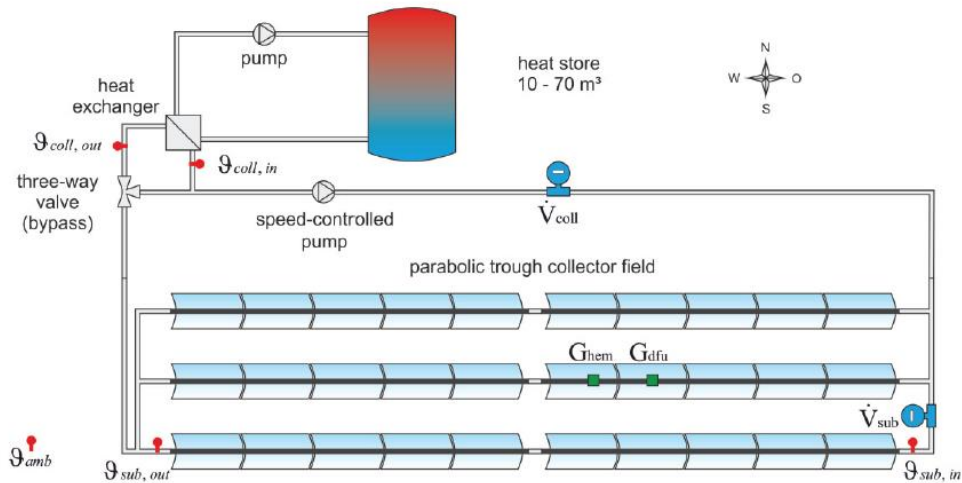


Figure 2.4: Current setup of the solar process heater and location of sensors [28]

A sample report for the performance of the collector throughout the period September 2013 till August 2014 is presented in Figure 2.5. The two parameters of interest from these charts are the *fractional primary energy savings* and the *primary energy savings*, which give indications on the performance of the system.

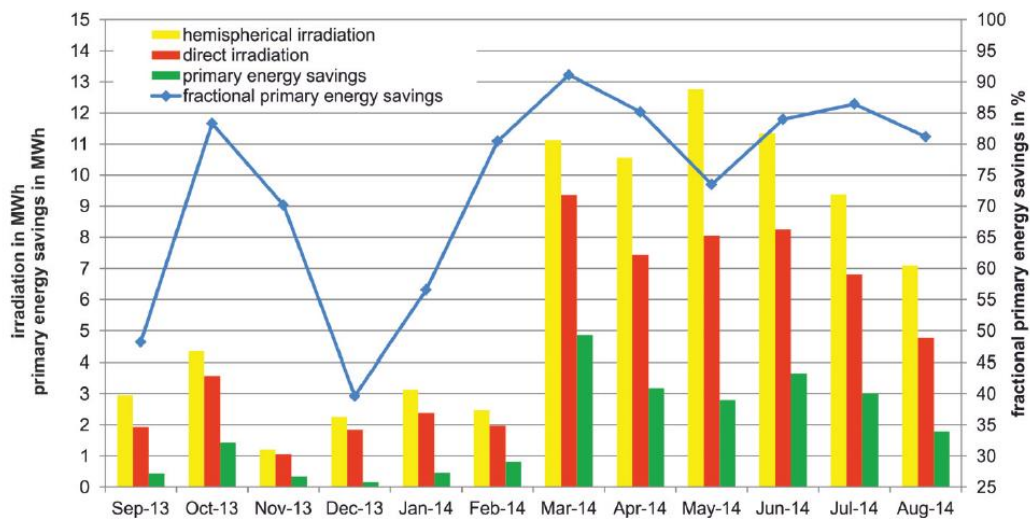


Figure 2.5: Monthly in-operation solar irradiation, primary energy savings and fractional energy savings for the period September 2013 to August 2014 [28].

During the analysis of the data obtained for the solar thermal system, it was deduced by the authors [28] that although the performance obtained was a good one, better results could be obtained if the tracking mechanism of the collector had to be improved. This was concluded after observing the large discrepancies between *primary energy savings*



and *solar irradiation* from the obtained charts. This observation would not have been possible without the monitoring system.

### 2.2.2.2 Onset Computer Corporation, Massachusetts California

Figure 2.6 depicts a system diagram of a solar-thermal monitoring system based in Massachusetts California. The device comprises of a series of sensors which continuously monitor collector water temperature, inlet and outlet collector temperatures, flow of hot water, and gas usage (in this case, the backup heater is replaced by an instant gas-powered water heater). The device also contains a GSM (Global System for Mobile Communications) cellular based data logging unit, which collects data at one-minute intervals and stores the information on a web-based platform, accessible from the device manufacturer's website.

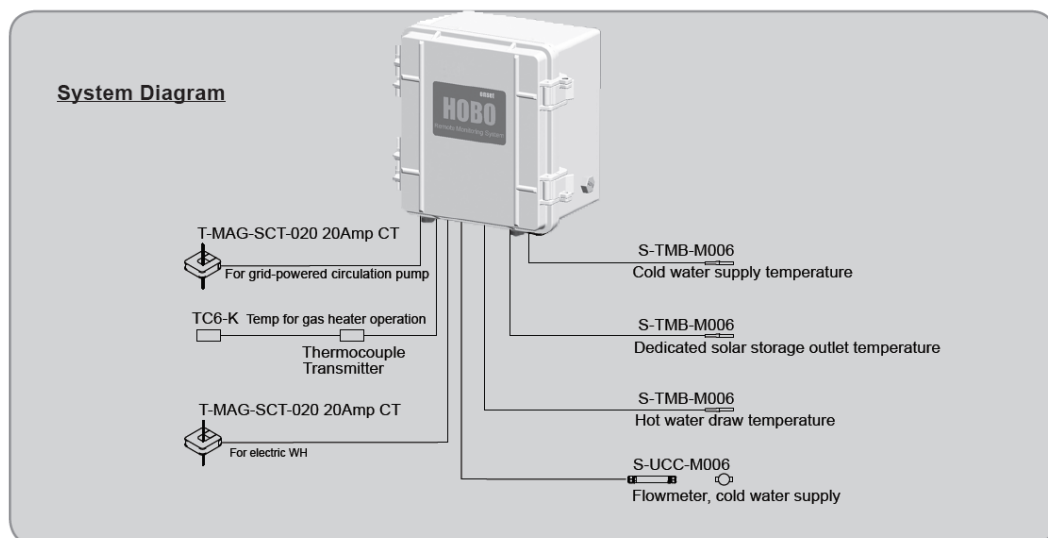


Figure 2.6: The HOBO® U30 Remote Monitoring System by Onset Computer Corporation [29]

The device is capable of executing performance analysis on the energy and cost savings incurred by the solar-thermal system, which will be reflected by the climate of the installation zone, the household size and the fuel for backup heating type [29].

### 2.2.2.3 Hotel Building in Bialystock University of Technology, Poland

The SWH system being monitored in this case is composed of two parallel connected subsystems, one of 35 flat plate collectors arranged in rows of 5 units, and the other of 21 evacuated tube collectors arranged in rows of 3 units. The total aperture areas are of 65.5m<sup>2</sup> and 67m<sup>2</sup> for the FPCs and ETCs, respectively. The system stores hot water in eight storage tanks of one cubic metre each, located on the inside of the building. The

monitoring setup consists of the following: 17 ultrasonic heat counters, 4 electrical power meters (for pumps' electrical consumption monitoring), and 42 temperature sensors of type PT500 platinum (for temperature monitoring of the entire system). Apart from the monitoring features, the system also includes a miniature weather station on the roof to monitor basic weather parameters such as the ambient temperature and solar irradiance. All the data captured is also stored online for easy reporting. The simplified system layout is depicted in Figure 2.7.

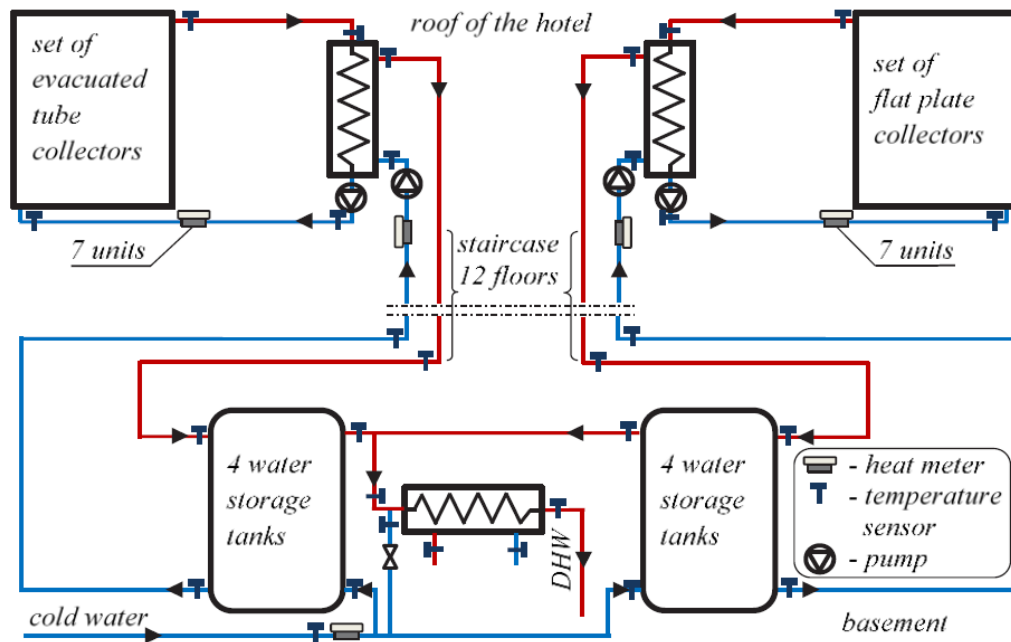


Figure 2.7: Simplified system layout highlighting the locations of the measuring instruments and sensors [24].

Zukowski et al. [24] in their report, define system energy efficiency ( $\eta_{Z-sys}$ ) as the useful solar heat energy supplied to the tap water system,  $Q_{Z-swh}$ , minus the electrical energy consumed by the pumps,  $E_P$ , divided by the incident solar energy on the collectors,  $E_{Solar}$ :

$$\eta_{Z-sys} = \frac{Q_{Z-swh} - E_P}{E_{Solar}} \times 100 \quad (1)$$

The advantage of having so many sensors is the ability to accurately trace sources of heat losses. The block diagram in Figure 2.8 outlines most heat energy transfers through the system. During the study, it was calculated by Zukowski et al. [24] that 13.4% of

the solar energy gain, were lost to the environment, through the piping network, the collectors themselves, or the storage.

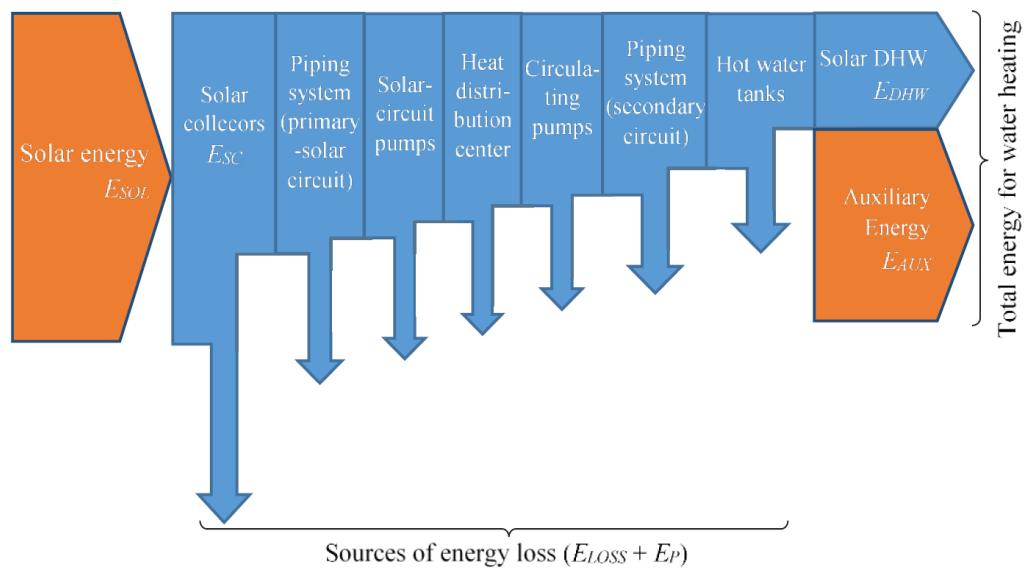


Figure 2.8: Energy transfers within a solar thermal system [24].

### 2.3 Attitudes and behaviours for renewable energies

Unlike fossil fuels, anyone in the residential sector could be part of the RE market by being part of the RE production. This is mostly visible by homeowners incorporating small scale solar energy systems (mainly solar PV and solar Thermal) in their home. This led to many countries adopting several schemes which would aid homeowners into incorporating RES into their homes. For example, such schemes allow homeowners to feed in generated electricity to the grid and get a price for it, known as the feed-in tariff. This encouraged homeowners to invest in such technologies which kicked off a demand fuelled development in the RE sector leading to price reductions and improved efficiencies for all the components making up the RES systems [30].

#### 2.3.1 The intentions to adopt renewable energy harvesting technologies: Economic, Social or Environmental?

The motives behind investing in RES systems in households, namely PV and solar thermal, has been researched thoroughly in different scenarios employing different methods. In California, the diffusion of PV systems was driven mainly by peer behaviour, meaning that a street or zip code area predicted further adoption as soon as the first adopters were observed. Hong Kong, however, saw a slow rate of adoptions due

to the many barriers imposed on the investors. For example, purchase prices for the systems were still high, along with inadequate infrastructure, long payback periods and lack of incentives [30]. The same applied for solar thermal systems however, to even a slower rate mainly due to the higher prices compared to solar PVs. As emphasised by Zhang et al. [31], incentivising RES technologies is not enough, and policy makers need to regulate the market as to provide a means of security for investors.

It was remarked by Masini et al. [32] that the willingness to invest in RETs depended heavily on the confidence in the technology. Investors seem to shift towards technologies which have already overcome the fear of reliability and long-payback periods. As a result, due to a general perception that solar PV payback period is shorter than for solar thermal systems, adopters tend to opt for the former. Moreover, investors focus more on established technologies and tend to shy away from new innovations. This shows that financial incentives alone are not sufficient, and campaigns and promotions are necessary to inform potential adopters about the advantages and selection processes of RES systems [30], [32], [33].

In brief, the adoption of RES systems is not solely pro-environment motivated, but also depends on prices, policies and incentives, infrastructure, knowledge on the technology and peer behaviour [30], [34]. Homeowners, when asked what it would take for them to adopt for RES systems, stated that they would opt for such systems for financial and environmental reasons. However, in a study by Nolan et al. [35], no significant correlation between energy saving campaigns (using leaflets mailed to homeowners), and actual energy consumption reductions were observed. This led to the understanding that social desirability (the act of replying as expected by society), played a role in data collection, resulting in over-emphasis on pro-environment reasons for adoption of RES technologies [30].

### **2.3.2 The role of monitoring devices**

The scope of this section is to review whether micro-RES system owners are conscious of their system's performance and energy production yields, and whether accompanying monitoring systems are made use of, if available. Although using PV systems as an example, it can be assumed that the same could apply for solar thermal systems due to public's general understanding that the two technologies are very related to each other.

Keirstead et al. [36], performed a study to assess changes in consumption patterns upon the adoption of PV in households. The study contained self-estimates of electricity consumption which is very sensitive to how energy consumption is assessed. Some responders in this study assessed their consumptions based on monthly electricity bills, whilst other were more energy-literate and assessed their consumption in kilowatt-hours (kWh) by taking regular readings. Most respondents (> 85%), had a monitoring device accompanying their PV system, with the main intention of reporting generation information to the household. The authors [36] asked questions related to the monitors, such as the instalment location, how frequent the monitors were viewed, which metrics were used etc. Results showed that approximately 60% of respondents had their monitoring device installed in frequently occupied areas such as kitchens and living rooms however, for older systems, the device was installed in more hidden areas close to the inverters (such as the attic or roof top). About 50% of the respondents stated that they viewed the monitoring device at least once daily, with a higher shift towards those with the easily accessible monitors. Most of the monitors displayed the instantaneous power generated by the PVs, as well as the cumulative energy generated since installation of the system. About 50% of the monitors included the cumulative kilograms of CO<sub>2</sub> saved since installation, a feature intended to give a sense of satisfaction to the respondents. Almost half of the respondents in this study reported to have participated in some form of load-shifting activities, primarily to match the output profiles of their PV system. Additionally, the monitors created an awareness of the electricity generated by PV, as respondents generally stated that PVs generate energy typically when it is not needed the most.

Keirstead et al. [36] reported that monitoring devices generally create a sense of encouragement for respondents to switch to more energy-saving appliances, whilst also encouraging them to consider other forms of microgeneration technologies in the future. Thus, opting for RES micro generating systems not only produces clean renewable energies, but also increases general awareness on use of energy, eventually reducing overall energy consumption [36], [37].

## 2.4 Summary of a SWH monitoring device's requirements

Summarizing all the above, an ideal monitoring system shall [38]:

- Accurately monitor the basic parameters of a SWH;
- Allow for a functionality and reliability check to homeowners, manufacturing firms, and installers of solar thermal systems;
- Detect failures and underperformances, and ease the troubleshooting process by providing fault information and pinpointing to the servicing personnel. The system shall also raise alarm to users of potential faults by issuing early warnings, as to prevent severe long-term damages on the overall system;
- Provide detailed visualisation of the systems' energy yield and performance to different user groups, including technicians (/servicing personnel), system owners, and the public;
- Ideally be installed in frequently occupied areas such as kitchens and living rooms; and
- Allow owners to control peripherals of the SWH, such as the backup heater and circulation pump, by providing a timer or other control features.

## 2.5 Thermal analysis of solar collectors

The collectors' thermal efficiency is defined as the ratio of useful converted energy to the total incident radiation energy (both direct and diffuse) on the collector's aperture [39]. Extensive work has been put into improving efficiencies of solar collectors, now reaching up to 70% in appropriate conditions and technologies [40].

Most effort has been done on flat plate collectors (FPCs), due to their working simplicity and reliability. The performance of FPCs can be estimated by evaluating a set of parameters and collector characteristics, such as selective coatings, insulation, tilt angles and working fluids [40]. In theory, if assuming steady-state conditions, the useful heat energy delivered by a solar collector is equal to the total heat gain by the collector's thermal transfer fluid minus the heat losses to the surroundings. The heat gain,  $q_u$  by the transfer fluid can be calculated using the formula [11]:

$$q_u = \dot{m}_c c_p \Delta T_c = A_c [G_c \tau \alpha - U_L (T_p - T_a)] \quad (2)$$

Where:

- $\dot{m}_c$  is the instantaneous mass flow rate of the transfer fluid in contact with the collector (kg);
- $c_p$  is the specific heat of the fluid at constant pressure (J/kg.K);
- $\Delta T_c$  is the temperature difference between the collector outlet ( $T_{co}$ ) and the inlet temperature ( $T_{ci}$ ).
- $A_c$  is the collector's total aperture area ( $m^2$ );
- $G_c$  is the total incident solar energy (direct and diffuse) incident on the collector ( $W/m^2$ );
- $\tau\alpha$  is the absorber transmittance-absorptance product;
- $U_L$  is the heat transfer loss coefficient of the collector ( $W/m^2 \cdot ^\circ C$ );
- $T_p$  is the average (stagnation) temperature of the absorber/ plate ( $^\circ C$ );
- $T_a$  is the ambient temperature ( $^\circ C$ ).

Alternatively, the formula may include the collector's correction factor,  $F_R$ , which replaces the average plate temperature ( $T_p$ ) with the inlet fluid temperature ( $T_{ci}$ ). The correction factor is given to solar collectors and is defined as the heat removal factor of a collector, i.e., the ratio of the actual heat delivered to the fluid to that delivered if the collector's temperature was the same as the inlet fluid's temperature. The factor is dependent only on the collector's characteristics, the fluid characteristics, and its flow rate through the collector. Equation (2) will result into:

$$q_u = A_c F_R [G_c \tau\alpha - U_L (T_{ci} - T_a)] \quad (3)$$

Where, the ratio  $F_R$  may be calculated using the formula:

$$F_R = \frac{\dot{m}_c c_p}{A_c U_L} \left(1 - \exp\left[-\frac{U_L F' A_c}{\dot{m}_c c_p}\right]\right) \quad (4)$$

Where  $F'$  represents the collector efficiency factor, i.e., the ratio of the actual useful heat gain that would result if the absorber and the local fluid were at equal temperature.

## 2.6 Performance analysis of solar collectors

Testing the thermal performance of collectors is an essential step in every verification process of FPCs. The ASHRAE (American Society of Heating, Refrigerating and Air-Conditioning Engineers) Standard 93:1986 [41] is the method most often adhered to for testing the performance and calculating efficiency figures of the collectors. The aim is to evaluate the collectors at different testing conditions and combinations of input parameters including incident radiation, ambient temperature, inlet fluid temperature, and expected outlet fluid temperature. Such testing requires determining the incident radiant energy falling on the collector (both direct and diffuse) as well as the total energy gain by the fluid passing through the collector at steady or quasi-steady conditions. Additionally, tests to determine steady state thermal efficiency variances with the variation of sun and collector positions are also required. Performance tests of collectors should also include transient testing conditions, to study the behaviour of the collectors in unforeseen conditions. The standard requires no significant storage of hot water, neither gives requirements on what fluids to be utilised as thermal-transfer fluids (provided that only single-phase fluids are used). With such tests in place, the behaviour and expected performance of any FPC could be approximated for any location and under any weather conditions, provided that the parameters are known.

### 2.6.1 Collector thermal efficiency

In reality, the heat loss coefficient,  $U_L$  in Equation (3) is not a constant but varies depending on the ambient temperature,  $T_a$ , and the collector inlet temperature,  $T_i$ . Thus [11]:

$$F_R U_L = c_1 + c_2(T_{ci} - T_a) \quad (5)$$

Where  $c_1$  and  $c_2$  are collector thermal efficiency constants.

Applying Equation (5) into Equation (3) and rearranging, we get:

$$q_u = A_a F_R [G_c \tau_\alpha - c_1(T_{ci} - T_a) - c_2(T_{ci} - T_a)^2] \quad (6)$$

Where  $A_a$  is the absorber area ( $m^2$ ). For FPC,  $A_a \cong A_c$ .



Therefore, the efficiency of the FPC may be written as:

$$\eta_{FPC} = F_R \tau \alpha - c_1 \frac{(T_{ci} - T_a)}{G_t} - c_2 \frac{(T_{ci} - T_a)^2}{G_c} \quad (7)$$

Let  $c_0 = F_R \tau \alpha$  and  $x = \frac{(T_{ci} - T_a)}{G_c}$ , then:

$$\eta_{FPC} = c_0 - c_1 x - c_2 G_c x^2 \quad (8)$$

For low temperature collectors, the 2<sup>nd</sup> order terms are neglected, which results in having  $c_2 = 0$ . Thus, Equation (8) now plots a straight-line graph relation of efficiency vs the heat loss parameter,  $\frac{(T_{ci} - T_a)}{G_c}$ . The y-intercept is  $c_0 = F_R \tau \alpha (= \eta_0)$ , while the gradient of the line is equal to  $-c_1 = -F_R U_L$  (from Equation (5) and putting  $c_2 = 0$ ).

Thus, a collector's performance can be experimentally calculated by plotting a best-fit straight line having efficiency on the vertical axis, and  $\frac{(T_{ci} - T_a)}{G_c}$  on the horizontal axis, the latter being a series of data experimentally gathered for various temperatures at discrete solar conditions. The y-intercept will correlate to the maximum efficiency of the collector, which occurs early morning when the inlet fluid temperature equals the ambient temperature. On the other hand, the x-intercept represents conditions where the collector's efficiency is zero. Such conditions are met either whenever radiation levels are very low, or when the collector reaches a stagnation temperature, meaning inlet temperature of the fluid is so high, that heat losses match solar absorption, and the collector is unable to further deliver useful heat. Stagnation temperatures are typically reached only when no thermal transfer fluid flow is present through the collector.

Figure 2.9 is a graph comparing the efficiencies of various types of collectors at two irradiation levels,  $500\text{W}/\text{m}^2$  and  $1000\text{W}/\text{m}^2$ . In this case, five types of collectors are represented, being [11]:

- Flat Plate Collector (FPC);
- Advanced Flat Plate Collectors (AFP) - These collectors are structurally similar to FPCs, but have their risers ultrasonically welded to the absorbing plate, as well as having an electroplated chromium selective coating for enhanced performance;
- Compound Parabolic Collector/ Concentrator (CPC);

- Evacuated Tube Collector (ETC);
- Parabolic Trough Concentrator Collector (PTC) with East-West tracking.

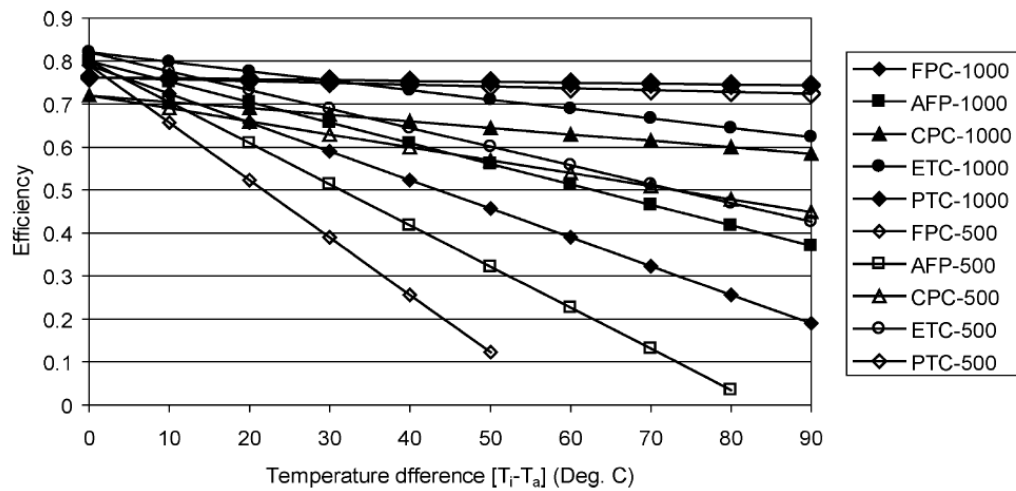


Figure 2.9: Comparison of efficiencies of various collectors, at irradiation levels of  $500\text{W/m}^2$  (hollow) and  $1000\text{W/m}^2$  (solid). In the case of PTCs, irradiation is considered as beam radiation [11].

As may be observed in the above figure, higher irradiation levels generally result in better performance (and efficiencies), even at higher inlet temperatures (larger  $T_{ci} - T_a$ ) for CPCs, ETCs and PTCs. It can also be observed that for concentrating collectors, namely PTCs and CPCs, the efficiency at high inlet fluid temperatures stays relatively high. The reason for this phenomenon is due to the relatively much smaller exposed aperture area of the absorber, compared to normal collectors such as the flat-plate collector, resulting in less heat losses to the surroundings.

The above equations cover all necessary collector design and operational parameters affecting steady-state performance, excluding solar incidence angle and flow rate. The latter naturally affects performance of a collector, through heat-removal factor principles. A too slow flow rate would generally result in an increased absorber temperature, directly increasing heat-losses to the surroundings. A fast flow rate thus generally improves performance of a collector as heat losses decrease. On the other hand, accounting for solar irradiance angle requires including the incidence angle modifiers for flat plate collectors [11].

### 2.6.2 FPC incidence angle modifier

For the previous equations, Equations (2-8), it was assumed that the solar irradiance is perpendicular to the plane of the FPCs. In the real world, this rarely occurs, and the sun is at an angle relative to the FPC, adversely affecting the performance of the collector. A fraction of the radiant solar energy is consequently reflected at the FPC glass cover interface, as a result reducing the absorber transmittance,  $\tau_\alpha$ . An incident angle modifier,  $k_{\tau\alpha}$ , is thus added and is defined as the ratio of  $\tau_\alpha$  at an incident angle  $\theta$ , to  $\tau_\alpha$  at normal to the plane of the FPC.  $k_{\tau\alpha}$  is expressed by [11]:

$$k_{\tau\alpha} = 1 - b_0 \left( \frac{1}{\cos(\theta)} - 1 \right) - b_1 \left( \frac{1}{\cos(\theta)} - 1 \right)^2 \quad (9)$$

Where  $b_0$  and  $b_1$  are angle modifier constants.

For a single glazed FPC,  $b_0 = -0.1$  and  $b_1 = 0$ , reducing to a single order equation. Thus, in such cases, Equation (9) can be rearranged to include the angle modifier [11]:

$$\eta = F_R(\tau\alpha)_n k_{\tau\alpha} - c_1 \frac{(T_{ci} - T_a)}{G_c} - c_2 \frac{(T_{ci} - T_a)^2}{G_c} \quad (10)$$

### 2.6.3 Collector time constant

The above-mentioned equations apply only whenever steady-state or quasi-steady-state conditions exist. Whenever transient conditions are present, the equations for the thermal performance do not apply as a portion of the absorbed solar energy is used to heat up the collector setup. An important consideration of collector testing is the determination of a time constant, which is a representation of the collector's heat capacity. This time constant will be the time response of a solar collector and is to be used to evaluate the transient behaviour of collectors, as well as to select the correct time intervals during quasi-/ steady efficiency testing. The time constant is defined as the time required for a fluid leaving the outlet of the collector to reach 63% of the final steady state value following a step change in incident radiation parameters. In other terms, the time constant is the time taken for the following relation to apply [11]:

$$\frac{T_{ot} - T_{ci}}{T_{oi} - T_{ci}} = \frac{1}{e} = 0.37 \quad (11)$$

Where:

- $T_{ot}$  is the collector outlet water temperature after time  $t$  ( $^{\circ}\text{C}$ );
- $T_{oi}$  is the collector's initial inlet water temperature following the step change ( $^{\circ}\text{C}$ );
- $T_{ci}$  is the collector's inlet water temperature ( $^{\circ}\text{C}$ ).

The test is performed according to the following procedure:

The collector is maintained at a steady-state condition, with inlet fluid collector temperature equal to the ambient temperature. The incident irradiance is then abruptly cut off (by shielding in the case of FPC or defocusing the beam in the case of concentrating collectors). Transfer fluid temperatures at the inlet and outlet are constantly monitored and the time taken for Equation (11) to be satisfied is noted [11].

## 2.7 Collector selection process

Sections 0 and 2.6 dealt with determining the performance of a solar collector. These methods allow for the possibility to make comparative testing of different collector types, to assure (or rate) their quality and identify the one mostly fit for a specific application. International Standard ISO (International Organization for Standardization) 9806:2017 (2017) [42] deals with testing conditions for collectors to determine their resistance to extreme operating conditions. The tests highlighted in the standard require several sequential tests in which sequence must be obeyed, such that degradation due to a specific test will be uncovered at some later stage. The tests mentioned in the standard are listed in Table 2.2 below:

Sequence	Test
1	Internal pressure
2	High temperature resistance
3	Exposure
4	External thermal shock
5	Internal thermal shock
6	Rain penetration
7	Freeze resistance
8	Internal pressure (re-test)
9	Thermal performance
10	Impact resistance
11	Final inspection

Table 2.2: Series of quality tests for solar collectors [42].

The final selection process for the type of collector should only be made after the energy requirements of an application are identified. Following that, a yearly (or more) energy output analysis of a complete system should be made, which includes parameters such as weather patterns and preliminary performance behaviours with different consumption patterns. The collector optimum fit for the application is the one that best matches the expected application load, with the optimum performance. One way of doing this is through studying the efficiency of the collector in terms of the heat loss parameter,  $\Delta T/G$ , similar to what is observed in Figure 2.10 below.

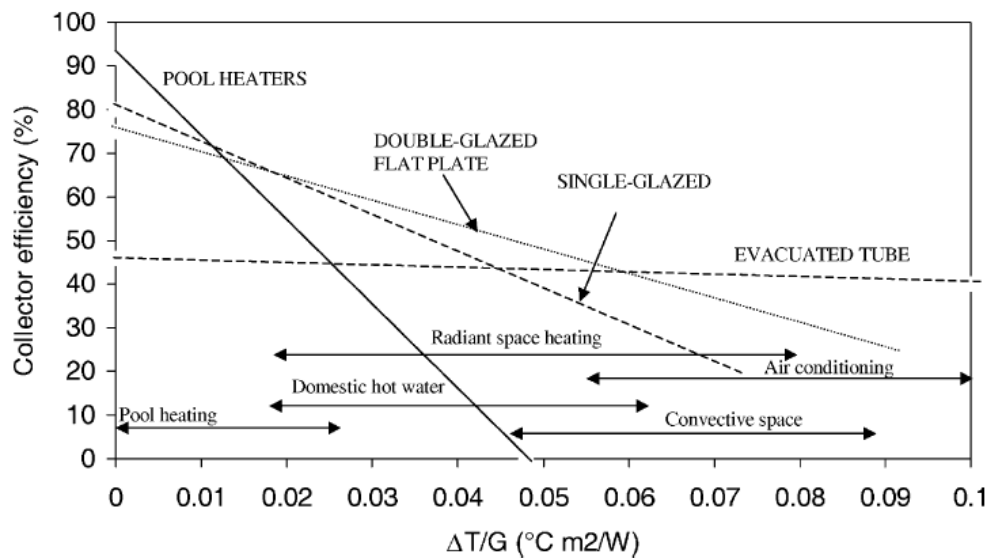


Figure 2.10: Efficiencies of various common liquid collectors and comparisons with various applications [11]

Such curves should only be used during preliminary phases, as they only illustrate the instantaneous behaviour of collectors. They exclude essential parameters such as incidence angles, cloud coverage effects on solar irradiance, system heat losses, and heat exchanger efficiencies. Thus, the final selection should be a product of years of performance cost-effectiveness analyses, and typically requires aid of specialised analysis tools such as *F-Chart* [43], TRNSYS (Transient Simulation) [44] and WATSUN [45] for annual performance of collectors.

### 2.7.1 Computer modelling and Performance Analysis Tools

Predicting performance of collectors and proper sizing of components is a complex task and requires both predictable and unpredictable parameters. Many techniques and

modelling software nowadays exist that can simulate and predict solar heating and cooling, according to specific applications and parameters. Using such aids can be advantageous, as they [11]:

- Eliminate the need to prototype;
- Provide a clearer layout of complex systems;
- Provide an understanding of how components interact with each other and the individual role in the overall system operation;
- Allow for the possibility to further optimise components;
- Give an estimate energy yield from the system;
- Give users the possibility of studying the behaviour of the system at different temperature variations;
- Give users the possibility of analysing the behaviour of the system at different design variables using the same weather conditions.

When designing solar thermal systems on computer modelling software, the system will always represent an imperfect copy of the real one. Opting for simplified analysers of systems have their own advantages, namely low cost, faster simulations, rapid computations, and ease of use. Such analysis is ideal for the initial design phases, i.e., for modelling, performance predictions and development.

### **2.7.2 Limitations of simulation**

Although as explained, simulations are advantageous and generally facilitate process design, they also bring some limitations. First and foremost, it is easy to make mistakes during the design stages, such as assuming or neglecting important parameters. One may require high levels of scientific knowledge to produce valuable simulation results.

Although the level of details that can be inputted in simulations software can be high to produce accurate results, some phenomena occurring in real life are difficult to predict. Simulations are ideal for predicting thermal performances of solar thermal systems but have their limitations when it comes to mechanical considerations. For example, unpredictable physical problems such as pipe breakages, leaks, clogs, scaling, failure of components, poor installation, poor installation, substandard controllers, etc. cannot be accounted for. Moreover, the performance of solar thermal systems depends heavily on the user behaviour and solar availability, as will be later discussed.

The ideal way to carry out performance tests of solar thermal systems is to have a combination of simulations and physical tests. This way, there is a better understanding of the overall system and the processes undergone, and any issues which are hidden in any of the scenarios may now be exposed and faced.

## 2.8 Performance analysis of Solar Water Heater (SWH) systems

Section 2.6 dealt with the performance analysis of just the solar collector. This section will review the methods to determine the overall system performance, which is affected by all components making up the SWH, including the storage tank insulative properties, the weather, the use of the backup heater (if available) and the water consumptions.

The ISO 9459-2 [46] international standard deals with the testing procedures for determining the performance of domestic SWHs (DSWHs) without a backup heater. An estimate annual performance of the SWH in any climatic or operating conditions may be then determined. This method is compatible with all types of solar water heating systems, including passive systems, active systems, and integrated collector-storage systems, provided that the solar storage capacity is less than 0.6m<sup>3</sup>. If operated with an automatic backup heater, the test procedures described in ISO 9459-3 are recommended, which quantify interaction between all energy inputs, including the backup heater. For systems with a manual backup heater, this should be kept off during the ISO 9459-2 performance testing.

### 2.8.1 Overall system Efficiency

In contrast to what is covered in Section 2.6.1, which considered the collectors' efficiency only, this section will go through the process of estimating the overall efficiency of a SHW system. Although dependent on each other, the two terms should not be interchanged. The overall system efficiency is a measure of how much of the total energy input is utilised, also taking into consideration the heat losses from the storage tank and any heat losses in the piping, as well as the use of backup electric heater (if applicable). The overall system efficiency,  $\eta_{\text{sys}}$ , of a SWH may be calculated using:

$$\eta_{\text{sys}} = \frac{\text{Output Energy}}{\text{Input Energy}} \times 100 = \frac{Q_{\text{demand}}}{Q_{\text{Elec}} + E_{\text{Solar}}} \times 100 \quad (12)$$

where:

- $Q_{\text{Demand}}$  is the total consumed heat energy (including that generated by means of electrical backup heaters);
- $Q_{\text{Elec}}$  is the electrical energy consumption of the overall system, namely the pumps (if any) and the backup heater (if any); and
- $E_{\text{Solar}}$  is the total solar irradiance incident on the collector.

### 2.8.2 Solar Energy Utilisation Factor (SEUF)

Unfortunately, values for the overall efficiency of a system do not really portray the capabilities of a SWH system, as values are very season specific and depend on the individual use of hot water, solar availability and use of backup electric heating. This often tends to confuse and alarm users, because the results often vary significantly from one day to another, with no easy interpretation of the values obtained. Typically, low results are associated with negative outcomes, while high results are associated with positive outcomes which often, is not the case. A term which may be more easily interpreted is the *Solar Energy Utilisation Factor*, SEUF, which may be defined as the ratio of the consumed heat energy provided by the SWH (solar means),  $Q_{\text{SWH}}$ , to the in-plane solar irradiance incident on the collector,  $E_{\text{Solar}}$  [24]:

$$\text{SEUF} = \frac{Q_{\text{SWH}}}{E_{\text{Solar}}} \times 100 = \frac{Q_{\text{Demand}} - Q_{\text{Elec}}}{E_{\text{Solar}}} \times 100 \quad (13)$$

To calculate any efficiency value of a SWH, including the SEUF value, a period of monitoring needs to be established. The efficiency of SWH will resemble that monitoring period. Thus, using this method, it would be easy to determine the efficiency of the SWH in different timeframes for comparative purposes, such that of seasonal differences, and water consumption changes.

The total heat energy demand,  $Q_{\text{Demand}}$  (Units: J), is equal to the sum of all instances of hot water consumption from the system:

$$Q_{\text{Demand}} = \sum \dot{m}_{\text{HW}} \cdot t \cdot c_p \cdot \Delta T \quad (14)$$



where:

- $\dot{m}_{HW}$  is the instantaneous mass flow rate at the hot water outlet (kg/s);
- $t$  is the total time per instance of detected water flow (s);
- $c_p$  is the specific heat capacity of water (J/kg. K); and
- $\Delta T$  is the difference between the outlet flow and the inlet flow temperatures (K).

For convenience, the value for  $Q_{Demand}$  will be then converted to kWh by the simple conversion:  $Q_{Demand}$  (Units: kWh) =  $3.6 \times 10^6 \cdot Q_{Demand}$  (Units: J).

$E_{Solar}$  and  $Q_{Elec}$  are calculated by also summing up all the instances of solar irradiance and electrical power, respectively, for the same monitoring period:

$$E_{Solar} = \sum G_c \cdot A_c \cdot t \text{ (Units: Wh)} \text{ and } Q_{Elec} = \sum P \cdot t \text{ (Units: Wh)}$$

### 2.8.3 Solar Fraction

The solar fraction (SF) is defined as the ratio of energy used provided by the solar thermal system to heat up the water to the total heat energy provided by all heating means, including the backup heating element. This value may be determined using the formula [24], [47]:

$$SF = \frac{Q_{SWH}}{Q_{Demand}} = \frac{Q_{Demand} - Q_{Elec}}{Q_{Demand}} = 1 - \frac{Q_{Elec}}{Q_{Demand}} \quad (15)$$

### 2.8.4 Surplus Hot Water Fraction

The *Surplus Hot Water Fraction* was added at the later stages of development and gives users indication of how much excess hot water is available for immediate consumption based on a period's SWH efficiency. The *Surplus Hot Water Fraction* for a specified period may be determined using the equation:

$$\begin{aligned} \text{Surplus Hot Water Fraction} &= \frac{\eta_{sys}/100 \times E_{solar}}{Q_{SWH}} \\ &= \frac{\eta_{sys}/100 \times E_{solar}}{Q_{Demand} - Q_{Elec}} \end{aligned} \quad (16)$$

The term may be helpful in determining whether the installed system is undersized; whether the consumption patterns are not ideal; or whether the backup heater is unnecessarily being used (or the combination of the latter two). A value above 1 indicates that a surplus of hot water is being generated by the SWH system over the consumed amount, which may be the result of overusing the backup heater or simply not utilising the SWH to its full potential. A value approximately equal to 1 is ideal and indicates that all hot water generated by the sun's radiative energy and the backup heater was effectively utilised. A consistent value below 1 is suggestive that the system may be undersized.

Now that the requirements for a monitoring system have been understood, and the performance analysis tools of a SWH have been reviewed, the next step would be to design a SWH monitoring system which incorporates these monitoring techniques into a capable, compact, versatile device. Chapter 3 will dive into the methods employed to create a prototype monitoring and controlling system, and the experimentation setup designed to put the device to the test.

## Chapter 3 Methodology

### 3.1 Monitoring Parameters

In order to define the most important parameters that need to be included in the thermal energy meter being developed, an overview of both ASHRAE Standard 93:1986 and ISO 9459-2:1995 standard for testing the performance of solar collectors and overall SWH performance was carried out. However, it was found that these standards are primarily designed to characterise the performance rather than monitor the performance of the SWH during everyday use. Therefore, the only useful part of these standards for the purpose of this dissertation is to extract the most important performance parameters that need to be monitored, rather than carrying out characterisation tests for the solar heater, which ultimately is not the scope of this project.

Moreover, the data to be monitored by the thermal energy meter needs to be only the essential figures that determine the energy savings from the SWH and a few other readings that provide essential information to enable the optimisation of the SWH system, such as the stored hot water temperature. Following careful analysis, it was deemed necessary to monitor the following parameters:

#### Primary monitoring parameters:

- 1)  $T_o$ , hot water outlet temperature ( $^{\circ}\text{C}$ );
- 2)  $Q_o$ , hot water outlet flowrate (L/min) – alternatively, one could monitor the cold-water inlet flowrate,  $Q_i$ ;

#### Optional monitoring parameters:

- 3)  $T_s$ , SWH storage tank temperature ( $^{\circ}\text{C}$ );
- 4)  $T_i$ , cold water inlet temperature ( $^{\circ}\text{C}$ ) – else taken as the yearly average;
- 5)  $G_{\text{coll}}$ , Instantaneous global solar irradiance on the collector ( $\text{W}/\text{m}^2$ );
- 6)  $Q_i$ , cold water inlet flow (L/min) – or instead,  $Q_o$ ;
- 7)  $W_a$ , Power rating of the backup heater (kW);
  - a.  $V_a$ , outlet voltage (V);
  - b.  $I_a$ , current drawn by the heater.

Monitoring just the two primary parameters ( $T_o$  and  $Q_o$ ), it is possible to sufficiently monitor most conventional SWHs. In such case, the monitoring device would serve as a thermal energy meter for the hot-water consumptions. However ideally, the monitoring system should monitor all parameters for complete, detailed, and accurate performance analyses. From these parameters, it would be possible to calculate the energy savings (in kWh), as well as other secondary parameters such as hot water consumption, electricity consumption and equivalent CO<sub>2</sub> savings.

Other requirements for the monitoring device are that data-logging of the system should be totally autonomous and monitored parameter values should be easily determined through the device itself or through another device at a remote location (such as a smartphone). Further, report generation on SWH performance should be straightforward and immediate. Ideally, the monitoring setup would require no permanent installations, and sensor installations should be non-destructive on the solar heating setup, meaning no permanent modifications should be done on the solar thermal system (excluding external pipework). Installation of device shall be straight-forward and non-complicated, able to be performed by the typical user with general understanding of electrical components and plumbing. Finally, the monitoring system shall be universal, meaning it should be compatible with all the standard types of solar heating systems.

### **3.2 Hardware and software configurations**

Multiple sensors and modules installed on the systems will all feed signals to a central microcontroller which interprets the signals and translates them to standardised recognisable values. The microcontroller will be capable of automatically distinguishing the installed sensors and modules and depending on the combination connected, will allow specific monitoring tasks and controls. The microcontroller will be a network supported device, based on IoT (Internet of Things), and hence will require a stable Wi-Fi connection to upload (and download) the monitored data. By default, the microcontroller will be configured to generate a UI accessed through the local network, which enables users to monitor and control their SWH in real-time. History performance analysis of the SWH should be allowed through the same UI, also allowing for custom-period performance analysis. Additionally, the UI shall give users a degree of control on their system, including managing the power of the backup heater, and calibrating parameters.

The development stages of the monitoring device are illustrated in Figure 3.1. The two sections dealt with during development are the hardware and the firmware/ software.

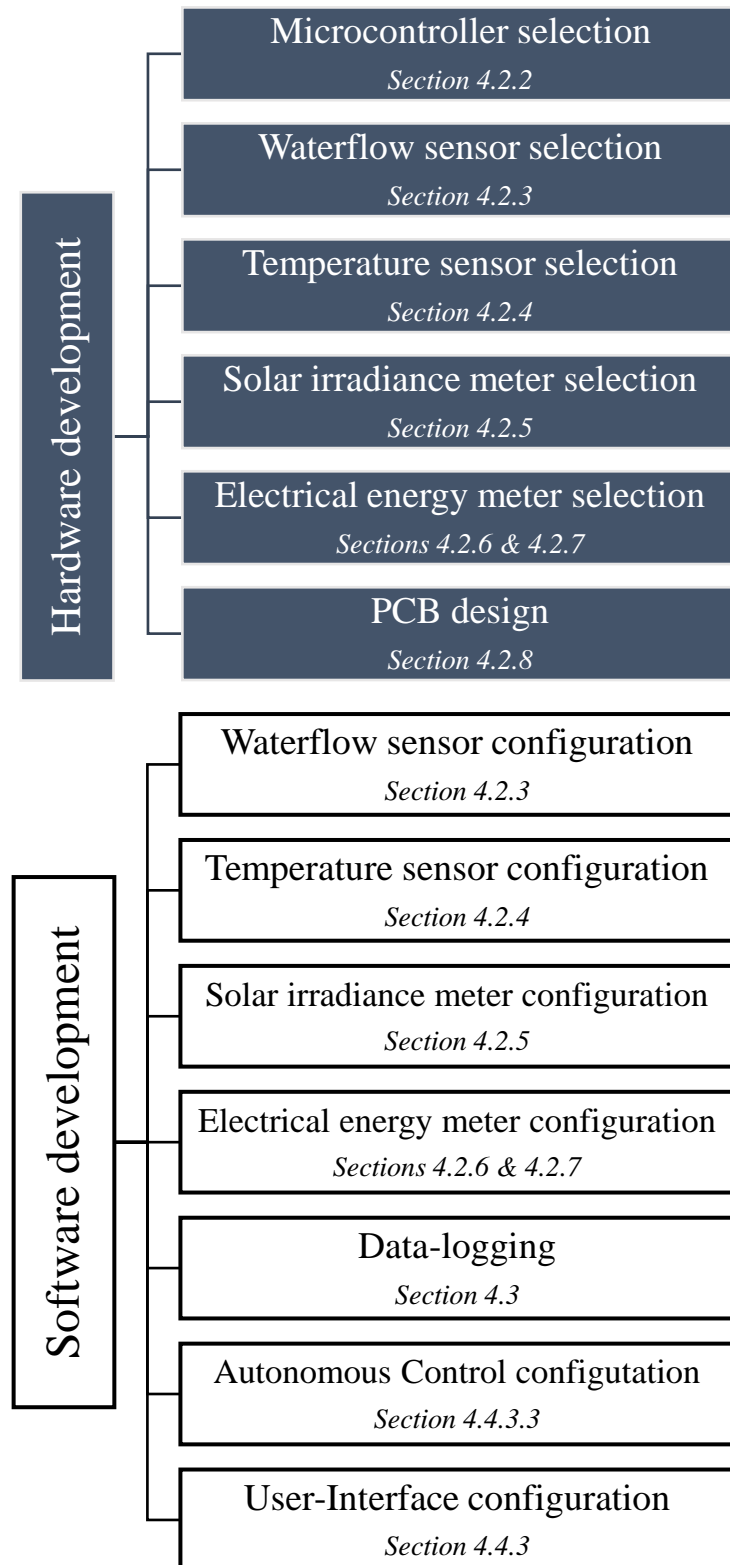


Figure 3.1: The hardware and software development stages for the SWH monitoring device.

All parameters mentioned in Section 3.1 will be monitored, excluding the outlet waterflow  $Q_o$ , as water consumption measurements will be taken from the inlet waterflow sensor,  $Q_i$ . The advantage of using the cold-water side is that the sensor will not be subjected to high water temperatures, thus reducing the chance of damage, and making it possible to opt for cheaper waterflow sensors.

The schematic representing data flows between the monitoring system hardware and the SWH are illustrated in Figure 3.2.

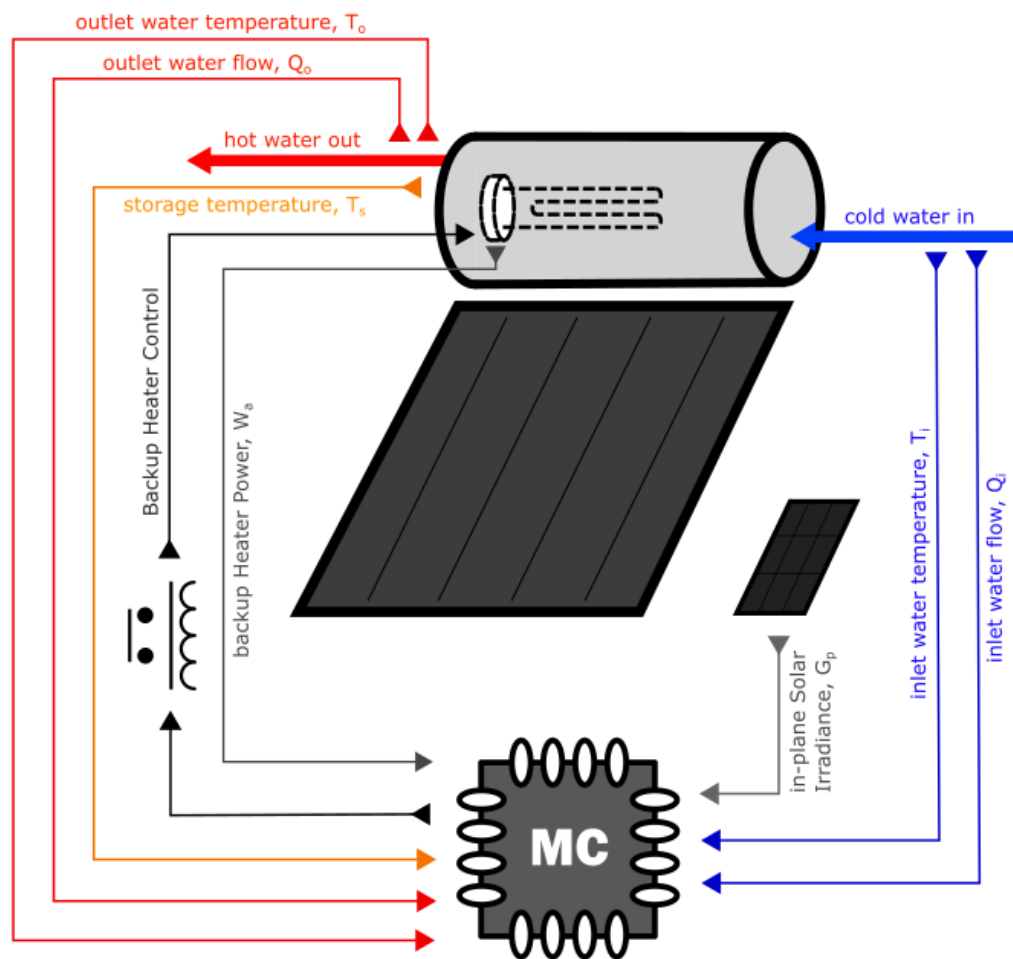


Figure 3.2: Monitoring system schematic for a common collector-storage type SWH. Dataflows through and from the microcontroller are also shown.

### 3.2.1 Solar Thermal Water Heater

For this study, a brand-new integrated collector-storage thermosyphon FPC type SWH with the following specifications (Table 3.1) was used:

Table 3.1: Specifications of the thermosyphon flat-plate solar heating system.

Description	Value
<b>Manufacturer</b>	COSMOSOLAR
<b>Model code</b>	MNE 16
<b>Circulation type</b>	Passive system (Thermosyphon)
<b>Collector type</b>	Flat plate (FPC)
<b>Heat transfer type</b>	Heat Exchanger with glycol mixture transfer fluid
<b>Transfer fluid volume</b>	1.2L
<b>Collector area</b>	1.55m <sup>2</sup> gross, 1.5m <sup>2</sup> aperture
<b>Stagnation temperature</b> (on paper)	127°C @ 1000W/m <sup>2</sup> , 30°C ambient temperature
<b>Backup heater rating</b>	2.3kW
<b>Water storage capacity</b>	150L
<b>Collector inclination angle</b>	45°
<b>Collector azimuth angle</b>	180° (South facing)
<b>Installed location</b>	Institute for Sustainable Energy, Marsaxlokk (MT)

The SWH has a 150-litre capacity, which would be sufficient for the washing needs of a family of four [48].

Depending on the need for solar heating, the angle of tilt of the collector should be the same as the latitude of the site  $\pm 15^\circ$ . Being located at a latitude of  $36^\circ$ , Malta experiences a wide range of sun elevations [48], [49] however, if opting for a fixed angle panel structure, which is the simplest and hence most common option, the ideal angle would be one which favours more the winter season (due to increased demand for hot water). For this reason, the tilt angle of the solar collector was kept at  $45^\circ$ , South-facing, throughout the entire testing phase, which is the prevailing setting for all domestic solar heating systems in Malta.

The inlet of the storage was connected directly to the water supply through a programmable watering timer for controlled draw-offs, to enable the simulation of showers autonomously. The outlet hot water valve was kept open and thus, flow in and out of the storage tank was controlled solely by the watering timer. Maximum flowrate possible through the system using this setup was measured to be around 6L/min.

The thermostat of the inbuilt backup heater was set at 55°C which although theoretically should never be triggered due to additional control (refer to Section 3.4.3.3), served as a safety limiter in case of controller malfunction.

Despite opting for a FPC SWH for this study, the controller shall also be compatible with all other solar collector types (ETCs, PTCs, AFPCs and CPCs – refer to Section 2.6) requiring minimal changes in the configuration and installation procedure. However, due to the FPCs increasing popularity and simplicity, the monitoring device shall be initially configured for FPCs.

### 3.2.2 Microcontroller

For this project, the microcontroller chosen was the *WiFi Kit 32 Module* by *Heltec Automation* [50], which incorporates the *ESP32* master chip by *Espressif Systems* [51]. The module, depicted in Figure 3.3, houses an onboard 0.96" OLED (Organic Light-Emitting Diode) display which will be useful for displaying key information such as Wi-Fi credentials and real-time updated parameters.

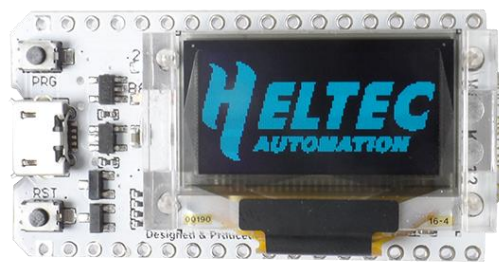


Figure 3.3: Heltec Automation WiFi Kit 32 module [51].

Before opting for the *Heltec* module, the *D1 Mini ESP32* by *AZ-Delivery* [52] was first considered. However, after many frequent brownout failures (type of power failures) and a poor Wi-Fi behaviour, the microcontroller was later changed to the *Heltec*.



The microcontroller was programmed in C++ language on the open-source platform of Arduino IDE (integrated development environment). Software development was initially done on the *ESP8266* due to unavailability reasons, but then was switched to the more advanced *ESP32*, which is the successor of the *ESP8266*. The *ESP32*, compared to the *ESP8266*, offers more GPIO (General Purpose Input/ Output) pins, has faster processing speeds, and provides more usable internal storage than the latter. Apart from being powerful, low-cost and low-power consuming, the microcontroller also contains an integrated Wi-Fi module which makes it ideal for IoT (Internet of Things) applications [51]. The specifications and the pinout diagram of the microcontroller module are provided in Table 3.2 and Figure 3.4 respectively below:

Table 3.2: Heltec ESP32 WiFi kit module specifications [50].

Description	Value
<b>Power supply input range</b>	3.3 – 5 Vdc
<b>GPIO pins voltage range</b>	0 – 3.3 Vdc
<b>SoC (System on a Chip)</b>	ESP32-WROOM-32
<b>Clock speed</b>	80MHz/ 240MHz
<b>External flash memory</b>	4MB
<b>Input/ output pins (GPIO)</b>	34
<b>Analog input pins (ADC channels)</b>	18 (only 8 pins usable if Wi-Fi is used)
<b>Max current per GPIO pin</b>	40mA
<b>Wi-Fi protocol</b>	802.11 b/g/n
<b>Dimensions</b>	39 × 28 × 6mm
<b>Cost</b>	< €10 /pc

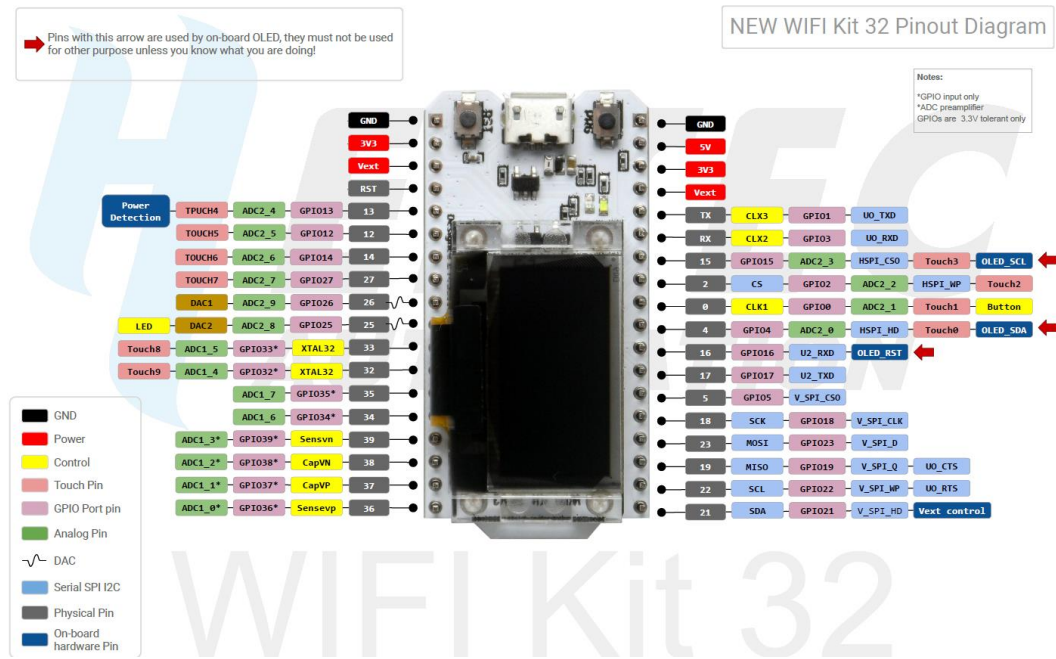


Figure 3.4: Heltec ESP32 WiFi kit module pinout diagram [50].

The GPIO pins function as communication lines between the sensors/ modules and the microprocessor. Each sensor/ module will be allocated to a unique GPIO pin, which depending on the function, will feed in signals (input) to the microprocessor, or signal out (output) a command to an external module. The inputs and outputs for this specific project and their allocated GPIO pin are listed in Table 3.3 below:

Table 3.3: Pin allocation of sensors and modules

Description	Input/ Output	Data Pin
Relay	Digital Output	GPIO33
Voltage transformer module	Analog Input	GPIO32
Current transformer module	Analog Input	GPIO34 + GPIO39
Inlet water flow sensor	Digital Input	GPIO19
Outlet water flow sensor	Digital Input	GPIO23
Solar irradiance (PV module)	Analog Input	GPIO35
Storage tank temperature sensor	Digital Input	GPIO18
Inlet flow temperature sensor	Digital Input	GPIO18
Outlet flow temperature sensor	Digital Input	GPIO18

### **Note on the integrated ADC (Analog-to-Digital Converter) pins of ESP32s.**

Unfortunately, the *ESP32*'s built in ADCs are non-linear and deliver readings with accuracies in the range of  $\pm 10\%$  if left uncalibrated. Although not a major issue for this project, improvements can be made to obtain the better readings from the monitoring device. Thus, a calibration method called `getVcal()` was created and added to all analogue type inputs to adjust for inaccuracies. The method simply passes raw ADC values through a polynomial equation obtained through experimentation and returns corrected values with an expected accuracy of  $\pm 1.5\%$ . The polynomial equation is unique to every microcontroller brand, and hence can be integrated in the coding. However, another constant, called `Vref`, which also is part of the calibration, is unique to every microprocessor (due to slight manufacturing inconsistencies). Thus, the value for `Vref` is automatically calculated during device bootup and is made use of by the `getVcal()` method. The `getVcal()` method is given below:

```
double getVcal(byte pin){
    double reading = analogRead(pin);
    double adjusted = ((reading/4095) * 3.3 * Vref);
    return -0.066109155 * pow(adjusted,2) + 1.240930493 * adjusted;
}
```

The correction polynomial equation,  $y = -0.066109155x^2 + 1.240930493x$ , was obtained by varying the input voltage on a microcontroller ADC pin, starting from 0Vdc up to 3.3Vdc, while noting down the output on the serial monitor. The Excel LINEST function was then used to determine the coefficients of the polynomial fit.

### **3.2.3 Water Flowmeters**

The hall-effect type waterflow sensor is a simple, low-cost and accurate flow sensor. The sensor comprises of a (typically) plastic body which serves as a path for water, a rotor with a magnet on one side, and a hall-effect sensor. The rotor rotates with speeds proportional to the water velocity flowing through the body, which induces a pulse signal by the magnet on the hall-effect sensor. The hall-effect sensor may then be interfaced with microcontrollers, which through a counter, will be able to compute the flow of the fluid inside the flowmeter [53]. An example of a hall-effect waterflow sensor and the one utilised in this project is the *YFS-201* [54]. The sensor specifications are provided in Table 3.4 below.

Table 3.4: *YFS-201* Hall Type Flow Sensor specifications

Description	Value
Power supply range	5 – 18Vdc
Flow rate reading range	1 – 30L/min
Accepted temperature range	–25 – +80°C
Accuracy	±10%
Number of pins	3 (voltage in pin, ground pin, data pin)
Maximum water pressure	20 bar / 2MPa
Maximum current draw	15mA (at 5V operating voltage)
Output type	Digital
Cost/ sensor	< €10

The sensor is compatible with most common microcontrollers due to its simple working principle and offers fairly accurate readings for a wide range of working flow rates. One drawback of such sensor is the requirement for it to be installed inline, meaning minor modifications on the pre-installed pipework are required. However, the instalment of the water sensor is very simple, and requires only a single cut, to which a push-fit assembly would fit.

The other option for monitoring flow would be to use ultrasonic flow sensors, but their drawback is that their price is much higher than the hall-effect flow sensor, which would defeat the whole scope of manufacturing a low-cost thermal energy meter.

### **Software configuration**

Waterflow readings are taken at one second intervals, by counting the number of pulses induced by the waterflow sensor in a second and computing the corresponding instantaneous waterflow in L/min. By means of an internal timer (`millis()`), the monitoring device compensates for possible delays obtained during the execution of the counting loop. The procedure to count for the number of pulses is performed through *interrupts*, which prioritises the detection and counting of pulses over other processes, so that no pulses are missed. Since the interrupts will be used solely for counting purposes, and hence require very short execution times, program execution flow will be unaffected.

The interrupt process takes the following format:

```
attachInterrupt(digitalPinToInterrupt(pin), ISR, mode)
```

The `pin` is the allocated GPIO number for the water flow sensors, in this case 19 and 23, for the inlet and outlet flow sensors, respectively. The `ISR` (Interrupt Service Routine) is the function to call whenever an interrupt occurs, in this case the function is used to increment the pulse counter. Finally, the `mode` describes what type of interrupt is expected, set to *FALLING*, meaning an interrupt is triggered when the pin goes from *HIGH* to *LOW*.

Since density of water varies slightly with temperature, a function to compensate for the variation is included in waterflow computations to obtain more accurate measurements. This is done by reading the temperatures of the inlet and outlet water flows and comparing the values with a temperature - density table obtained from literature [55].

In order to allow for further fine-tuning calibrations by the user, a factor, `water_CF`, is added, which can be updated from the UI.

Further to instantaneous flows, the monitoring device keeps track of the cumulative water consumptions which are used for thermal energy consumption calculations. Instantaneous waterflow readings and cumulative water consumptions are presented on the inbuilt display and on the UI in L/min and m<sup>3</sup>, respectively.

### 3.2.4 Temperature Sensors

The temperature sensors chosen for this project are the type *DS18B20* Digital Temperature Sensors by *Maxim Integrated* [56]. These high-precision and low-cost sensors are advantageous over the common resistive-type counterparts. Firstly, multiple sensors may be hooked up to the same data bus (GPIO data pin) due to a unique 64-bit serial address stored in an onboard ROM (Read Only Memory) for each sensor, thus preserving GPIO pins. Secondly, the precise readings over a wide range of temperatures makes it ideal for this application. Finally, the sensors require no additional components to function and can be powered using the same power-line provided by the microcontroller [56]. The specifications of the sensor are listed in Table 3.5 below:

Table 3.5: *DS18B20* temperature sensors specifications [56]

Description	Value
Power supply range	3.0V to 5.5V
Temperature reading range	-5°C to +125°C
Accuracy	±0.5°C
Resolution	User-definable from 9-bit up to 12-bit
Number of pins	3 (supply pin, ground pin, data pin)
Standby current draw	750nA
Active current draw	1mA (at 5V operating voltage)
IC output type	Digital
Cost/ sensor	<€5

### **Software configuration**

The software is configured to automatically detect the number of temperature sensors hooked up to the monitoring system and assigns them in the order of: Outlet Temperature; Storage Tank Temperature; and Inlet Temperature. Thus, if just two sensors are hooked up, only the outlet and storage water temperatures are monitored, whilst the inlet temperature is taken as the average yearly water temperature of the area of installation. If only one temperature sensor is hooked up, it will be assigned to the outlet temperature, and the *autonomous control* feature is purposely disabled for safety reasons (without the storage temperature, the monitoring device would be unable to control the backup heater). In such cases, electricity consumptions for the backup heater are not monitored, and the backup heater cannot be controlled by the monitoring device but only by the inbuilt thermostat. Other functions of the monitoring system would still work as intended, such as solar system performance monitoring, and monitoring of consumptions. If no sensors are attached, an error is displayed to the user during device initialisation (displayed on the inbuilt screen).

Temperature readings are done at 10-second intervals, which was determined experimentally and is approximately equal to the time it takes for the temperature probe to adjust to the surrounding fluid. Thus, more frequent temperature readings are unnecessary. Since temperature readings are of digital type and hence not affected by

the inaccuracies of the ADC channels, measurements are expected to carry the same accuracy as specified by the manufacturer, being  $\pm 0.5^\circ\text{C}$ .

Readings are done through a function from a preconfigured library (file written in C/C++ which the firmware can refer to for specific functions), and shall take the following format:

```
float temp = temp_sensors.getTempC(deviceAddress);
```

The only variables that the function requires are the GPIO number (being `temp_sensors / GPIO18`), and the temperature sensor's 64-bit address, which is determined automatically during boot-up of the monitoring device.

Temperature readings are presented on the inbuilt display and on the UI in  $^\circ\text{C}$ .

### 3.2.5 Solar Irradiance Meter (Photovoltaic panel)

Using a high grade pyranometer would defy the scope of producing a low-cost thermal monitoring device due to their high costs. Thus, for solar irradiation measurements, a generic polycrystalline PV (photovoltaic) panel was used, which is low-cost and readily available. The panel specifications were obtained experimentally and are listed in Table 3.6 below:

Table 3.6: Generic PV panel specifications.

Description	Value
Aperture area	110mm × 60mm
Rated wattage (at STC)	1W
$V_{OC}$ (Open circuit voltage)	6V
$I_{SC}$ (Short circuit current)	167mA
Cost/ panel	< €4

A custom-made solar PV panel frame was designed and 3D-printed (refer to Figure 3.5) for waterproofing purposes, which also held the panel at a  $45^\circ$  tilt for solar irradiation exposures identical to that of the solar thermal collector. The 3D printed material of choice was that of PET-G (Glycol modified Polyethylene Terephthalate), which is a durable, warp-resistance plastic able to withstand harsh weather conditions.



Figure 3.5: 3D rendering of the solar panel fixture to be installed for irradiance monitoring.

Since the microcontroller's analogue to digital converter (ADC) accepts voltages in the range of 0 – 3.3Vdc, an additional circuit which limits voltage to the accepted range had to be designed. Unfortunately, monitoring the solar PV's open circuit voltage by a simple voltage divider was not possible, due to the photovoltaics IV characteristics. For all photovoltaics, the short circuit current varies linearly with a change in solar irradiance. On the other hand, the open circuit voltage remains fairly constant with changes in solar irradiance, making monitoring using open circuit voltages impractical. Thus, converting the short circuit current to voltages was necessary to calculate the in-plane solar irradiance.

This was made possible by coupling a shunt (small resistance) in series to the solar PV panel. The voltage drop across the shunt was monitored by the microcontroller which represented the short-circuit current of the PV module (linear behaviour to the solar irradiance). To choose the appropriate shunt resistance value, the following procedure was followed:

The panel was hooked up to a variable load in a shorted circuit, starting from  $0\Omega$ , according to the schematic shown in Figure 3.6:



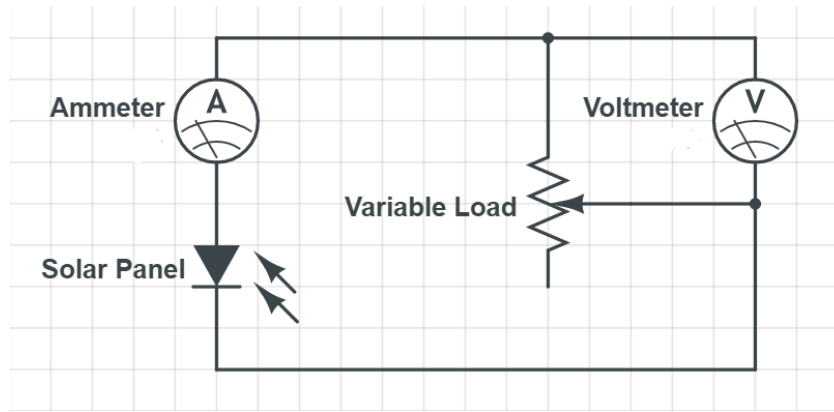


Figure 3.6: Circuit schematic for obtaining the IV curve of the panel.

The variable load had a maximum resistance of  $20\Omega$  and was varied using a knob. Starting from the lowest possible value, being  $0\Omega$  (short circuit), the resistance was increased in small increments, each time recording values of the current flow (though an ammeter hooked up in series) and voltage drop across the resistance (through a voltmeter hooked up in parallel to the resistance). The resistance value was also noted at each increment by measuring the resistance using the Ohmmeter function of a multimeter. Larger resistance increments were made as soon as the current flow was noted to decrease significantly. Once all data was gathered, the IV characteristics curve of this specific configuration of PV module could be plotted (Figure 3.7) and the resistance at the required voltage range was noted.

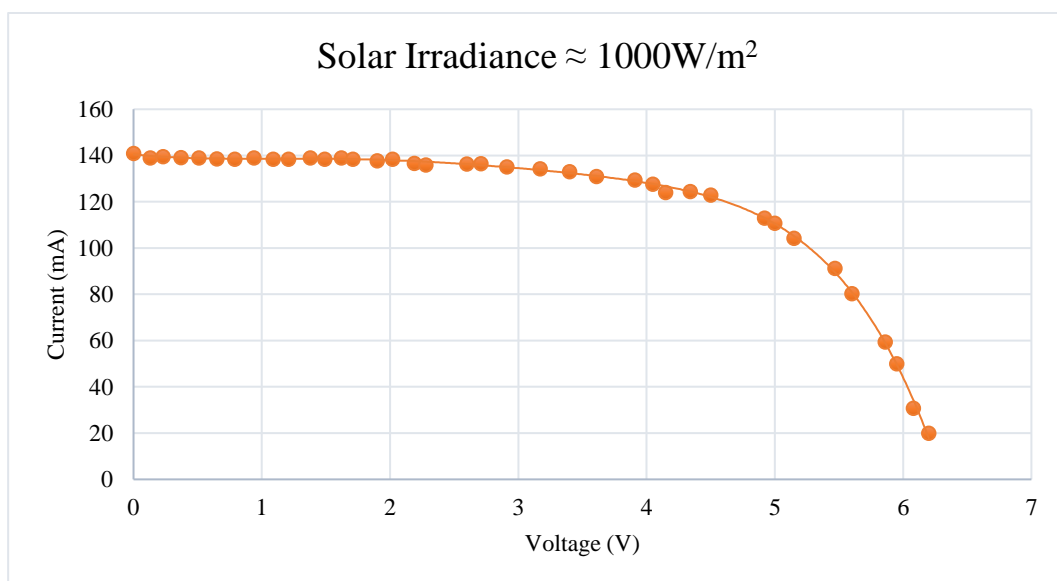


Figure 3.7: IV curve of a generic PV panel at global solar irradiance levels of  $\sim 1000\text{W/m}^2$ .

For a 3.3Vdc maximum input voltage at  $\sim 1000\text{W}/\text{m}^2$  solar irradiance, a  $23.7\Omega$  shunt resistance should be used however, for this project, a  $15\Omega$  resistance was instead used, which gives a potential difference of  $\sim 2.0\text{Vdc}$  across the resistor at  $1000\text{W}/\text{m}^2$  of solar irradiance. A lower than rated resistance value was deliberately chosen to protect for the microcontroller from unplanned overvoltage which may cause damages to the microcontroller. Further, a  $10\text{k}\Omega$  resistor was hooked up in series to the GPIO35 for blocking current flow through the pin, which serves as further protection to the microcontroller. Figure 3.8 illustrates the schematic of the solar irradiance meter setup utilised in the monitoring device.

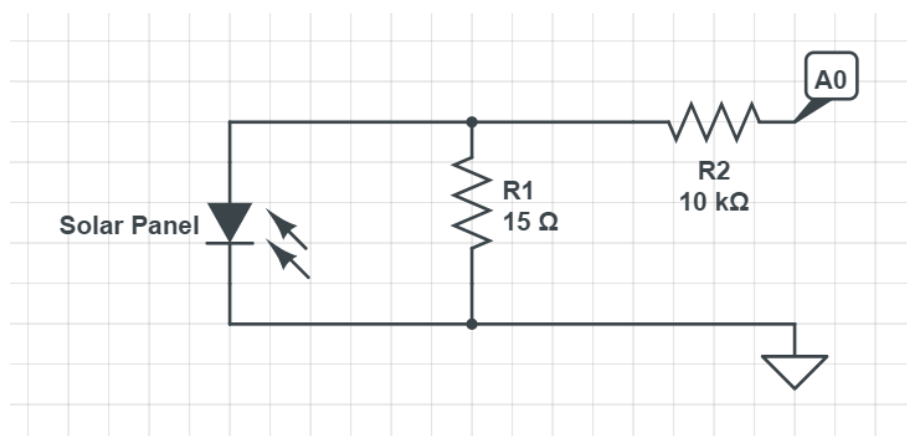


Figure 3.8: Solar Irradiance meter schematic

### **Software configuration**

Solar intensities are automatically measured every 30 seconds using the `analogRead(pin)` function. Experimental results have shown that 30-second intervals are enough to track variations in solar irradiance such as due to passing clouds. At each interval, the microcontroller averages out 100 sample readings, executed in less than 0.2s which filters out any noise and increases accuracy. The procedure to calculate solar irradiance is as follows:

```
int currentSolar_avg = 0;
for (uint8_t i = 1; i < 100; i++)
{
    float currentSolar = getVcal(solarpanel);
    currentSolar_avg = (currentSolar_avg * (i-1) + currentSolar) / i;
    delay(1);
}
currentSolar_avg = map(currentSolar_avg, 0.0, 3.3, 0, 1023);
solar_power = solar_calib * solar_CF * currentSolar_avg;
```

A moving average method is used to obtain the average, which has shown to provide better smoothing results compared to other averaging methods.

The solar irradiance meter was calibrated against a lab-grade certified global pyranometer provided by the Institute for Sustainable Energy. Both irradiance meters were tilted at the  $45^\circ$  to replicate the tilt of the installed SWH system, as depicted in Figure 3.9. A calibration factor, termed Solar Correction Factor, was determined for a clear day, and utilised in the code. Additionally, a calibration factor, `solar_CF`, is added, which provides a means for calibrating solar irradiance values from the UI. Readings below  $10\text{W}/\text{m}^2$  are neglected, as these are considered as noise or artificial light sources.



Figure 3.9: Solar Irradiance calibration setup

Using a user configured collector panel area, the device also computes the cumulative solar irradiance falling on the collector. Solar intensity readings and cumulative solar irradiance falling on the collector are displayed on the inbuilt display and on the UI in  $\text{W}/\text{m}^2$  and kWh, respectively.

### 3.2.6 AC voltage sensor

The *ZMPT101B* [57] voltage transformer module was chosen for this project to measure mains input AC voltage, namely for power consumption measurements of the backup heater. The module can measure up to 250Vac, for both 50Hz and 60Hz supplies. The voltage waveform will be converted to RMS (Root Mean Square) value in software configuration before energy consumption calculations could be performed. The transformer specifications are provided in Table 3.7 below:

Table 3.7: ZMPT101B Voltage transformer specifications [57]

Description	Value
<b>Input measurement range</b>	0 – 250Vac
<b>Rated output</b>	0 – 5Vdc
<b>Accuracy</b>	1%
<b>Number of pins</b>	4 (supply pin, data pin, GND pin, GND pin)
<b>Active current draw</b>	2mA
<b>Response time</b>	< 16ms
<b>Cost/ sensor</b>	< €10

#### Software configuration

The voltage transformer outputs an analogue signal, in the range of 0 – 5Vdc. A simple voltage divider limits the voltage to 3.3Vdc, which is the maximum input rated voltage for the microcontroller data pin.

For voltage readings, procedure to calculate the RMS voltage was utilised. A total of 500 samples are taken at each voltage calculation, with a 500 $\mu$ s delay in-between each sample. The code below is executed every 90 seconds and takes less than 0.5s to return a voltage reading.

```

for ( int i = 0; i < 500; i++ )
{
    float rawVoltage = getVcal(voltage_sensor);;
    voltageSampleRead = rawVoltage- 1.48;
    voltageSampleSum = voltageSampleSum + sq(voltageSampleRead) ;
    voltageSampleCount ++;
    delayMicroseconds(500);
}
voltageMean = voltageSampleSum/voltageSampleCount;
RMSVoltageMean = sqrt(voltageMean);
RMSvoltage = ((RMSVoltageMean) * VperVoltValue)- VmanualOffset;

```

The 500 samples readings at 500 $\mu$ s delays method was obtained experimentally using the following method:

First, the mid-value of the AC transformer module was found by trial-and-error, by slightly varying the value until an equal peak amplitude waveform was observed, as shown in Figure 3.10 (b) (initial waveform shown in Figure 3.10 (a) ). In this case, the mid-value was found to be 1.48V.

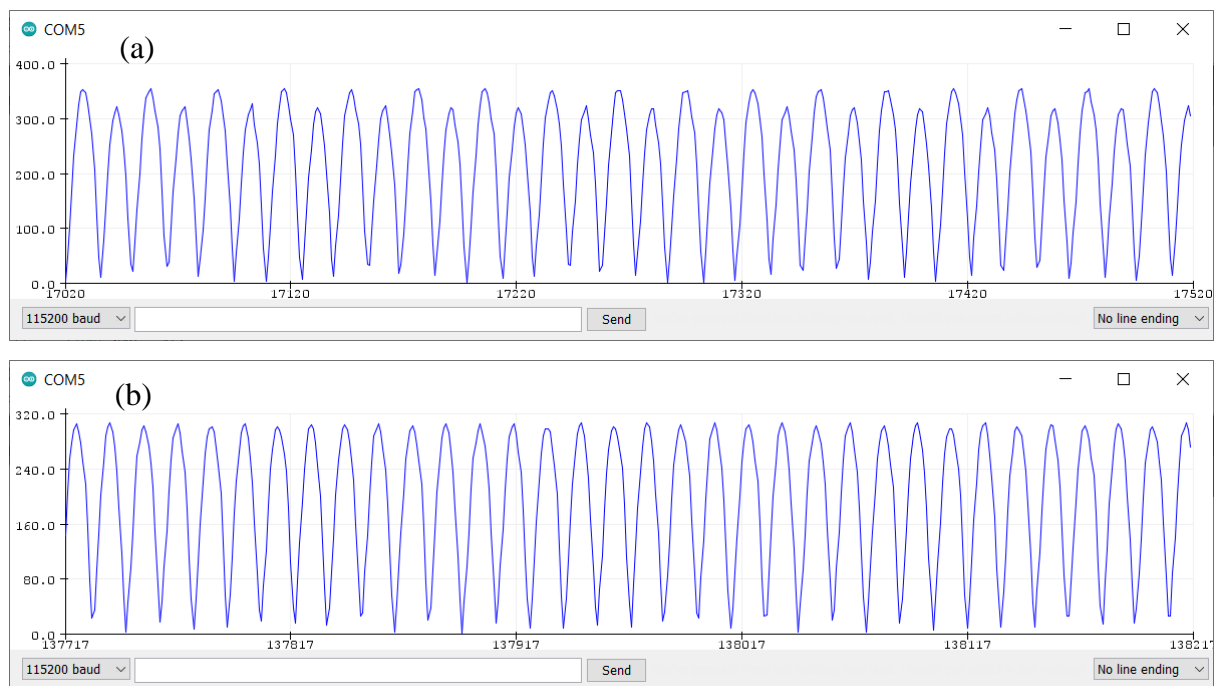


Figure 3.10: Raw waveforms from the AC voltage module for a (a) incorrect mid-value and (b) correct mid-value.

Then, to translate to RMS voltages, the sample number and the delay (in microseconds) were changed until a stable output was obtained. Figure 3.11 (a) is the output when too few samples are taken, resulting in very noisy and unstable signals, which would provide inaccurate voltage readings. Figure 3.11 (b) is the signal obtained when many samples

are taken, but without adding delay, which although produces fairly accurate readings, is a slow and processor intensive process. Stable readings with fast execution speeds were obtained when adding very small delays (in  $\mu\text{s}$ ) in-between readings. Figure 3.11 (c) is the signal obtained for a 500-sample reading with a  $500\mu\text{s}$  delay in-between readings, which is the chosen configuration for Voltage readings. Accuracies of  $\pm 1\%$  (not taking into consideration the accuracy of the voltage module itself) were achievable using this method.

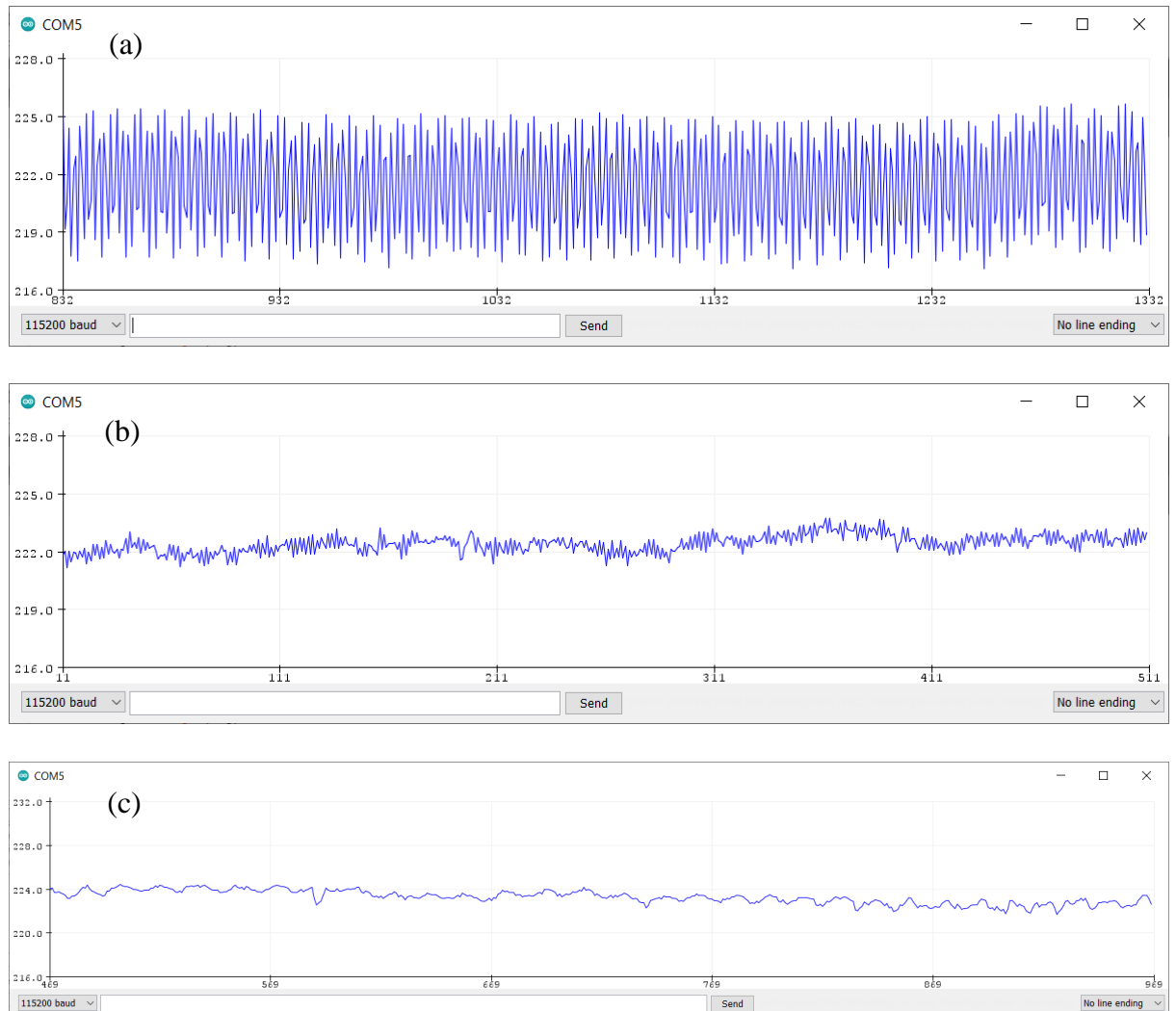


Figure 3.11: RMS signal of a  $\sim 240\text{Vac}$  source using a (a) 5,000 sample reading with no in-between delays; (b) 50,000 sample reading with no in-between delays; and (c) 500 sample readings with a  $500\mu\text{s}$  in-between delay.

In all cases described above, the calibration factor, 'VperVoltValue' was yet undetermined, hence the shift towards  $220\text{Vac}$  rather than the input source of  $240\text{Vac}$ .

Later, the factor was found to be 675.83, which produced an overall accuracy of  $\pm \sim 2V$  for a 240Vac source (observed  $\sim 10Vac$  above the nominal national standard due to an electricity sub-station being nearby).

The function ignores voltage readings below 85Vac and above 300Vac, which are common due to the high sensitivity of the module, even when an AC voltage source is not present. Voltage readings are displayed on the inbuilt display only in V (Volts).

### 3.2.7 Hall Effect Current Transformer

The current transformer chosen for this project is the *HST016L-20A* split core transformer by *YHDC* [58]. The transformer can measure both AC and DC currents, without needing physical connection or any modification to the circuitry. The device works by internally utilising both a hall-effect sensor and a current transformer, to form a Hall Effect Current Transformer. The sensor has a voltage output range of  $2.5V \pm 0.625V$ , thus requiring no additional circuitry due to the maximum output voltage falling in the accepted range of the microcontroller. To increase accuracy of the readings, a second analogue pin is provided, which functions as the calibration pin. The specifications of the *HSTS016L* current transformer are listed below in Table 3.8 [58]:

Table 3.8: *HSTS016L* specifications [58]

Description	Value
Supply voltage	+5V
Input measurement range	$\pm 150A$
Rated output	$2.5 \pm 0.625V$
Accuracy	1%
Linearity	< 0.1%
Number of pins	4 (supply pin, GND pin, data pin, calibration pin)
Active current draw	15mA (at 5V operating voltage)
Response time	< $3\mu s$
Cost/ sensor	< €15

### **Software configuration**

In this project, the sensor will be used to measure the current draw by the backup heater for power consumption measurements. However, the same sensor may be utilised for measuring the total current draw of the overall SWH system, which includes current draw by circulation pumps (if any), backup heaters (if any) and the monitoring device itself. Like the solar irradiance meter and AC transformer module, the current transformer outputs an analogue signal. Thus, the same `analogRead(pin)` and the `getVcal()` function can be used. The same procedure to obtain an RMS (root mean square) value as for voltage readings is utilised. A total of 500 samples are taken at each interval with a 500 $\mu$ s delay between each reading, and the RMS value is calculated during each interval.

Current readings are done every 90 seconds and displayed on the inbuilt display only in A (Amperes).

The current value, in combination with the source voltage, will be used to estimate the backup electric heater energy consumption, using the basic equation:

$$P_{RMS} = I_{RMS} V_{RMS} t \quad (17)$$

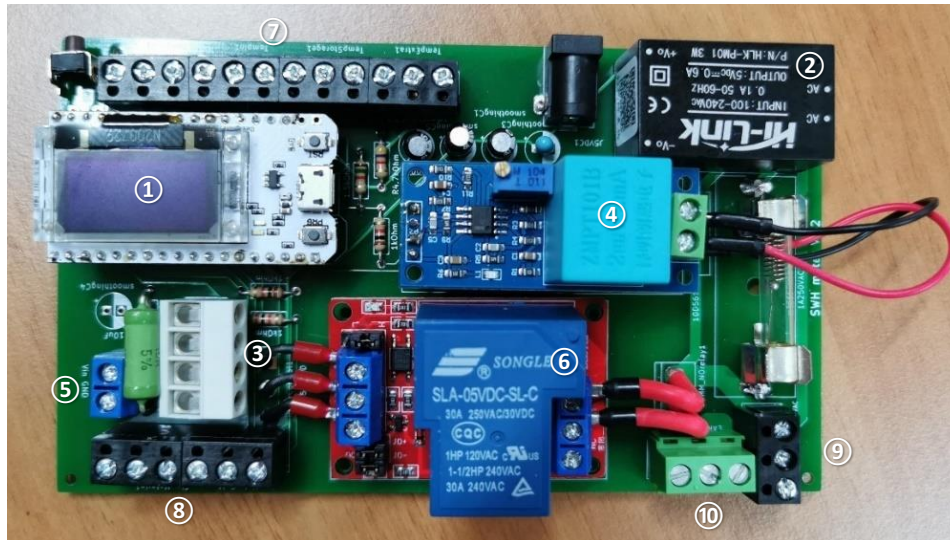
The software is configured to also measure the cumulative total of the backup heater electrical consumption and present it on the UI in kWh.

### **3.2.8 Custom PCB (Printed Circuit Board)**

To facilitate assembly and concept testing, a custom PCB was designed using Ki-Cad [59], which is an open-source software for Electronic Design Automation (EDA). The PCB will mechanically support and electrically connect all components and modules of the project. The PCB includes two power levels on a single board, isolated from each other to prevent interference. At one side lies the high-level AC supply, which provides power for the backup heater and the power supply. The low-level side, at the opposite side of the PCB, supplies the 3.3Vdc supply, 5Vdc supply and ground (backplane) required by the microcontroller and sensors. The PCB will also allocate space for passive and active components, such as capacitors and resistors, for further signal smoothing and circuitry protection.



Two versions of the PCB were made, the first made to fit the rejected microcontroller, which as discussed in Section 3.2.2, was later changed to the *Heltec* module due to occasional power failures and Wi-Fi connectivity issues. *Version 2* of the board, depicted in Figure 3.12, fits the *Heltec* board, while also improves on other features such as isolated power lines, and the better smoothing capabilities.



- |                                 |                              |                           |
|---------------------------------|------------------------------|---------------------------|
| ① Microcontroller module        | ② Power supply module        | ③ Current module terminal |
| ④ Voltage Transformer module    | ⑤ Solar PV terminal          | ⑥ Relay module            |
| ⑦ Temperature sensors terminal  | ⑧ Waterflow sensors terminal | ⑨ AC power input terminal |
| ⑩ Backup heater output terminal |                              |                           |

Figure 3.12: The second version PCB designed to fit the Heltec WiFi kit 32 module (①).

### 3.3 Internet of Things (IoT) / Data-Logging

All parameters tracked by the device were constantly uploaded to ThingSpeak™, a cloud IoT data aggregation and analytics service. ThingSpeak™ allows for prototyping and building of IoT systems without setting up complicated servers. Eight fields are provided with the free ThingSpeak™ service, on which parameter values are stored. Data is made easily accessible through the ThingSpeak™ *HTTP GET API* service, which allows devices, such as a common PC or the microcontroller, to easily access and download data. API, or Application Programming Interface, is a software intermediary which allows communication between two applications, such as the monitoring device and the ThingSpeak™ service [60], [61]. The data is transferred through JavaScript Object Notation (JSON), which is a cross-platform text-based format for presenting structured data based on JavaScript object syntax [62].

ThingSpeak™ allows for MATLAB® analytics inside ThingSpeak™ itself, where MATLAB™ code could be executed to perform pre-processing, visualisations, and analyses. Despite this useful feature, all pre-processing, visualisations, and analyses were done outside of ThingSpeak™ to ease up the setup process for new devices. Instead, these were included in the monitoring system environment coding using HTML/JavaScript (for the UI), and C++ programming languages (for the microcontroller)

Dataflows to and from the monitoring device is illustrated in Figure 3.13. The ThingSpeak™ data can be accessed and downloaded by any device (API keys required for secure data access). Similarly, the monitoring device can upload data to the ThingSpeak™ server, which cannot be done through another device due to a unique security key provided with each channel. The UI and the monitoring device communicate together through a network connection.

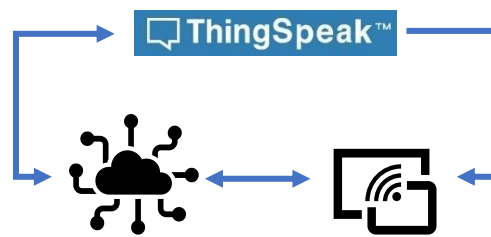


Figure 3.13: Data flows to and from the monitoring device

A total of eight parameters are stored in the ThingSpeak™ servers, which are listed in Table 3.9 along with their corresponding field number.

Table 3.9: Field numbers and corresponding parameters stored on the ThingSpeak™ database.

Field	Parameter name	Description	Units
1	Outlet Temperature	Outlet flow temperature	°C
2	Storage Temperature	Storage tank temperature	°C
3	Qo Solar Tank Consumption	Total hot water consumption (outlet)	m <sup>3</sup>
4	Qi Inlet Consumption	Total hot water consumption (inlet)	m <sup>3</sup>
5	Solar Flux	Instantaneous solar irradiation	kW/m <sup>2</sup>
6	Solar Irradiance Total	Total cumulative solar irradiance	kWh
7	Consumed Heat Energy	Total consumed heat energy	kWh
8	Consumed Electrical Energy	Total consumed electrical energy	kWh

### 3.3.1 Data uploads and downloads / Data-logging feature

Uploading of data to the ThingSpeak™ servers is done exclusively by the device. The process utilises a preconfigured library which makes it simple for the device to upload and download data to and from the ThingSpeak™ servers. Data uploads are done at three-minute intervals using the function call `ThingSpeak.setField(1, float(To));`. In this example, the variable *To* (Outlet Temperature) value is uploaded to *field 1* of the channel.

Similar to uploads, data downloads are done through a preconfigured function with the following structure:

```
temp_volumeQi = ThingSpeak.readFloatField(Channel_ID, 4, myReadAPIKey.c_str());
delay(500);
statusCode1 = ThingSpeak.getLastReadStatus();
delay (500);
```

In this example, the *inlet consumption* is being downloaded from *field 4* of the channel. The *channel ID* and the *read API key* are also passed for the function to access the data. In all cases, the last entry will be downloaded. Additionally, a *return read status* process is added to verify that the data has been successfully downloaded and depending on the value (eg. 200 for successful), the program will either pass to the next variable, or retry the download. Data downloads are done during device bootup only and are used to load the last updated parameter values.

### 3.3.2 Internet disconnections and upload failures

The device is configured to automatically restart upon 12 minutes of successive failed uploading attempts. Typically, upload failures occur due to an internet connection issue, such as disconnection to the Thingspeak™ servers. Although the device code features Wi-Fi error handlers such as reconnection and automatic IP (Internet Protocol) reassigning, it is possible that conflicts occur while assigning of new IPs to other devices in the network, requiring a device reboot to establish a new connection. In such cases, the data gathered during the 12 minutes of being offline are lost.

### 3.4 Design of a User-Interface (UI)

To maximise accessibility of the gathered data, a web-based UI was programmed with JavaScript, HTML and CSS programming languages. The UI is presented by the monitoring device itself and is accessed through any device connected on the same network, using the same IP address the monitoring device is assigned to. This IP address is displayed on the monitoring device display and is only required to be entered in the address bar of any web browser on any same network connected device. Alternatively, one may access the UI by entering <https://swh/> as the URL (Uniform Resource Locator) in the address bar on the web browser.

#### 3.4.1 Data requests/ UI parameter value updates

The UI requests data from the device using the *HTTP\_GET* function. An identifier is sent with the request, along with a *GET/* tag. If the device recognises the identifier, the variable data is sent back to the UI as a character string, which is then converted back to the original data type. Data requests are done automatically by the UI: fixed parameters such as the variables in the *Settings* tab, are requested once during UI page loading, while real-time monitored variables such as temperatures and flowrates are updated at specified intervals, for this project set at 10 seconds. The requests sent by the UI take the following format:

```
setInterval(function ( ) {
var xhttp = new XMLHttpRequest();
xhttp.onreadystatechange = function() {
    if (this.readyState == 4 && this.status == 200) {
        document.getElementById("To").innerHTML = this.responseText;
    }
};
xhttp.open("GET", "/To", true);
xhttp.send();
}, 10000 );
```

In this case, the variable *To*, which is the *Outlet Temperature*, is requested at 10-second intervals using the *GET/* function. The device responds by sending the variable value in a string format using the code:

```
server.on("/To", HTTP_GET, [])(AsyncWebServerRequest *request){
    request->send_P(200, "text/plain", String(To).c_str());
};
```

When the UI receives the response, the variable is updated on the UI. The process repeats for as long the UI is open.

### 3.4.2 Parameter/ Settings updating

A similar procedure is followed for updating parameters from the UI. Again, an identifier is sent to the device representing the parameter being requested, however this time, a value is sent along with the identifier, which represents the user submitted value. As the device receives the request, the variable (in String data format), is saved in the internal memory of the microcontroller, then converted to the assigned data type to replace the contents of the original variable. Below, is the sample code which is used when the *storage temperature limit* for the *backup heater control* feature is updated from the UI:

```
if (request->hasParam("temperature_control_range"))
{
  String temperaturecontrolrange = request->getParam("temperature_control_range")->value();
  writeFile(SPIFFS, "/temperaturecontrol.txt", temperaturecontrolrange.c_str());
  temperature_control_range = temperaturecontrolrange.toFloat();
  request->send(200, "text/text", temperaturecontrolrange);
} else
```

### 3.4.3 UI walkthrough

Upon UI loading, the user is presented with five main tab headings, namely: *Current Readings*, *View Charts*, *Autonomous Control*, *Efficiencies*, and *Settings* (Figure 3.14). Each tab gathers related data in a presentable and user-friendly manner, as follows:

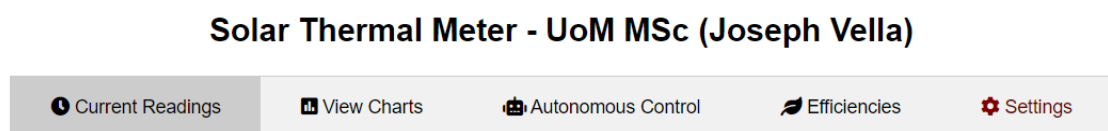


Figure 3.14: User-interface heading showing the 5 main tabs upon page loading.

#### 3.4.3.1 Current Readings Tab

The first page shown upon loading the UI is the *Current Readings* tab. All real-time monitored parameters of the SWH system (excluding power of the backup heater) are gathered in this tab. A snapshot of the page as presented to the user upon page loading is provided in Figure 3.15. The parameters in this tab are updated every 10 seconds by the UI itself, by requesting refreshed data directly from the monitoring device using the process described in Section 3.4.1. This tab requires the monitoring system and the data

viewing device to be connected to the same network (a Virtual Private Network connection would also suffice).

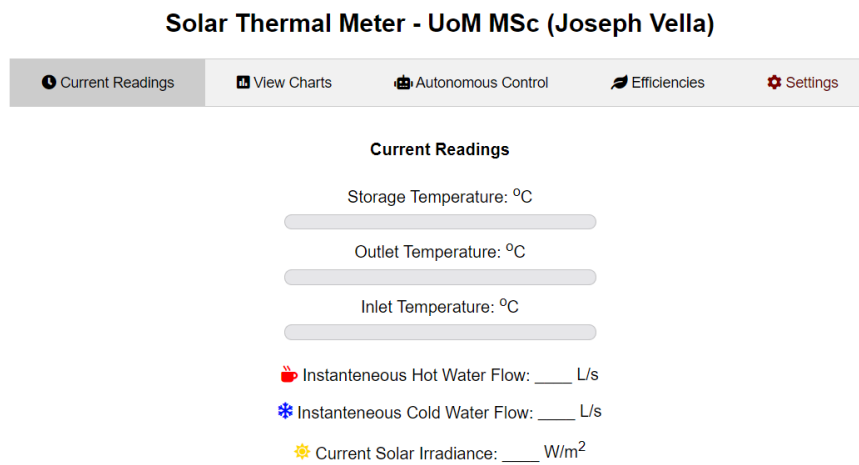


Figure 3.15: The Current Readings tab as presented on the first page of the UI.

### 3.4.3.2 View Charts Tab

This tab holds a *Highcharts* [63] interactive chart of the parameters being monitored, listed in Table 3.9. Using this chart, one may easily visualise gathered data and follow consumption trends for specified date ranges. Individual variables may be hidden/isolated for easier comparative observations. Hovering over a data series will view time and value details of that instance. Data is uploaded every three minutes directly from the monitoring device, thus all data entries presented on the chart are also at three-minute intervals.

Apart from custom date ranges, seven different zoom levels are available to the user, which aggregate the plot area to periods of 30 minutes, 12 hours, 1 day, 1 week, 1 month, 1 year and ‘all’. Additionally, users can download snapshots of the data plots and export raw data in *.csv* format. A snapshot of the *Chart* section is presented in Figure 3.16, including the additional options offered in the side menu.

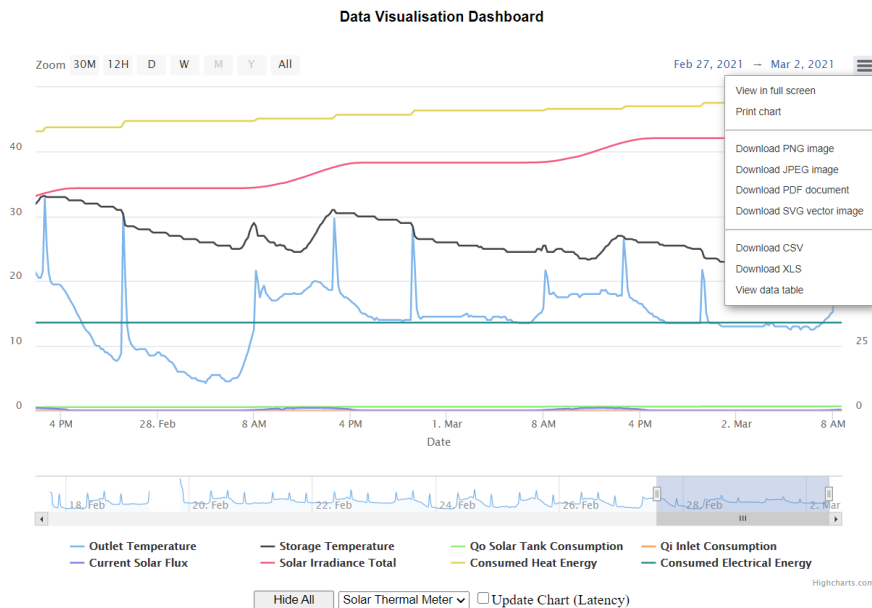


Figure 3.16: *Highcharts* [63] chart presenting all gathered parameter data viewed in the *View Charts* tab. Also displayed is the additional menu accessed by clicking the menu icon on the right.

### 3.4.3.3 Autonomous Control Tab

This section deals with the *automatic control* feature for the control of the backup heating element. The feature gives the user three levels of control, namely *Temperature Control* (automatically selected with the activation of *Autonomous Control*), *Time Control* and *Solar Irradiance Control*.

***Temperature Control (Autonomous Control)*** controls the state of the backup heater depending on the current storage water temperature. When the storage temperature goes below the set temperature (configurable in the *Settings* tab), the backup heater is switched on, and stays on until the storage temperature reaches 3°C above the set temperature. This is commonly referred to as the hysteresis band and is included to prevent very frequent power switching of the heating element which may cause damages to the switching relay and the heating element itself.

***Solar Irradiance Control***, if selected, will add control on the backup heater depending on the current solar irradiance intensity. A solar irradiance reading above the pre-configured limit (configurable in the *Settings* tab) keeps the backup heater off. This option allows for proper solar energy utilisation and prevents avoidable electrical energy usage.



Finally, **Time Control**, if selected, will add a time-control feature on the backup heater. The user is required to enter up to two time-control ranges during which the heater will be allowed to turn on. This feature will prevent unwanted wastage of electricity to heat up water during periods of no demand, particularly at night. The second time-control may be ignored by keeping time values at “00” (configurable in the *Settings* tab).

The three features may be independently activated to allow different levels of automated control. Although *solar irradiance control* and *time control* are independent of each other, both require the *autonomous control* feature to be enabled for these options to be available. The hierarchy showing the availability of the control options are illustrated in Figure 3.17 (a), and the corresponding UI menu is shown in Figure 3.17 (b).

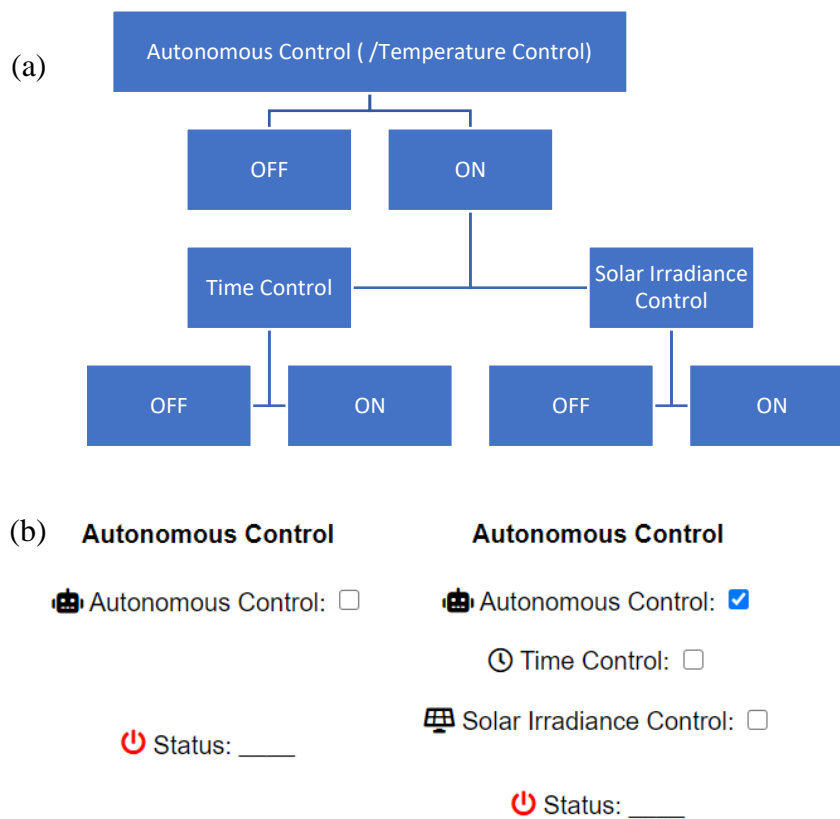


Figure 3.17 (a) Hierarchical order of control options and (b) User-interface control options showing instance where *Autonomous Control* is disabled (left) and instance where *Autonomous Control* is enabled (right).

The UI is solely used to change the control limits (from the *Settings* tab) and change the state of the control options (from the *Autonomous Control* tab). The microcontroller will then control the switching of the backup heater in the background, without requiring an open UI instance. The backup heater control decision process which is programmed in the microcontroller is illustrated in Figure 3.18.



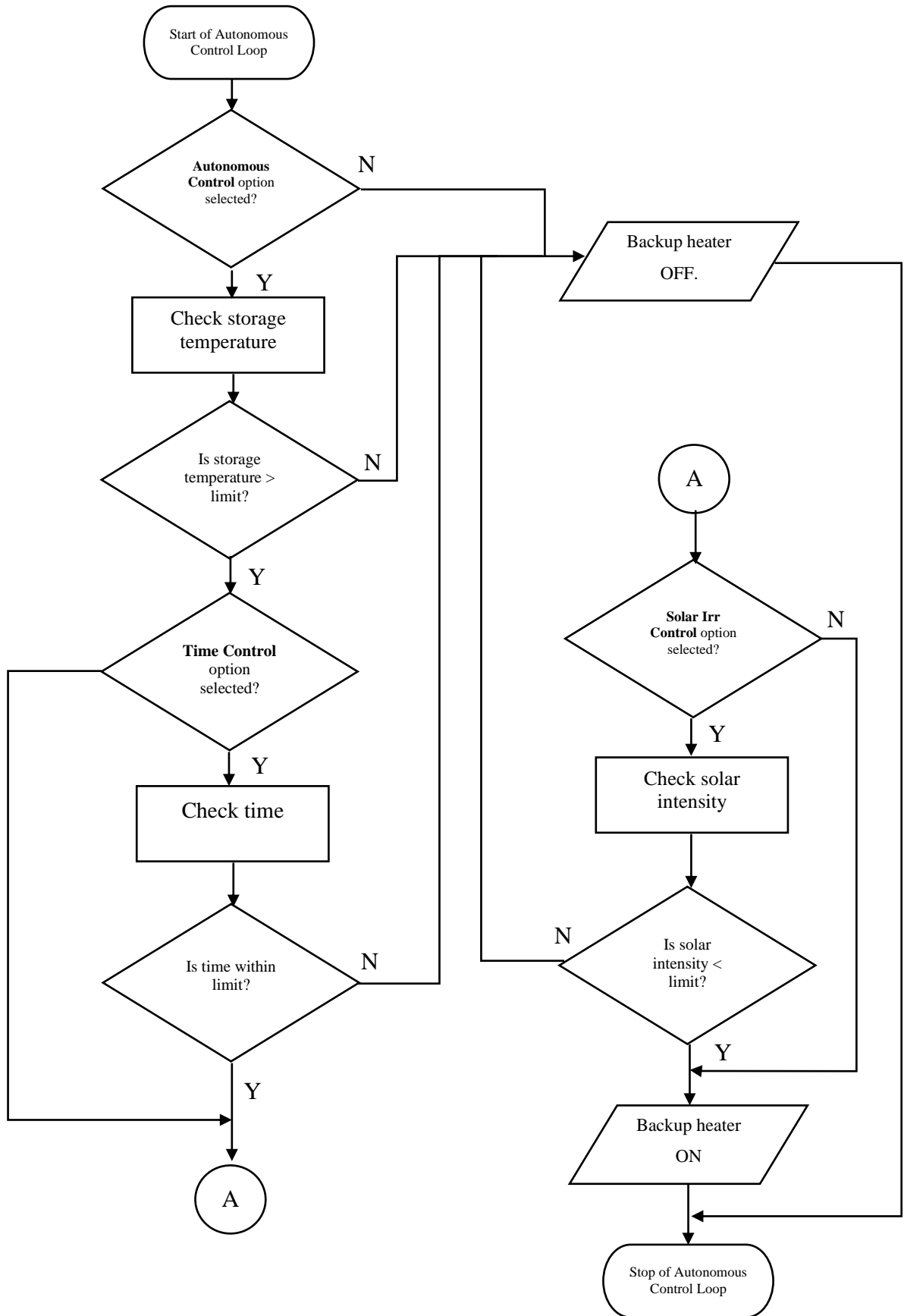


Figure 3.18: Flowchart showing the execution flow of the *autonomous control* process.

### 3.4.3.4 Efficiencies Tab

All performance related analyses of the SWH are done through the *efficiencies* tab. Two tables are presented on the page, being **Solar Water Heater Primary Efficiencies** and **Energy Utilisation Efficiencies**, which provide detailed reports on important energy characteristics including system efficiencies and energy generation and consumption.

#### Solar Water Heater Primary Efficiencies

This section determines the system efficiencies, termed *Primary Efficiencies*, of the overall SWH system. The user is requested to select a specific monitoring date, for which the storage tank heat gains during the day, losses during the night and system (*primary*) efficiencies are computed using historical data from the online database. The generated results also provide the storage temperature rise/ fall,  $\Delta T_S$ , for the evaluated period, alongside the average ambient temperature,  $T_{A-avg}$ , and the consumptions,  $\Delta Q$  and  $\Delta E$  for hot water and electricity, respectively. Since no dedicated ambient temperature sensors are available, the inlet temperature sensor is also utilised for ambient temperature readings. Ambient temperature readings are taken at instances of no water consumptions, which have proven to provide fairly true results. *Primary efficiencies* provide three main results: *day efficiency*, *night efficiency* and *combined efficiency*.

The *day efficiency*,  $\eta_{day}$ , is a measure determining the SWH's efficiency in converting sunlight into useful heat to raise the temperature of the water inside the storage tank, and is a function of ambient temperature, storage temperature (and difference), solar irradiance, and the absorber transmittance-absorptance product as described in Section 2.6.1. The value also caters for heat convective and radiative losses from the storage tank and the collector, although during the day these are significantly lower than during the night. The value for  $\eta_{day}$  is obtained by:

$$\eta_{day} = \frac{mc\Delta T_S}{G'_{period}} \quad (18)$$

Where:

- $G'_{period}$  is the period solar irradiance on the collector, in J;
- $m$  is the storage tank capacity, in kg; and
- $c$  is the specific heat capacity of water = 4200 J/kg. K.

Three timeframe options are available for *day efficiency* calculations, being: 06:00 – 09:00, 11:00 – 14:00 and 14:00 – 17:00.

The *night efficiency*,  $\eta_{\text{night}}$ , is a measure determining the SWH's efficiency in keeping the heat losses at a minimum during hours of no solar irradiance. In simpler terms, the *night efficiency* is an indication of how much of the generated energy during the day is preserved after the following night. *Night efficiencies* are computed by comparing the heat energy lost from the storage tank during the night to the heat gains inside the storage tank during the day had the SWH performed with the *day efficiency*,  $\eta_{\text{day}}$  for the entire day, i.e.:

$$\eta_{\text{night}} = \frac{G'_{\text{day}} \times \eta_{\text{day}} - \Delta H_{\text{night losses}}}{G'_{\text{day}} \times \eta_{\text{day}}} = \frac{G'_{\text{day}} \times \eta_{\text{day}} - mc\Delta T_{\text{S}}}{G'_{\text{day}} \times \eta_{\text{day}}} \quad (19)$$

Where:

- $G'_{\text{day}}$  is the daily solar irradiance on the collector, in J.

The value, thus, is a representation of the heat convection and radiative losses of the system, and is a function of the ambient temperature, storage temperature (and difference) and the thermal conductivity of the storage insulation (and to a lesser extent, other components of the SWH).

Finally,  $\eta_{\text{combined}}$ , provides the overall (*primary*) system efficiency for that specific monitoring period and is equal to the product of the two efficiencies,  $\eta_{\text{day}}$  and  $\eta_{\text{night}}$ .

A snapshot of a blank *primary efficiencies* report is shown in Figure 3.19 below:

**Solar Water Heater Primary Efficiencies**

Monitoring Day   Storage Capacity (L):

	Time	T <sub>A-avg</sub>	T <sub>S-first</sub>	T <sub>S-last</sub>	ΔT <sub>S</sub>	ΔG	ΔQ <sup>*</sup>	ΔE <sup>*</sup>	ΔH <sub>gain/loss</sub>	η <sub>coll/store</sub> <sup>**</sup>	η <sub>combined</sub>
☀	11:00 till 14:00 ▾	___	___	___	___	___	___	___	NaN	NaN	NaN
☾	00:00 till 06:00	___	___	___	___	___	___	___	NaN	NaN	

T<sub>A</sub>= Ambient Temperature and T<sub>S</sub>= Storage Temperature

\* For accurate estimates, choose monitoring periods with no hot water and electricity consumptions.

\*\* When day efficiencies are negative, night efficiency will be based on temperature differences. This method is less accurate.

Figure 3.19: Blank SWH Primary Efficiencies report.

The estimates work best when no water and electricity are consumed during the monitoring period, as these will cause temperature fluctuations which produce misleading efficiency figures. The UI is configured to give a green colour to the consumptions when none are detected, and red when otherwise.

Moreover, whenever the *day efficiencies* are negative, meaning the storage tank water sustained a net heat loss during the day, the *night efficiency*,  $\eta_{\text{night}}$ , is based on temperature differences during the night, such that:

$$\eta_{\text{night}} = \frac{T_{S-\text{min}}}{T_{S-\text{max}}} \times 100 \quad (20)$$

Whenever this is the case, the *night efficiency* value will be shown in red colour, implying an inaccurate estimate.

### **Energy Utilisation Efficiencies**

This section deals with the effects on SWH's performance with other factors in play including user behaviour on water consumptions and the backup heater use. Results are collated in two columns, one representing results for the entire monitoring period since initialisation, under *Total*, while the other represents results for a user specified monitoring period, under *Period*. The *Total* column loads the current parameter values as are from the monitoring device and computes the rest of the results depending on these parameter values. On the other hand, the *Period* column uses downloaded data from the online-database for the user-selected observation range and produces results based on these values.

The first four rows presented in the *Energy Utilisation Efficiencies* results, namely *Hot Water Consumption*, *Thermal Energy Consumption*, *Electricity Consumption*, and *Input Solar Irradiance* contain values as loaded from the device and the online database for the *Period* and *Total* results, respectively. The rest are computations coded in the UI and executed by the browser, and are described below:

- The *Solar Contribution to Hot Water*,  $Q_{\text{swh}}$ , is the consumed energy in the form of hot water less the electricity consumption, as described in Section 2.8;
- The *CO<sub>2</sub> equivalent reduction* is the mass of CO<sub>2</sub> emissions avoidance that the solar heating system has offset, had the same amount of energy been generated from a

conventional Open Cycle Gas Turbine power plant. The value is determined by multiplying the energy value in kWh by a factor, in this case 0.5 [64], [65]:

$$\text{CO}_2 \text{ equivalence} = 0.5 \times Q_{\text{swh}} \text{ (kg)} \quad (21)$$

The *CO<sub>2</sub> equivalence* is a value easily understood by the general public and gives an indication of the ecological contributions of using the SWH system. This factor is highly dependent on the means of hot-water storage and distribution means. For example, for a common household water heater installed inside, only ~75% of the stored heat-energy is retrievable. The remaining ~25% is lost to heat external components, mainly the insulation and piping. The same happens for SWH storage tanks however, that amount of heat that can never be retrieved is not generating CO<sub>2</sub>. Thus, in practice, the CO<sub>2</sub> equivalence reduction would be greater than what is obtained in Equation ( 21 );

- The *Solar Energy Utilisation Factor (SEUF)* (refer to Section 0), is a measure of the total utilised solar energy incident on the collector;
- Similarly, the *Overall Energy Utilisation Factor*, is indicative of how much of the input energy is utilised, but also includes the heat generated from the electrical backup heater as an input, i.e.:

$$\text{Overall Energy Utilisation Factor} = \frac{Q_{\text{Demand}}}{E_{\text{Solar}} + Q_{\text{Elec}}} \times 100 \quad (22)$$

- The *Solar Fraction* (refer to Section 2.8.3) is displayed to show users what fraction of the consumed energy in the form of hot water is coming directly from the sun's energy;
- Finally, the *Surplus Hot Water Fraction* (refer to Section 2.8.4) is shown. Although not truly accurate due to assuming hot water generation on a single efficiency, can give an indication on whether the backup heater is being unnecessarily switched on, or whether water consumptions could be optimised to match the hot water production patterns of the solar thermal system.

Ideally, such performance measurements are taken for periods of three days or longer, to avoid inaccuracies due to non-steady-state conditions (generation and consumption

of yesterday may affect today's performance). A snapshot of a blank *Energy Utilisation Efficiencies* report is shown in Figure 3.20.

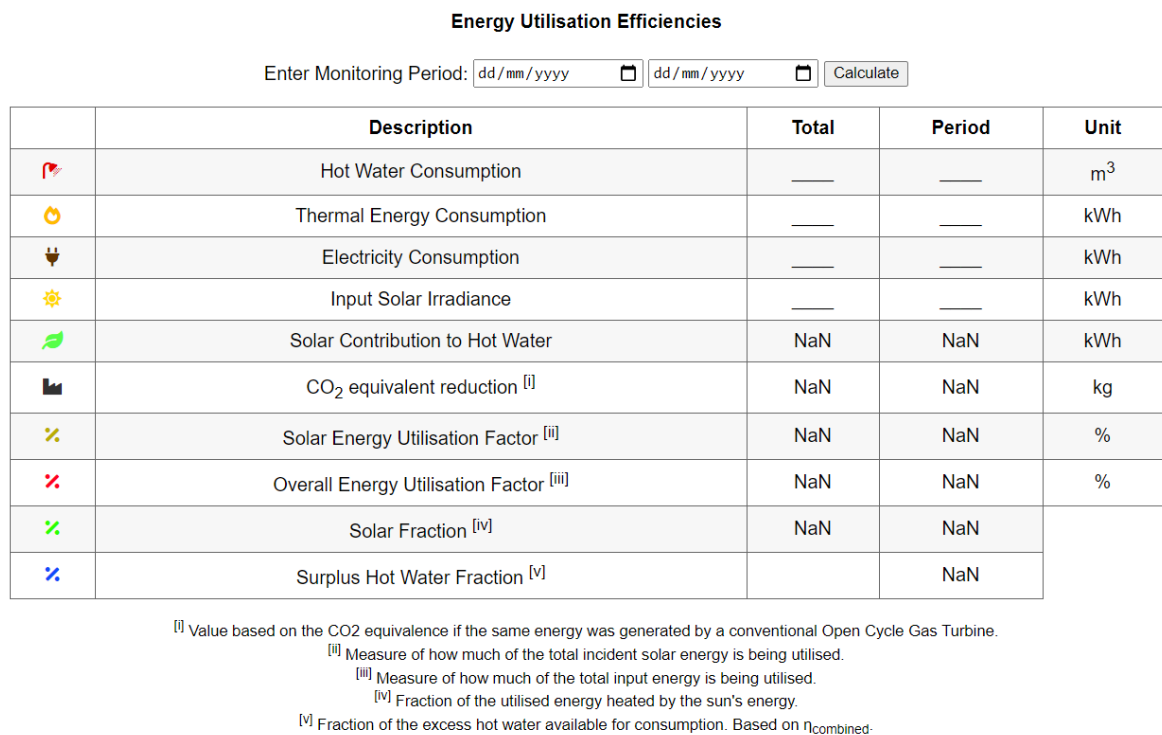


Figure 3.20: Blank Energy Unitisation Efficiencies report.

### 3.4.3.5 Settings Tab

Some parameters of the monitoring system may be updated directly from this tab. These parameters are:

- Solar collector aperture area ( $m^2$ );
- Backup heater power rating (used only in situations where a power meter is not available) ( $kWh$ );
- Waterflow correction factor (for calibration purposes);
- Solar Irradiance correction factor (for calibration purposes);
- Temperature control limit ( $^{\circ}C$ );
- Solar Irradiance control limit ( $W/m^2$ );
- Time Control ranges (2 ranges are possible);
- Location details (for time keeping purposes);
- Channel settings (Channel ID and Keys – for data-logging purposes).

The full *Settings* menu as displayed to the user is presented in Figure 3.21. The contents of the fields are updated with current parameter values when a direct network connection with the monitoring device is provided.

**Solar Thermal Meter - UoM MSc (Joseph Vella)**

📊 Current Readings
📈 View Charts
🔧 Autonomous Control
📊 Efficiencies
⚙️ Settings

**Update Parameters**

⚡ Filament Power:  kW

📏 Panel Area:  m<sup>2</sup>

📍 Update Location:

**Calibrations**

⊕ Solar Correction Factor:   (x 0.01)

⊕ WaterFlow Correction Factor:   (x 0.01)

**Control Limits**

🕒 Time Control 1:  :00 and  :00

🕒 Time Control 2:  :00 and  :00

Heater allowed to turn on in between the set time ranges.  
Time Control 2 is optional! Set to 00 and 00 to skip!  
Only enter the hours in hh (24hr) format.

📏 Update Solar Irr Control Limit:  W/m<sup>2</sup>

🌡 Update Temperature Control Limit:  °C

**Keys**

🔑 Read Key:

🔑 Write Key:

⚠ Channel ID:

Figure 3.21: Blank *Settings* page showing all updatable parameters.

Being in control of these parameters lets users configure their monitoring system to best fit their installed SWH, while also providing tools for optimising the performance. Changes are saved in the internal memory of the microcontroller and are reloaded automatically during device initialisation. In future versions, some of these settings will be hidden, such as the *Keys*, to ensure that no tampering with data is possible.

The *filament rating*, typically ranging between 1kW and 3kW, is the backup heater's power rating, and will be used if no electrical consumption metering means (Voltage and Current sensors) is provided. In such cases, the monitoring device will perform electrical energy consumption measurements in kWh using the *filament rating*.

The *panel area* is the total aperture area of the SWH collector, excluding the framing of the collector. This value will be used to compute the total solar irradiance incident on the panel, in kWh.

Although the sensors are pre-calibrated, the *Settings* tab in the UI allows for fine adjustments, namely for the water-flow and solar irradiance measurements. A value between 0.00 and 2.00, with 0.01 step increments is allowed, which by default is set to 1.00. Once updated, the new value, termed *correction factor*, will be stored in the monitoring device's internal memory and used in waterflow and/ or solar-irradiance measurements and computations.

### 3.5 Prototype installation and development timeline

The first prototype monitoring system performed basic energy metering tasks and was composed of three temperature sensors and one waterflow sensor. The monitoring device installation process was straightforward, requiring only minor modifications on the existing system mainly on external pipework to fit the sensors, and some sealing for waterproofing. The first monitoring system installation on the SWH, shown in Figure 3.22, was done on the 9<sup>th</sup> of February 2021.



Figure 3.22: Monitoring system prototype installation on a common thermosyphon type SWH, located at the Institute for Sustainable Energy in Marsaxlokk, Malta.



The SWH system was tested in different weather conditions, consumption patterns, and user preferences (set via the UI). The results generated by the monitoring system were continuously supervised, to verify correct functionality of the system. Along with the testing, frequent corrective updates were done on the monitoring system which improved reliability, responsiveness, and accessibility. Later, the second and then the third prototypes of the monitoring device replaced the first, which enabled more detailed and more accurate performance analysis with the addition of more sensors and features. The full timeline of prototype installations and their corresponding description and features are presented Table 3.10.

Table 3.10: Prototypes developed showing progress timeline. All prototypes were installed on the same SWH located at the Institute for Sustainable Energy in Marsaxlokk, Malta.

Prototype #	Description	Installation date	Features							
			Temperature monitoring	Waterflow monitoring	Solar irradiance monitoring	Power consumption monitoring	User-Interface	Autonomous (temperature) control	Time control	Solar-Irr control
1	ESP8266 + breadboard	09/02/2021	✓ (max 3 sensors)	✓ (max 1 sensor)						
2	ESP8266 + breadboard	02/03/2021	✓ (max 3 sensors)	✓ (max 2 sensors)	✓			✓		✓
3	ESP32 + PCB V1	19/04/2021	✓ (max 3 sensors)	✓ (max 2 sensors)	✓	✓	✓	✓	✓	✓
4	ESP32 + PCB V2	05/05/2021	✓ (max 4 sensors)	✓ (max 2 sensors)	✓	✓	✓	✓	✓	✓

### 3.6 Design of experiments

The possible testing combinations for the monitoring system are endless, thus, testing conditions were set up in a way to allow the most diverse data to be gathered as to fully test the capabilities of the monitoring system. Combinations may be categorised into three groups, namely: *Weather conditions*, *Draw-off timings*, and *Autonomous control*, as presented in Figure 3.23, together with the testing combinations for each category.

The monitoring system will be tested over the span of four months, from February 2021 till end of May 2021. Conditions were arbitrarily chosen to, where possible, imitate real life ones.

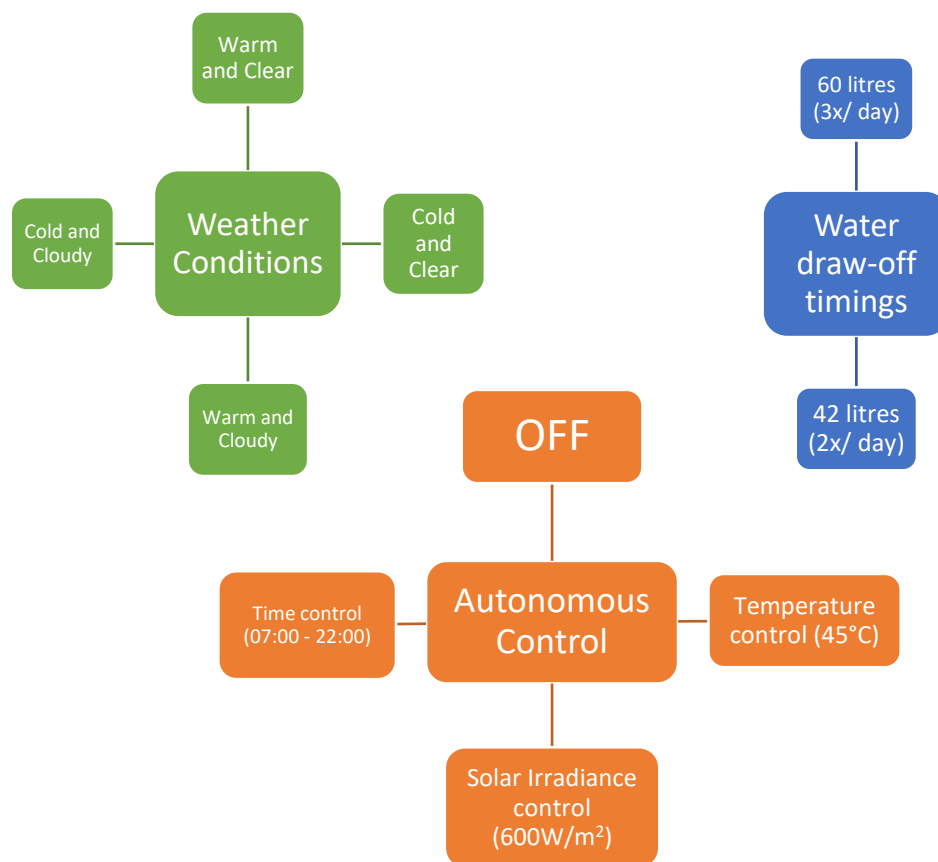


Figure 3.23: Combination of tests to be performed to test the capabilities of the monitoring system. Warm weather signifies ambient temperature highs  $> 25^{\circ}\text{C}$  and lows  $> 18^{\circ}\text{C}$ ; Cold weather signifies ambient temperature highs  $< 15^{\circ}\text{C}$  and lows  $< 5^{\circ}\text{C}$ . Clear signifies total daily solar irradiance  $> 8\text{kWh}$ ; Cloudy signifies total daily solar irradiance  $< 5\text{kWh}$ .

### 3.6.1 Control of water consumptions

The water consumptions were based on a single shower per person per day, for a household of 2-3 persons. Makki et. al [66], during a water consumption study in Australia, concluded that approximately 40L of water are consumed per shower. The commonly preferred time and water temperature for each shower are 8.5 – 10 minutes and 40°C, respectively [67].

Having a maximum flow rate of 6L/min (as covered in Section 3.2.1), it would take about 6.7 minutes for the SWH to draw-off the 40L of hot water. In practice, the direct hot water from the SWH would be mixed with cold water for a comfortable water temperature, thus the actual hot water consumption would be less.

The timer which controlled water draw-offs was set to the two testing conditions:

- 1) 7-minute showers, thrice per day – represents a family of three taking average length showers (~42L hot water per shower);
- 2) 10-minute showers, twice per day – represents a family of two taking longer than usual showers (~60L hot water per shower).

### 3.6.2 Control of backup heater

As shown in Figure 3.17, the backup heater is given three levels of control that are autonomous but at the same time interdependent. The following three sections explain the rationale adopted for these control limits.

#### 3.6.2.1 Temperature control limit

The *temperature control limit* for controlling the backup heater's switching was set to 45°C as:

- 1) Preliminary tests have shown that the SWH set up for testing stagnated at around 65°C, thus approaching this water temperature will make it difficult in predicting whether the solar effect is causing any storage water temperature rise;
- 2) Storage tank heat losses increase significantly with an increase in storage temperature, especially during winter nights. Thus, this value limited temperature rise to 48°C (due to the hysteresis allowance of the heating element discussed in

Section 3.4.3.3), avoiding repetitive switching on of the backup heater due to the much rapider temperature drops obtained;

- 3) As discussed above, the preferred showering temperature is in the range of the set temperature limit.

### **3.6.2.2 Solar irradiance control limit**

The value of  $600\text{W}/\text{m}^2$  for the solar irradiance limit was randomly chosen, based on assumptions that solar irradiance levels below this value are not sufficient in generating useful heat energy to provide a net temperature rise of the water inside the storage tank. In practice, this value should be set after some preliminary testing, and should vary with the type of collector in use and climatic conditions of the area of installation.

### **3.6.2.3 Time control limit**

The time limit of 07:00 till 22:00 is based on the time during which the average person is awake. Taking showers at night is not common, hence this time limit will prevent the backup heater from turning on at night.

## Chapter 4 Results and Observations

This Chapter analyses the results of this dissertation to evaluate the level of success in achieving the required functionality, reliability, and longevity of the monitoring device when it was tested in a real field application. The device was connected to a flat-plate thermosiphon type SWH and had all features tested extensively over the span of four months. During this period, regular corrective hardware and firmware updates were applied to further optimise the device. The Chapter closes with several UI generated results for different monitoring periods, for which a general review on the performances are provided.

The contents of this Chapter are divided into nine main parts, overviewed in Table 4.1 below:

Table 4.1: Description of the contents of this chapter.

Section #	Description	Scope
4.1	SWH functionality check	Preliminary tests to verify correct functionalities of the SWH and the inbuilt backup heater.
4.2	Software and UI functionality check	Verify all programmed features in the software and the UI are working as intended. This section does not focus on performance results, but rather the functionality of the features, including the <i>autonomous control</i> feature which shall take control of the switching times of the backup heater.
4.3	Parameter accuracies and precisions	Obtain accuracies and precisions of the monitored parameters and evaluate the long-term stability of the sensors.
4.4	Solar shading instances	Test whether the solar irradiance meter can trace solar shading instances and present them on the charts.
4.5	Tracing water draw-offs	Verify that the timed water draw-offs are accurately being traced and quantified by the monitoring device and presented on the UI.

<b>4.6</b>	<i>Primary Efficiencies</i> results section	Observe SWH main efficiencies for the day and the night with varying climatic conditions. Results depend mainly on the SWH and the weather.
<b>0</b>	<i>Energy Utilisation Efficiencies</i> results section	Observe the long-term performance results of the SWH with varying backup heater use. Results depend on water consumptions, use of backup heater and weather conditions.
<b>4.8</b>	Investigating an ideal consumption pattern.	Determine whether it would be possible for anyone to improve performance of their SWH based on their consumption patterns, backup heater use and the weather conditions.
<b>4.9</b>	Determining the stagnation point of the SWH.	Determine whether it would be possible to estimate the stagnation point of the SWH by observing results provided by the UI.

#### 4.1 Solar Water Heater functionality check

From the 9<sup>th</sup> of February till the 11<sup>th</sup> of March 2021, the SWH was unintentionally operated without sufficient water-glycol transfer fluid mixture in its primary circuit between the panel and the tank heat exchanger due to an unnoticed leakage. The performance of the SWH was in turn a poor one, with overall system efficiencies consistently below 10%, and often below zero, meaning that the storage tank water was sustaining a net temperature drop during the day. Since it was amidst the peak of the winter season, and the first time operating the SWH, it was at first assumed that the performance obtained was a typical one for a cloudy day. During this period and when the backup heater was allowed to operate, it succeeded in raising the water temperature to the set point. The leakage was then repaired and the SWH was refilled with the water-glycol primary fluid. Improvements were instantaneous, with *day efficiencies* surpassing 50% during the first few hours in operation.

As a result of this event, the UI was updated to display possibility of malfunctioning warnings when system efficiencies dropped below a certain threshold. Presently, the threshold is set at 30% *day efficiencies* for solar irradiance yields greater than 3kWh during sun peak hours (11:00 till 14:00). Similarly, a possibility of malfunctioning warning is displayed on the UI when *night efficiencies* drop below 50%. In such cases,

the malfunction, such as insulation breakages and leakages, would be causing major heat losses in the storage tank. Table 4.2 shows the *SWH Primary Efficiencies* results for a scenario when both *day* and *night efficiencies* obtained were below the threshold values.

Table 4.2: Functionality check of SWH, displaying alerts due to the obtained low efficiencies.

Solar Water Heater Primary Efficiencies											
Monitoring Day		02/03/2021		Calculate		Storage Capacity (L):		150			
	Time	$T_{A-avg}$	$T_{S-first}$	$T_{S-last}$	$\Delta T_S$	$\Delta G$	$\Delta Q^*$	$\Delta E^*$	$\Delta H_{gain/loss}$	$\eta_{coll/store}^{**}$	$\eta_{combined}$
☀	11:00 till 14:00	17.80	23.00	23.50	0.50	4.01	0.00	0.00	0.09	2.24	0.33
☾	00:00 till 06:00	13.42	21.00	20.00	-1.00		0.00	0.00	-0.17	14.54	

$T_A$  = Ambient Temperature and  $T_S$  = Storage Temperature

\* For accurate estimates, choose monitoring periods with no hot water and electricity consumptions.

\*\* When day efficiencies are negative, night efficiency will be based on temperature differences. This method is less accurate.

Day efficiency too low! Check for malfunctions such as leaks, blocks or shading.  
Night efficiency too low! Check for malfunctions such as leaks or insulation breakages.

## 4.2 Software and UI functionality check

The UI was tested thoroughly for correct feature functionality and performance reporting. As the only full interaction with the SWH, the UI had to be responsive and always updated with the latest parameter values. During all occurrences of testing, the UI was quick to respond, with page loading times varying from 0.5s up to 5s, depending on the network connection quality and the connecting device. The slowest loading time was encountered when the monitoring device was accessed through a VPN (Virtual Private Network) connection from a laptop at a remote location. The UI also worked without limiting any functionality when accessed through a smartphone, although loading times were on the slower side.

All features which required the downloading of online-stored data, such as charts and efficiency calculations, worked as intended, provided a good internet connection was available. Despite requiring miniscule amounts of data to be downloaded from the ThingSpeak™ servers, the internet connection download speed was the governing factor to the features' loading time. Nevertheless, in all testing cases, a common household internet connection was more than adequate for the UI to function properly.

Real-time updated parameters, which are found on the first screen of the UI, were confirmed to update as intended. The feature also worked well through a VPN

connection; one instance is shown in Figure 4.1, which shows real-time parameter values during a water draw-off instance.

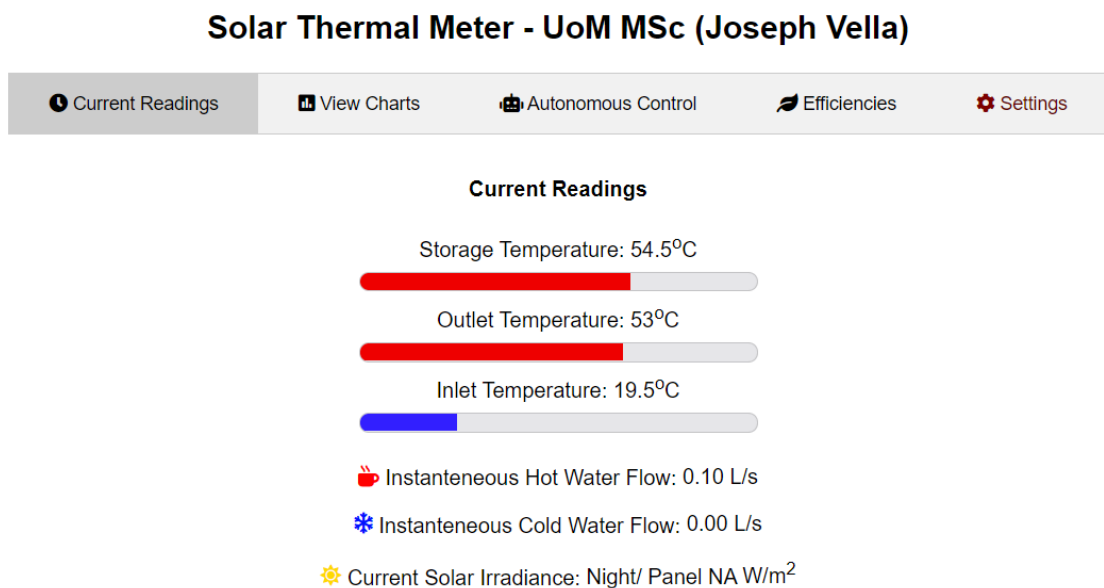


Figure 4.1: Real-time monitored parameter values displayed on the homepage of the UI during a water draw-off instance.

The *Settings* section was tested by submitting both allowed and disallowed parameters and observing the behaviour of both the UI and monitoring device. Embedded data validation functions in the UI only accepted correct data-types and data-ranges. This prevented the device from encountering logic, syntax, and arithmetic errors due to invalid data submissions. Figure 4.2 depicts an alert instance displayed during an out-of-range value submission. Data-type validations were immediate, meaning the UI would block characters of incorrect data types from being inputted in the first place.

#### Control Limits

🕒 Time Control 1:  :00 and  :00

🕒 Time Control 2:  ⚠️ Value must be less than or equal to 24.

**Heater allowed to turn on in between the set time ranges.**  
 Time Control 2 is optional! Set to 00 and 00 to skip!  
 Only enter the hours in hh (24hr) format.

Figure 4.2: Embedded data-validation in the UI.



### 4.2.1 Changes in *Settings* and offline saving

Accepted parameter changes from the *Settings* tab were traced back to the monitoring device and confirmed of being stored in the microcontroller's built-in memory, also verifying that the data was not erased after device reboots. The user is shown a pop-up message similar to the one in Figure 4.3 whenever a submitted *Settings* change is accepted. The UI refreshes to load the new values as soon as *OK* is pressed.



Figure 4.3: UI alert confirming that the changed parameters from the *Settings* tab is accepted.

### 4.2.2 Autonomous control feature functionality test

The *autonomous control* feature was tested against varying sets of conditions set via the UI. The two types of testing performed on this feature are the instantaneous (real-time) testing, and long-duration testing.

Instantaneous monitoring was straightforward and quick, as parameters were set, and the backup heater was monitored in real-time following the changes. The backup heater was switched on via the *Autonomous Control* tab in the UI and the heater state was observed from the same tab. Additionally, the relay's inbuilt LED indicator turns on when the relay is triggered. Both were confirmed to react correctly. The status of the heater in the 'on' position as presented by the UI is shown in Figure 4.4 (left), along with the triggered indicator LED on the relay module in Figure 4.4 (right).

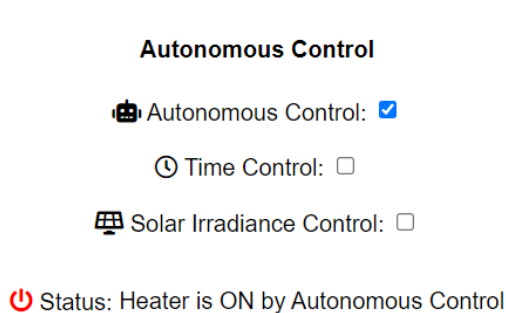


Figure 4.4: UI displaying an 'ON' status for the backup heater (left), and the indicator lights showing 'closed position' status on the relay module (right)

For long-duration testing, the *autonomous control* feature was enabled, and the behaviour of the backup heater was observed over a span of consecutive days. Correct functionality of the feature was verified by observing the storage water temperature and electrical consumption trends on the graphs from the *Charts* tab. Figure 4.5 depicts the *storage temperature* and *electrical consumption* plots with the *autonomous control* feature enabled with only the storage temperature as the control factor.

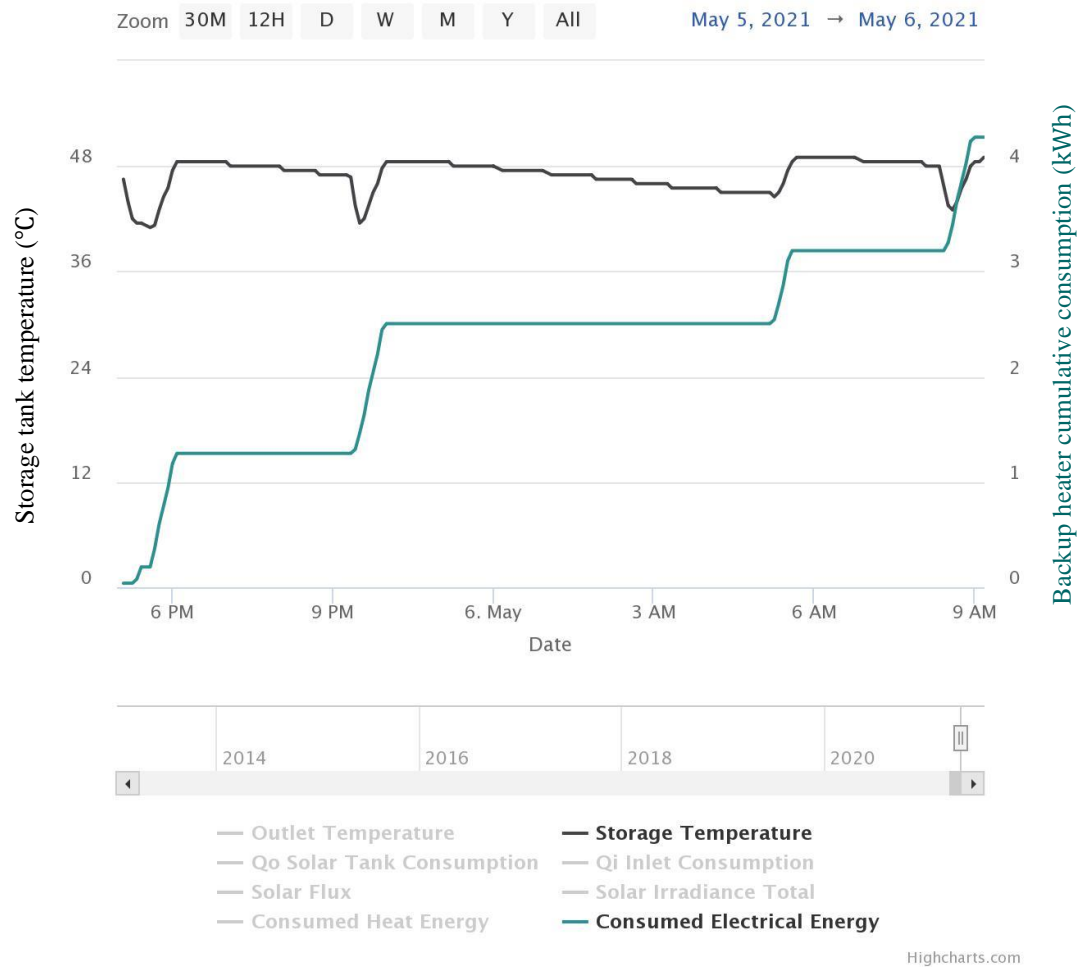


Figure 4.5: *Storage temperature* (black) and *consumed electrical energy* (blue) chart for the 5<sup>th</sup> (17:00) till the 6<sup>th</sup> (09:00) of May 2021 with *Autonomous Control* feature enabled with only the storage temperature as the controlling factor.

As can be observed, whenever *storage temperatures* dropped below 45°C, the backup heater kicked in until the storage water temperature was raised to +3°C of the set temperature, in this case 48°C. The *electrical consumption* (on the right y-axis) was confirmed to increment accordingly whenever the backup heater was in use. For the period displayed in Figure 4.5 , being the 5<sup>th</sup> of May at 17: 00 till the 6<sup>th</sup> of May at

09:00, the backup heater switched on four times, at 17:38, 21:26, 05:16 and 08:29. All instances except the third were triggered due to sudden drop in storage temperature due to hot water draw-offs. On the other hand, the third instance was triggered due to a gradual temperature drop during the night.

The *autonomous control* feature was also tested with all control conditions enabled, as described in Section 3.6.2, and with two draw-offs timed at 08:00 and 18:00. The feature was given three days to operate autonomously, between the 12<sup>th</sup> and the 15<sup>th</sup> of May 2021, during which it functioned as intended, as can be observed by the *solar irradiance* (purple) – *storage temperature* (black) – *electricity consumption* (teal) vs time plots shown in Figure 4.6.

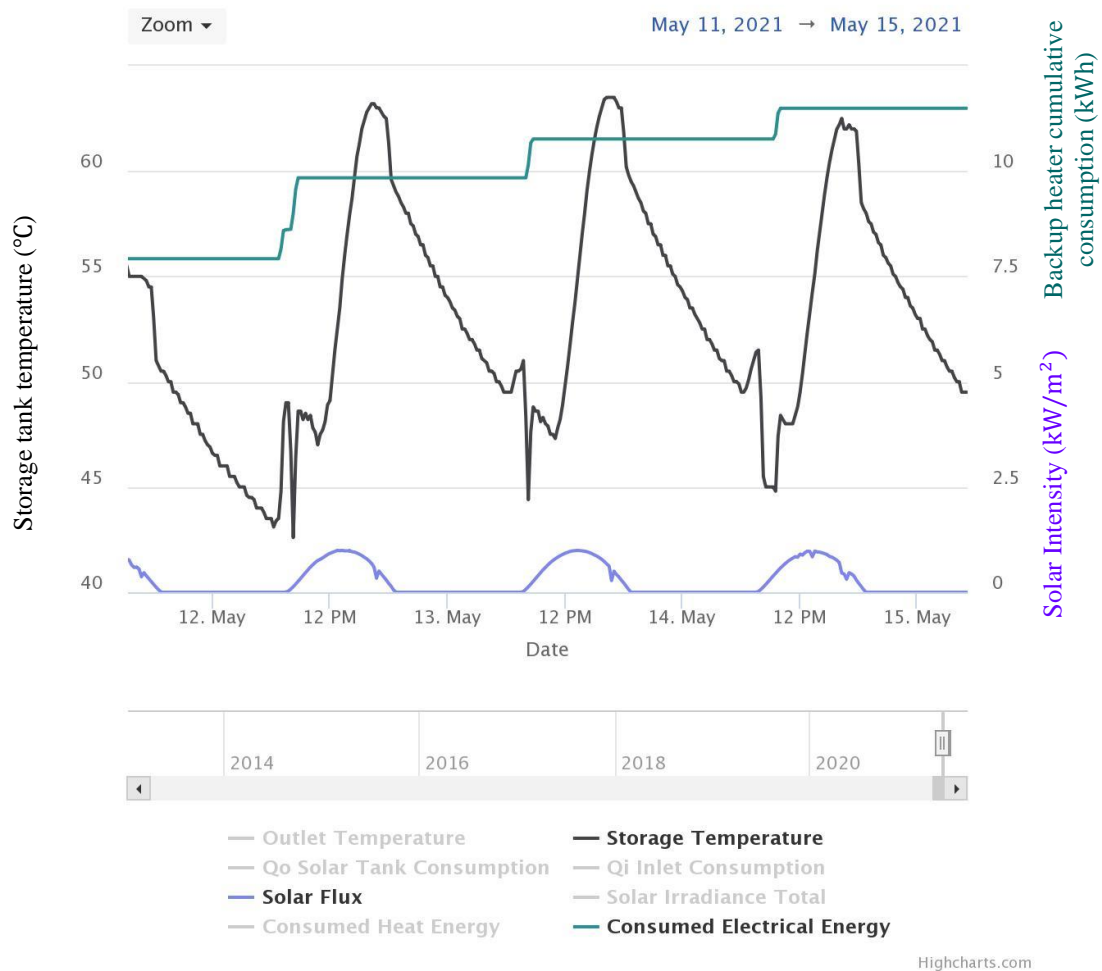


Figure 4.6: Storage temperature (black), electrical consumption (teal) and solar irradiance (purple) chart for 12<sup>th</sup>-15<sup>th</sup> of May with Autonomous Control feature turned on with all control features enabled.

On the 12<sup>th</sup> of May, two successive instances of backup heater use may be observed, at 07:00 and at 08:15. For the following days, the 07:00 backup heating instance did not take place, due to the storage water temperature being  $> 45^{\circ}\text{C}$ . Summarising, all instances have adhered to the programmed set conditions:

1. Switch on only if storage temperature is below  $45^{\circ}\text{C}$ ;
2. Enabled only between 07:00 and 22:00;
3. Enabled only if solar irradiance is less than  $600\text{W}/\text{m}^2$ .

### 4.2.3 Internet Disconnection Timeouts

As discussed in Section 3.3.1, the device is configured to automatically reboot after 12 minutes of offline activity. During the testing of the monitoring system, multiple occurrences of internet disconnections occurred due to internet issues, mainly related to security protocols imposed by the University of Malta *eduroam* hotspot. In Figure 4.7, the monitoring device disconnected and successfully reconnected after a restart, observed by the gap in the chart data between 13:03 and 13:18 on the 21<sup>st</sup> of April 2021. The device functioned as intended after the internet connection was re-established, showing a robust firmware.

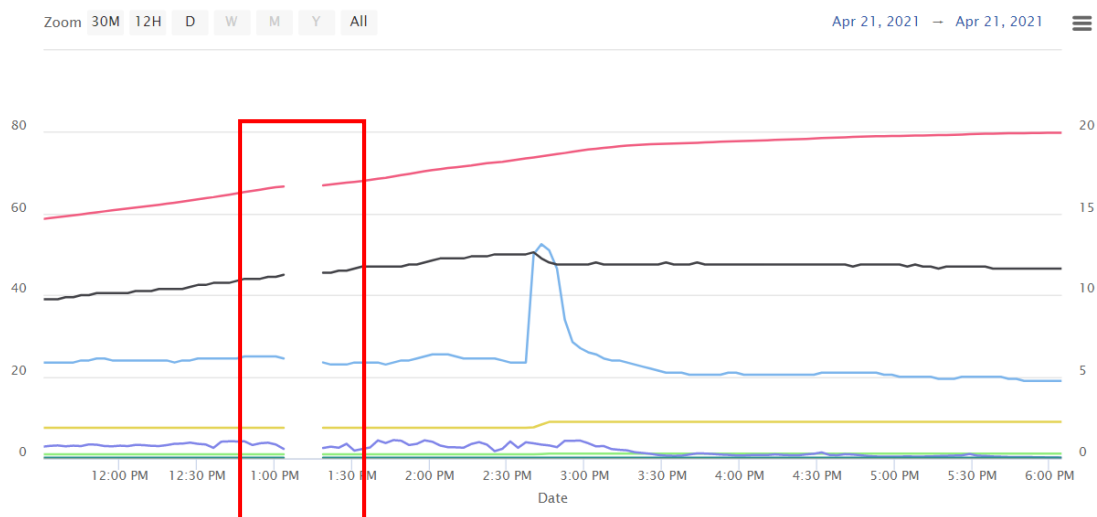


Figure 4.7: Reconnection to the internet after rebooting due to a disconnection timeout.

Unfortunately, however, despite the parameter changes still being tracked by the monitoring device during this offline period, these were lost during rebooting because of upload failures. The issue was resolved by adding a programmed procedure, which

temporarily stores variable data inside the microcontroller's internal memory when internet disconnection is detected. The device then reloads the data from the internal memory upon rebooting. This solution has enabled the reduction in the number of device reboots. As a result, internet timeouts were increased to 30 minutes instead of previously configured 12 minutes as covered in Section 4.3.2.

### **New internet hotspot**

On the 10<sup>th</sup> of May 2021, a separate new internet hotspot was purchased and installed, given that the issue of disconnection of the internet of the UoM *eduroam* hotspot could not be solved.

### **4.3 Parameter accuracies, precisions, and calibration requirements (long-term stability)**

Sensor accuracies and precisions were evaluated twice; the first during installation of the second version of the prototype monitoring device (19<sup>th</sup> April 2021), and the second after 21 days of uninterrupted use. The latter test was made to check the long-term stability of the sensors and their calibration. Table 4.3 compares the readings from the monitoring device with parameter values obtained by other means (termed *actual*) and lists the corresponding accuracies and precisions. Precisions were calculated using the average deviation method.

Waterflow accuracies were determined by filling up a bucket of known capacity and recording the time taken to fill up. The flow rate was then calculated and compared to the value obtained by the waterflow sensor of the monitoring device. Naturally, using this method, inaccuracies in the *actual* readings are expected. Similarly, for *actual* temperature measurements, a common thermistor was used which also possesses its own inaccuracies. However, by repeating the tests several times consecutively, the errors would statistically cancel out and one can get a reliable *actual* result to be used for comparison.

All instruments were observed to perform well, even after 21 days of continuous use. As expected, the worst performing sensors were of the analogue type, specifically solar irradiance measurements, with accuracies ranging from  $-15.62\%$  to  $+1.77\%$  for day one (similar for day 22). However, it was noted that inaccurate solar irradiance readings

were obtained only for intensities of less than  $500\text{W}/\text{m}^2$ , otherwise the readings were relatively accurate especially for solar irradiance intensities exceeding  $900\text{W}/\text{m}^2$ .

Summarising, all sensors produced satisfactory results, well within the acceptable ranges of accuracies and precisions for the scope of this project.

**Note on cleanliness of solar PV module.**

Long-term observations have shown that the sensor seemingly requiring most frequent calibrations is the solar irradiance meter however, upon further inspection, it was noted that small PV panel's surface was occasionally found in a soiled state (covered in a thick layer of dust), especially after precipitation, most notably after red soil rains. Upon wiping the surface of the solar PV panel, solar irradiance measurements returned to the previous accuracies.

Table 4.3: Parameter accuracies and precision calculations for 19/04/2021 (top/ blue) and 03/05/2021 (bottom/ green). Also presented are the % changes in accuracies and precisions after 21 days of consecutive monitoring.

Parameter	Actual Reading	Day 1			Accuracy	Precision		
		1st reading	2nd reading	3rd reading				
<i>Water flow rate - high (L/min)*</i>	5.79	5.88	5.90	5.86	+1.55%	99.77%		
<i>Water flow rate - low (L/min)*</i>	3.71	3.65	3.68	3.68	-1.08%	99.64%		
<i>Water draw-off - high (L)*</i>	9.00	9.11	9.15	9.10	+1.33%	99.78%		
<i>Water draw-off - low (L)*</i>	9.00	8.87	8.94	8.95	-0.89%	99.63%		
<i>Temperature - high (°C)</i>	45.00	44.00	44.50	44.00	-1.85%	99.50%		
<i>Temperature - low (°C)</i>	14.00	13.00	13.00	13.50	-5.95%	98.31%		
<i>Solar Irradiance - high (W/m<sup>2</sup>)</i>	1092.00	1100.00	1148.00	1086.00	+1.77%	97.80%		
<i>Solar Irradiance - low (W/m<sup>2</sup>)</i>	239.00	202.00	209.00	194.00	-15.62%	97.47%		
<i>Voltage (V)</i>	244.00	245.00	243.00	243.00	-0.14%	99.64%		
<i>Current (A)</i>	9.97	9.83	9.89	9.32	-2.91%	97.52%		
Parameter	Actual Reading	Day 22			Accuracy	Precision	% change from day 1	
		1st reading	2nd reading	3rd reading			Accuracy	Precision
<i>Water flow rate - high (L/min)*</i>	5.86	5.96	5.98	5.98	+1.93%	99.85%	+0.38%	+0.08%
<i>Water flow rate - low (L/min)*</i>	3.10	3.05	3.02	3.06	-1.83%	99.49%	-0.75%	-0.15%
<i>Water draw-off - high (L)*</i>	9.00	9.15	9.18	9.19	+1.93%	99.83%	+0.59%	+0.05%
<i>Water draw-off - low (L)*</i>	9.00	8.85	8.77	8.89	-1.81%	99.50%	-0.93%	-0.13%
<i>Temperature - high (°C)</i>	48.00	47.50	47.50	48.00	-0.69%	99.53%	+1.16%	+0.04%
<i>Temperature - low (°C)</i>	23.00	22.00	22.50	22.00	-3.62%	99.00%	+2.33%	+0.69%
<i>Solar Irradiance - high (W/m<sup>2</sup>)</i>	982.00	998.00	1001.00	991.00	+1.49%	99.62%	-0.28%	+1.82%
<i>Solar Irradiance - low (W/m<sup>2</sup>)</i>	565.00	489.00	502.00	512.00	-11.33%	98.40%	+4.29%	+0.94%
<i>Voltage (V)</i>	242.00	248.00	245.00	241.00	+1.10%	99.00%	+1.24%	-0.63%
<i>Current (A)</i>	9.93	10.02	9.89	9.84	-0.13%	99.31%	+2.77%	+1.78%

\*Inaccuracies in the actual readings are expected as no calibrated tools for these parameter measurements were available.

#### 4.4 Solar shading instances

The UI detected daily occurrences of very low levels of solar irradiance. In some cases, such as the months of March and April 2021, sudden drops in solar irradiance were noted twice daily, occurring close to each other, as can be observed by the successive dips in Figure 4.8. For instance, during the end of March (GMT+1), the low irradiance readings were detected at around 10:30 and 13:00, while during the end of April (GMT+2 – daylight saving time), dips were detected at around 15:45 and 16:50, as can be observed in Figure 4.8.



Figure 4.8: Solar shading effect on solar irradiance readings. Charts showing solar irradiance (in kWh/m<sup>2</sup>) for the 25<sup>th</sup> and 26<sup>th</sup> of April 2021.

Further examination concluded that during these occurrences, the solar irradiance meter was temporarily shaded by a metal structure surrounding the area where the SWH was



installed. A solar shading occurrence is shown in Figure 4.9, where a partial shade on the solar irradiance meter (solar PV panel) may be observed.



Figure 4.9: Solar shading occurrence due to a metal structure surrounding the installation area.

#### 4.5 Water draw-offs

The daily water draw-offs could be monitored using the *Energy Utilisation Efficiencies* section under the *Efficiencies* tab of the UI. The minimum observation period using this feature is of a full day (00:00 till 23.59), thus an average water consumption per draw-off could be determined by dividing the total daily consumption by the number of daily draw-offs. For the 24<sup>th</sup> of April, water was drawn-off three times per day as described in Section 3.6.1. The daily hot water consumption added up to 0.13m<sup>3</sup>, as reported by the UI, shown in Table 4.4. This value averages out at 43.33L per draw-off, 1.33L more than the predicted value applying the previously calculated flowrate and draw-off duration, which is sufficiently accurate (3%).

Alternatively, the water consumption could be determined by tracing the *Qo Solar Tank Consumption* plot under the *View Charts* tab, which gives greater detail on consumption occurrences. Figure 4.10 verifies that indeed, water was drawn-off three times during the day: at 08:00, 14:30 and 21:00; each draw-off lasting ~7 minutes.

Table 4.4: Energy Utilisation Efficiencies results for the 24th of April 2021.

**Energy Utilisation Efficiencies**

Enter Monitoring Period:

	Description	Total	Period	Unit
	Hot Water Consumption	---	0.13	m <sup>3</sup>
	Thermal Energy Consumption	---	3.21	kWh
	Electricity Consumption	---	0.00	kWh
	Input Solar Irradiance	---	8.72	kWh
	Solar Contribution to Hot Water	NaN	3.21	kWh
	CO <sub>2</sub> equivalent reduction <sup>[i]</sup>	NaN	1.60	kg
	Solar Energy Utilisation Factor <sup>[ii]</sup>	NaN	36.81	%
	Overall Energy Utilisation Factor <sup>[iii]</sup>	NaN	36.81	%
	Solar Fraction <sup>[iv]</sup>	NaN	1.00	

<sup>[i]</sup> Value based on the CO<sub>2</sub> equivalence if the same energy was generated by a conventional Open Cycle Gas Turbine.

<sup>[ii]</sup> Measure of how much of the total incident solar energy is being utilised.

<sup>[iii]</sup> Measure of how much of the total input energy is being utilised.

<sup>[iv]</sup> Fraction of the utilised energy heated by the sun's energy.



Figure 4.10: *Qo Solar Tank Consumption* trend showing instances of hot water consumptions for the 24th of April 2021.

### **Solar Energy Utilisation Factor (SEUF) behaviour with water consumption and the addition of the Surplus Hot Water Fraction**

Table 4.4 also shows key information on the performance of the SWH for that day, above all the *Solar Energy Utilisation Factor*. As described in Section 2.8.2, the SEUF value gives an indication of how much of the incident solar irradiation on the collector is being utilised. For the 24<sup>th</sup> of April, 36.81% of the total incident solar irradiation on the panel was consumed as hot water, which is a fair value, although may be misleading as such calculations are more reliable for long term studies. The *Overall Energy Utilisation Factor* is also at 36.81%, as the backup heater was not turned on at any time during the day, confirmed by the 0.00kWh value for the *Electricity Consumption*. Unfortunately, to this point, it is still not very clear to users viewing such reports of the consumptions and backup heater uses ‘score’, and whether optimisations to improve this ‘score’ are possible. At this stage, the *Surplus Hot Water Fraction* term (see Section 2.8.4) was added, so as to better interpret the results obtained and give an indicative ‘score’ on the thermal energy consumption and use of the backup heater. The same day, the 24<sup>th</sup> of April, obtained a *Surplus Hot Water Fraction* value of 1.55, meaning 1.55 times the energy consumed as hot water on that day remained available for consumption at a later time, considering that day’s SWH efficiency. This factor also gives an idea on the sizing of the solar heater in relation to the hot water consumption of the user. Frequent values above 1 imply that the system is well sized to cater for cloudy days, as it would still have hot water potential stored in the tank.

#### **4.6 Primary efficiencies results section with different weather conditions**

The SWH performance was observed for the conditions described in Section 3.6. The primary aim of these tests was to test the response of the monitoring device with the Maltese climate, and validate the reports obtained for the varying weather conditions. The four main weather conditions encountered in Malta are explored in the following:

##### **4.6.1 Cold and clear weather**

During the month of February, the SWH was exposed to the coldest weather conditions for this monitoring period, with temperatures occasionally plummeting close to 0°C during the night, and highs reaching just below 15°C. The 16<sup>th</sup> of February 2021 was the coldest day recorded by the monitoring device. During the day, the recorded average

ambient temperature was that of 13.7°C, while during the night (of the 17<sup>th</sup> of February), the average ambient temperature dropped to 2.7°C. Between the 16<sup>th</sup> and 17<sup>th</sup> of February, the autonomous feature was configured to allow the backup heater to switch on at any time during the day if storage temperatures dropped below 45°C. Thus, the efficiency figures obtained for this period were portraying the overall system efficiency, including that of the backup heater. Apart from electrical energy consumption by the backup heater, the night also contained hot water draw-offs, which explains the red font colour given to  $\Delta Q$  and  $\Delta E$  in Table 4.5. In such case, the 100% figure obtained for the night efficiencies does not mean that no heat losses were sustained by the storage tank during the night, but that the backup heater kept storage temperature constant, thus obscuring any thermal losses.

Table 4.5: SWH primary efficiencies report for the 16th of February 2021.

**Solar Water Heater Primary Efficiencies**

Monitoring Day:    Storage Capacity (L):

	Time	$T_{A-avg}$	$T_{S-first}$	$T_{S-last}$	$\Delta T_S$	$\Delta G$	$\Delta Q^*$	$\Delta E^*$	$\Delta H_{gain/loss}$	$\eta_{coll/store}^{**}$	$\eta_{combined}$
☀	11:00 till 14:00	13.68	44.50	45.50	1.00	4.07	0.00	0.19	0.17	4.18	4.18
☾	00:00 till 06:00	2.72	45.00	45.00	0.00		0.01	0.53	0.00	100.00	

$T_A$ = Ambient Temperature and  $T_S$ = Storage Temperature

\* For accurate estimates, choose monitoring periods with no hot water and electricity consumptions.

\*\* When day efficiencies are negative, night efficiency will be based on temperature differences. This method is less accurate.

Day efficiency too low! Check for malfunctions such as leaks, blocks or shading.

The SWH was still malfunctioning during this monitoring period, as described in Section 4.1. Thus, the performance of the SWH was much worse than expected. In fact, the UI correctly gave a bad *primary efficiency* score for this day and displayed the possibility of malfunction warning.

During March and following the leakage fix, the SWH performed well, as reported by the *primary efficiencies* report in Table 4.6. For days with high levels of solar irradiance, such as the 17<sup>th</sup> of March 2021, the SWH attained efficiencies often exceeding 70% during the day, and above 90% during the night.

Table 4.6: SWH Primary Efficiencies for the 17<sup>th</sup> of March 2021.

**Solar Water Heater Primary Efficiencies**

Monitoring Day   Storage Capacity (L):

	Time	T <sub>A-avg</sub>	T <sub>S-first</sub>	T <sub>S-last</sub>	ΔT <sub>S</sub>	ΔG	ΔQ <sup>*</sup>	ΔE <sup>*</sup>	ΔH <sub>gain/loss</sub>	η <sub>coll/store</sub> <sup>**</sup>	η <sub>combined</sub>
☀	<input type="text" value="11:00 till 14:00"/>	19.82	37.00	54.50	17.50	4.37	0.00	0.00	3.06	70.02	63.71
☾	00:00 till 06:00	12.08	46.50	42.50	-4.00		0.00	0.00	-0.70	90.99	

T<sub>A</sub>= Ambient Temperature and T<sub>S</sub>= Storage Temperature

\* For accurate estimates, choose monitoring periods with no hot water and electricity consumptions.

\*\* When day efficiencies are negative, night efficiency will be based on temperature differences. This method is less accurate.

From 11:00 till 14:00 and from 00:00 till 06:00, the backup heater was not allowed to turn on, and no water draw-offs were timed, as correctly reported by the UI, also giving a green font colour to ΔQ and ΔH. In such case, the UI is indicating that 70.02% of the solar irradiance incident on the collector in the sun-peak hours was converted to heat energy in the storage tank, raising the temperature by 17.5°C. On the other hand, during the following night, just 0.7kWh, or 9.01% of this energy collected during the day was lost from the storage tank as radiative and convective losses, which dropped storage tank temperatures by 4°C.

The storage tank water temperature rise during the day may be seen in Figure 4.11 by observing the black *Storage Temperature* trend during the sun-peak hours, most prominent between 12:00 and 16:00. The sudden drop in storage temperature at around 16:00 is due to a hot water draw-off timed at 16:00 which lasted 10 minutes. The solar irradiance drops to very low levels at c. 09:00 and 12:30, due to shading occurrences as highlighted in Section 4.4.



Figure 4.11: *Storage temperature rise and current solar flux trend between 07:00 and 19:00 for the 17<sup>th</sup> of March 2021.*

#### 4.6.2 Warm and clear weather

May was characterised by warm and clear weather, with ambient temperatures often exceeding 25°C during the day and staying above 15°C during the night. The primary efficiencies for the 17<sup>th</sup> of May are presented in Table 4.7. As expected, the day efficiency is lower than what is obtained for a cold and clear day (refer to Section 4.6.1). The reason is that the starting temperature of the storage tank for the 17<sup>th</sup> of May at 11:00 is much higher than that of the 17<sup>th</sup> of March, resulting in slower rates of net heat gain. The same phenomenon was noted by Jiao et al. [68], during a performance analysis on a solar heating installation in a dormitory in LuoYang City, China, where it was noted by the authors that the overall storage water temperature rise was small in cases where the storage water temperature was initially already high, resulting in lower system efficiencies.

Table 4.7: SWH primary efficiencies report for the 17th of May 2021.

**Solar Water Heater Primary Efficiencies**

Monitoring Day   Storage Capacity (L):

	Time	T <sub>A-avg</sub>	T <sub>S-first</sub>	T <sub>S-last</sub>	ΔT <sub>S</sub>	ΔG	ΔQ <sup>*</sup>	ΔE <sup>*</sup>	ΔH <sub>gain/loss</sub>	η <sub>coll/store</sub> <sup>**</sup>	η <sub>combined</sub>
☀	11:00 till 14:00 ▾	27.61	54.50	63.50	9.00	3.97	0.00	0.00	1.57	39.55	34.02
☾	00:00 till 06:00	18.87	56.50	53.50	-3.00		0.00	0.00	-0.53	86.03	

T<sub>A</sub>= Ambient Temperature and T<sub>S</sub>= Storage Temperature

\* For accurate estimates, choose monitoring periods with no hot water and electricity consumptions.

\*\* When day efficiencies are negative, night efficiency will be based on temperature differences. This method is less accurate.

Possibly, at the end of the monitoring period (around 13:00), the stagnation temperature is approached, and is close to 63.5°C (actual temperature determined in Section 4.9). At this point, minimal net heat transfers occur in the system as energy collected approximates the energy lost to ambient and thus, efficiency is close to or equal to zero. Transfer fluid flow between the collector and storage tank is also greatly reduced due to both having approximately equal temperatures. On the other hand, the balance between heat losses and heat gains implies that FPC SWHs are very well suited for Maltese climate and does not cause undue overheating or damage to the SWH or the hot water pipes.

Night efficiencies reported by the monitoring device are also lower for this day, despite experiencing less net heat losses than the 17<sup>th</sup> of March (0.53kWh compared to 0.70kWh). The main reason behind this is that during the day, heat gains by the storage tank water were minimal due to the already high storage temperatures, thus heat losses at night are viewed as relatively large.

### 4.6.3 Cold and cloudy weather

The 16<sup>th</sup> of March was a cold, overcast day, with very low solar irradiance levels, as reported by the UI's *primary efficiencies* results shown in Table 4.8. The monitoring device recorded a solar irradiance yield of just 1.33kWh on the collector from 11:00 till 14:00. As a result, the storage tank water temperature rose by just 1°C, gaining 0.17kWh of net heat energy. This resulted in the system having a *day efficiency* of just 12.78%. During the following night (00:00 till 06:00), the storage tank sustained a temperature fall of 2.5°C, amounting to 0.44kWh. Losses during the night were greater than the gains during the day, explaining the low *night efficiency* figure of 34.17%. Even



though efficiencies were very low, the possibility of malfunctioning alert was rightly not triggered, as solar irradiance levels were also very low.

Table 4.8: SWH primary efficiencies report for the 16th of March 2021.

**Solar Water Heater Primary Efficiencies**

Monitoring Day   Storage Capacity (L):

	Time	T <sub>A-avg</sub>	T <sub>S-first</sub>	T <sub>S-last</sub>	ΔT <sub>S</sub>	ΔG	ΔQ*	ΔE*	ΔH <sub>gain/loss</sub>	η <sub>coll/store</sub> **	η <sub>combined</sub>
☀	<input type="text" value="11:00 till 14:00"/>	12.43	33.00	34.00	1.00	1.33	0.00	0.00	0.17	12.78	4.37
☾	00:00 till 06:00	9.25	31.00	28.50	-2.50		0.00	0.00	-0.44	34.17	

T<sub>A</sub>= Ambient Temperature and T<sub>S</sub>= Storage Temperature

\* For accurate estimates, choose monitoring periods with no hot water and electricity consumptions.

\*\* When day efficiencies are negative, night efficiency will be based on temperature differences. This method is less accurate.

#### 4.6.4 Warm and cloudy weather

The 1<sup>st</sup> of May of 2021 was also very cloudy, as can be observed in the *SWH Primary Efficiencies* results in Table 4.9.

Table 4.9: SWH primary efficiencies report for the 1<sup>st</sup> of May 2021.

**Solar Water Heater Primary Efficiencies**

Monitoring Day   Storage Capacity (L):

	Time	T <sub>A-avg</sub>	T <sub>S-first</sub>	T <sub>S-last</sub>	ΔT <sub>S</sub>	ΔG	ΔQ*	ΔE*	ΔH <sub>gain/loss</sub>	η <sub>coll/store</sub> **	η <sub>combined</sub>
☀	<input type="text" value="11:00 till 14:00"/>	23.69	39.50	44.00	4.50	2.11	0.00	0.00	0.79	37.44	31.21
☾	00:00 till 06:00	18.47	41.50	39.50	-2.00		0.00	0.00	-0.35	83.37	

T<sub>A</sub>= Ambient Temperature and T<sub>S</sub>= Storage Temperature

\* For accurate estimates, choose monitoring periods with no hot water and electricity consumptions.

\*\* When day efficiencies are negative, night efficiency will be based on temperature differences. This method is less accurate.

The monitoring device registered a solar irradiance yield of 2.11kWh incident on the collector between 11:00 and 14:00, raising the storage water temperature by 4.5°C and gaining 0.79kWh of stored internal energy in the process. The ambient temperature for this day was approximately double that of the previous example, which meant that heat losses were lower and therefore the net temperature rise in the storage tank was higher than that of 16<sup>th</sup> March. Similarly, the heat losses from the tank at night was lower due



to the higher ambient temperature. Again, the UI correctly did not display the possibility of malfunctioning warning as solar irradiance yields during the day were also low.

#### 4.7 Long duration tests and *Energy Utilisation Efficiencies* results

The main objective of the long duration tests is to verify that the generated results reflect a SWH performance which also depends on external factors, namely consumption patterns, backup heater use and the weather. Moreover, these tests determine whether optimisation of the SWH performance is possible by simply observing the results.

The *Energy Utilisation Efficiencies* section could only be fully tested once long-term uninterrupted data of at least three days were gathered. Three testing periods were chosen to test this feature: one which included few backup heater usages, one which made heavy use of the backup heater, and one which did not include any occurrences of backup heater use. For all long duration testing, water draw-offs were timed twice per day, at 08:00 and 18:00, lasting 10 minutes each. The weather during these 12 days of testing was mostly warm and clear, with ambient temperatures generally above 25°C and 15°C during the day and night, respectively. The *combined efficiency* of 54.29% obtained on the 4<sup>th</sup> of May was chosen for performing *Surplus Hot Water Fraction* calculations, which was the highest obtained *combined efficiency* for the month of May.

##### 4.7.1 Few backup heater uses

Between the 20<sup>th</sup> and 23<sup>rd</sup> of May 2021, the *autonomous control* feature could turn the backup heater on only if all conditions described in Section 3.6.2 were satisfied. This, in turn, resulted in the backup heater being turned on once daily at around 08:00 following the morning draw-off. The *Energy Utilisation Efficiencies* results for this period are provided in Table 4.10.







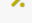



The monitoring device reported that the *thermal energy consumption* (thermal energy consumed as hot water) for this period was of 14.18kWh, of which 10.65kWh, or 75% was directly heated by the sun (determinable by the *solar contribution to hot water* and *solar fraction* values respectively). The rest was heated by the backup heater, consuming 3.53kWh of electrical energy in the process. The results show that 27.87% of the solar irradiance on the collector was utilised, which although not a bad figure, improvements were possible. This is evidenced by the *Surplus Hot Water Fraction* value of 1.95, meaning that almost twice of the energy used as hot water was available as extra (heated

by a combination of solar and electrical means). Thus, from such results, it could be concluded that improvements can be made by further limiting the backup heater use and changing consumption patterns to ones which favour the afternoon and evening consumptions.

Table 4.10: Energy Utilisation Efficiency results for the 20<sup>th</sup> (00:00) till the 23<sup>rd</sup> of May (23:59) 2021.

**Energy Utilisation Efficiencies**

Enter Monitoring Period:

	Description	Total	Period	Unit
	Hot Water Consumption	_____	0.47	m <sup>3</sup>
	Thermal Energy Consumption	_____	14.18	kWh
	Electricity Consumption	_____	3.53	kWh
	Input Solar Irradiance	_____	38.21	kWh
	Solar Contribution to Hot Water	NaN	10.65	kWh
	CO <sub>2</sub> equivalent reduction <sup>[i]</sup>	NaN	5.33	kg
	Solar Energy Utilisation Factor <sup>[ii]</sup>	NaN	27.87	%
	Overall Energy Utilisation Factor <sup>[iii]</sup>	NaN	33.97	%
	Solar Fraction <sup>[iv]</sup>	NaN	0.75	
	Surplus Hot Water Fraction <sup>[v]</sup>		1.95	

<sup>[i]</sup> Value based on the CO<sub>2</sub> equivalence if the same energy was generated by a conventional Open Cycle Gas Turbine.

<sup>[ii]</sup> Measure of how much of the total incident solar energy is being utilised.

<sup>[iii]</sup> Measure of how much of the total input energy is being utilised.

<sup>[iv]</sup> Fraction of the utilised energy heated by the sun's energy.

<sup>[v]</sup> Fraction of the excess hot water available for consumption. Based on  $\eta_{combined}$ .

#### 4.7.2 No backup heater use











The backup heater was not allowed to turn on at any time during this testing period hence, good performance results are expected. Table 4.11 reports the *Energy Utilisation Efficiencies* for the 16<sup>th</sup> till the 19<sup>th</sup> of May 2021.

The results validate that no electrical energy was consumed by the backup heater, and the water's only means of heating was the sun's energy. A *Solar Fraction* of 1.00 further confirms this statement. The *SEUF* obtained for this period is of 34.8%, indicating that about a third of the sun's energy incident on the collector was effectively converted and used up as hot water. On the other hand, a reported *Surplus Hot Water Fraction* of 1.56 suggests a good performance of the SWH however, with such weather conditions and water consumptions, the SWH has the ability to provide more hot water than what is consumed.

Table 4.11: Energy Utilisation Efficiency results for the 16<sup>th</sup> (00:00) till the 19<sup>th</sup> of May (23:59) 2021.

**Energy Utilisation Efficiencies**

Enter Monitoring Period:

	Description	Total	Period	Unit
	Hot Water Consumption	---	0.47	m <sup>3</sup>
	Thermal Energy Consumption	---	13.78	kWh
	Electricity Consumption	---	0.00	kWh
	Input Solar Irradiance	---	39.60	kWh
	Solar Contribution to Hot Water	NaN	13.78	kWh
	CO <sub>2</sub> equivalent reduction <sup>[i]</sup>	NaN	6.89	kg
	Solar Energy Utilisation Factor <sup>[ii]</sup>	NaN	34.80	%
	Overall Energy Utilisation Factor <sup>[iii]</sup>	NaN	34.80	%
	Solar Fraction <sup>[iv]</sup>	NaN	1.00	
	Surplus Hot Water Fraction <sup>[v]</sup>		1.56	

<sup>[i]</sup> Value based on the CO<sub>2</sub> equivalence if the same energy was generated by a conventional Open Cycle Gas Turbine.

<sup>[ii]</sup> Measure of how much of the total incident solar energy is being utilised.

<sup>[iii]</sup> Measure of how much of the total input energy is being utilised.

<sup>[iv]</sup> Fraction of the utilised energy heated by the sun's energy.

<sup>[v]</sup> Fraction of the excess hot water available for consumption. Based on  $\eta_{combined}$ .

### 4.7.3 Heavy backup heater use







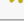

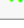

Between the 20<sup>th</sup> and 23<sup>rd</sup> of May 2021, the backup heater could turn on every time storage temperatures dropped below 45°C, irrelevant of the time and solar intensity. During this period, the backup heater was observed to kick in twice; during the early hours and following the morning draw-off. The *Energy Utilisation Efficiencies* results for this period are provided in Table 4.12.

Undeniably, results indicating a bad performing SWH were obtained for this period. The *Solar Contribution to Hot Water* was just of 8.12kWh, which is small compared to the 38.21kWh of incident solar irradiance on the collector. The result in a *SEUF* value of just 21.25% and a *Solar Fraction* of 0.53, meaning that close to half of the consumed hot water was heated by the backup heater. Moreover, the obtained *Surplus Hot Water Fraction* of 2.55 indicates that more than 2.5 times the amount of consumed hot water was already heated and available for consumption. Thus, anyone viewing such report could easily arrive to the conclusion that the SWH was either malfunctioning, or the backup heater was unnecessarily used for such weather conditions. In this case it was the latter.

Table 4.12: Energy Utilisation Efficiencies report for the 10th till 17th of February 2021.

**Energy Utilisation Efficiencies**

Enter Monitoring Period:

	Description	Total	Period	Unit
	Hot Water Consumption	—	0.47	m <sup>3</sup>
	Thermal Energy Consumption	—	15.44	kWh
	Electricity Consumption	—	7.32	kWh
	Input Solar Irradiance	—	38.21	kWh
	Solar Contribution to Hot Water	NaN	8.12	kWh
	CO <sub>2</sub> equivalent reduction <sup>[i]</sup>	NaN	4.06	kg
	Solar Energy Utilisation Factor <sup>[ii]</sup>	NaN	21.25	%
	Overall Energy Utilisation Factor <sup>[iii]</sup>	NaN	33.91	%
	Solar Fraction <sup>[iv]</sup>	NaN	0.53	
	Surplus Hot Water Fraction <sup>[v]</sup>		2.55	

<sup>[i]</sup> Value based on the CO<sub>2</sub> equivalence if the same energy was generated by a conventional Open Cycle Gas Turbine.

<sup>[ii]</sup> Measure of how much of the total incident solar energy is being utilised.

<sup>[iii]</sup> Measure of how much of the total input energy is being utilised.

<sup>[iv]</sup> Fraction of the utilised energy heated by the sun's energy.

<sup>[v]</sup> Fraction of the excess hot water available for consumption. Based on  $\eta_{combined}$ .

#### 4.8 Investigating an ideal consumption using the monitoring device







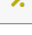



In Section 4.7.2, a good SWH performance was obtained when the backup heater was deliberately kept switched off. Still, it was possible to obtain better results with better water consumptions. To test this proposition, another period which included an additional draw-off was chosen. Between the 1<sup>st</sup> and the 4<sup>th</sup> of May 2021, the backup heater was not allowed to turn on at any point. Three water draw-offs per day were timed, at 08:00, 14:30 and 21:00 and each lasting 7 minutes. Table 4.11 lists the *Energy Utilisation Efficiencies* results for this period.

Again, the results correctly indicate that no electricity consumption was recorded, thus the water's only means of heating was the sun's energy. The *SEUF* obtained for this period is of 45.26%, indicating that about a half of the sun's energy incident on the collector was effectively converted and used up as hot water. The resulting *Surplus Hot Water Fraction* of 1.20 (using  $\eta_{combined} = 54.29\%$  for the 4<sup>th</sup> of May) shows an improvement over the previously attained value of 1.56, indicating a very good performance of the SWH. Only minor improvements are possible when it comes to water consumption timing, such as shifting morning consumptions towards the afternoon.

Table 4.13: Energy Utilisation Efficiency report for the 1<sup>st</sup> (00:00) till the 4<sup>th</sup> of May (23:59) 2021.

**Energy Utilisation Efficiencies**

Enter Monitoring Period:

	Description	Total	Period	Unit
	Hot Water Consumption	—	0.51	m <sup>3</sup>
	Thermal Energy Consumption	—	10.42	kWh
	Electricity Consumption	—	0.00	kWh
	Input Solar Irradiance	—	23.02	kWh
	Solar Contribution to Hot Water	NaN	10.42	kWh
	CO <sub>2</sub> equivalent reduction <sup>[i]</sup>	NaN	5.21	kg
	Solar Energy Utilisation Factor <sup>[ii]</sup>	NaN	45.26	%
	Overall Energy Utilisation Factor <sup>[iii]</sup>	NaN	45.26	%
	Solar Fraction <sup>[iv]</sup>	NaN	1.00	
	Surplus Hot Water Fraction <sup>[v]</sup>		1.20	

<sup>[i]</sup> Value based on the CO<sub>2</sub> equivalence if the same energy was generated by a conventional Open Cycle Gas Turbine.

<sup>[ii]</sup> Measure of how much of the total incident solar energy is being utilised.

<sup>[iii]</sup> Measure of how much of the total input energy is being utilised.

<sup>[iv]</sup> Fraction of the utilised energy heated by the sun's energy.

<sup>[v]</sup> Fraction of the excess hot water available for consumption. Based on  $\eta_{combined}$ .

Such results make it easy for SWH users to agree that in similar weather conditions and with similar water consumptions, the backup heater is not needed.

#### 4.9 Determining the stagnation point using the monitoring device

As described earlier in Section 4.6.2, the stagnation point of a SWH system is the point of zero efficiency, at which no net heat transfers are obtained. At this temperature, no collector-storage tank flow exists, and heat gained by the system is equal to the heat lost to the surroundings. The stagnation point varies from one SWH to another and is sensitive to surrounding conditions such as ambient temperature and solar irradiance intensity. With the monitoring device installed, it was possible to approximately determine the stagnation point of the SWH for a particular day, such as for 18<sup>th</sup> of May 2021. For this day, the morning and afternoon water draw-offs were skipped, to allow the storage tank to reach the highest possible temperatures for such conditions. The *storage temperature vs time* trend for the 18<sup>th</sup> of May is provided in Figure 4.12. During the sun-peak hours, the *storage temperature* (black) can be observed to rise to ~66°C, at which point stagnates, despite the solar irradiance levels (blue) being still significantly high. This may be an indication that the stagnation point for these conditions have been reached and is about 66°C. Upon analysis of historical data, it was noted that in no cases

was this temperature exceeded however, it is highly plausible that in hotter days such as those in July, this temperature point could be exceeded due to the warmer ambient conditions and higher solar irradiance intensities.

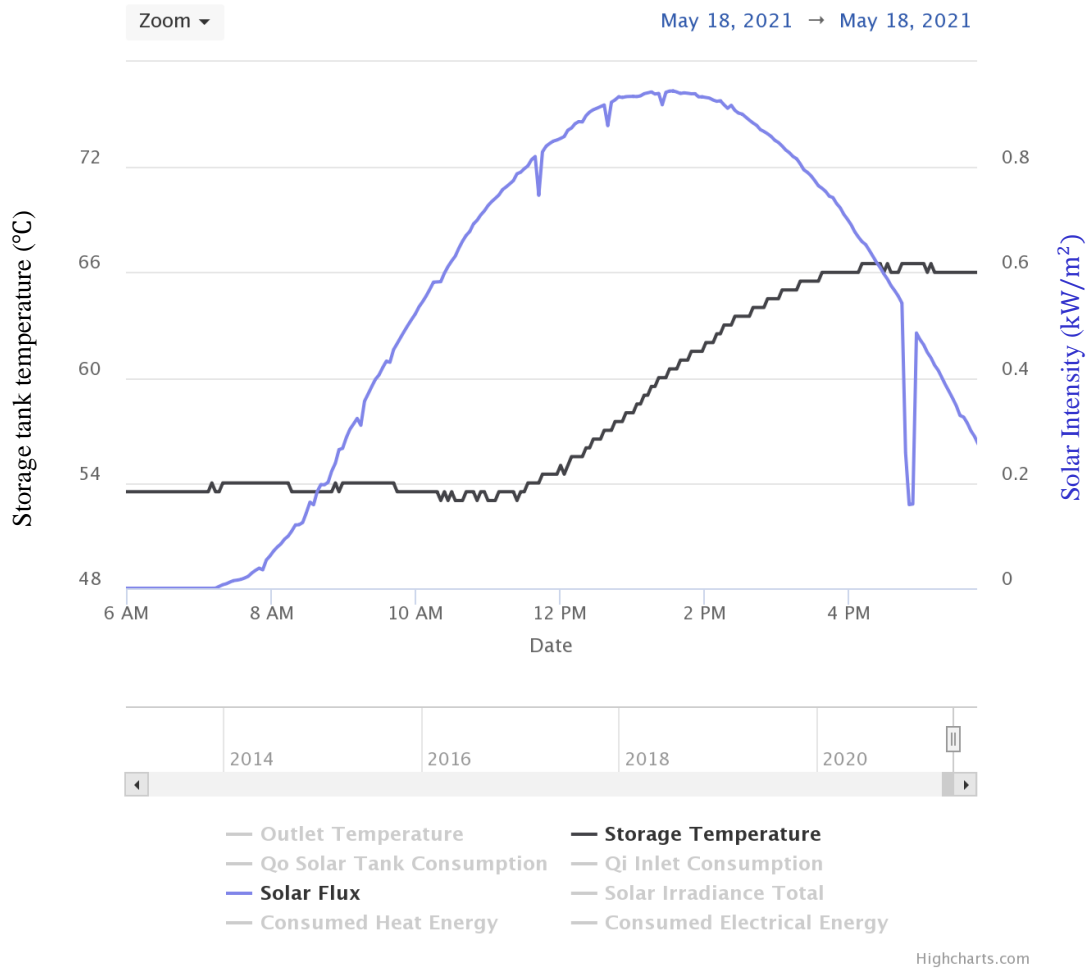


Figure 4.12: Storage temperature rise and current solar flux trend between 06:00 and 18:00 on the 18<sup>th</sup> of May 2021.

## Chapter 5 Conclusion & Future Works

### 5.1 Conclusions

A compact, low-cost, versatile, accurate and reliable device for monitoring parameters, storing data and controlling operation of solar thermal systems was successfully prototyped, installed and tested on a SWH in real operating conditions. It may be concluded that:

- A microcontroller-centred development board based on Arduino provides more than enough computing power to monitor all necessary parameters of a SWH system for performance analysis. Furthermore, the monitoring device proved to be also well capable of storing and loading a preconfigured web-based user-interface, while also serving as a smart controller for the backup heater;
- The cost of the prototype rounded up to about €90 (including the costs for PCB development). However, it is expected that the product cost would significantly decrease (up to a margin of 50-60%) upon acquiring the parts in bulk and miniaturizing the components. The target price of the monitoring device is around €70-€120, depending on the level of functionality and features of the device (several options with varying levels of functionality and features shall be offered);
- The ADC channels of the microcontroller required complex software calibrations and compensations to acquire stable and precise results;
- Solar irradiance readings as monitored by the device had accuracies of less than  $\pm 3\%$  for solar irradiance ranges exceeding  $500\text{W}/\text{m}^2$ , and were less accurate ( $\pm 20\%$ ) for ranges of less than  $500\text{W}/\text{m}^2$ . The low-cost solar PV panel however, provided a reliable means of measuring solar irradiance yields on the collector which helped in determining the performance characteristics of the SWH system;
- The waterflow sensor correctly quantified the amount of discharged water at each timed draw-off with accuracies of less than  $\pm 5\%$ . This exceeded the manufacturers accuracy rating of  $\pm 10\%$ ;
- Temperature reading accuracies obtained were of less than  $\pm 5\%$  however, it is important to mention that the thermistor used for the accuracy tests also possess inaccuracies, thus the accuracy from the utilised sensors (DS18B20) is expected to be better;

- Sensor accuracies and precisions stayed relatively stable during 21 days of continuous operation. This gives indication of good long-term stability of the monitoring device, and that frequent calibrations are not required;
- The UI was responsive and performed well in all feature functionality checks, provided that a good network connection was available. All gathered data was well presented on the *Highcharts* chart, and the level of functions (such as zoom levels, graph snapshots, raw-data downloads etc.) offered with the charts meet the requirements for both basic and advanced users.
- A stable internet connection is required for the data logging feature to work as intended. Several internet connection issues arose during the testing phase, which caused interruptions in the data. Later, corrective updates were done on the monitoring device firmware to temporarily store offline data when internet disruption occur, to prevent data losses;
- The backup heater control feature using the *autonomous control* worked as intended, always adhering to the set condition limits. The multitude levels of autonomous control on the switching on of the backup heater allowed for improved SWH performances by avoiding unnecessary backup heater operation;
- The *efficiencies* tab provided detailed performance reports which contained both easily interpreted information for the basic user, as well as information for the more advanced user. This feature provided means of visually observing the performance of a SWH, as well as the means to alter water consumption patterns and backup heater uses to optimise the performance.

Overall, the project has achieved its aim of designing and assembling a prototype low-cost, reliable, versatile, and accurate thermal energy meter that can be easily fitted to any SWH system. Moreover, the objectives of monitoring and storing performance data, as well as controlling the operation of the backup heater and optimising the use of solar energy without compromising hot water availability were fully attained. The user-interface's objectives of serving as a responsive platform interacting the monitoring device with the user, presenting data in a well-interpretable manner, providing real-time updated parameter values, as well as alerting users of malfunctions were also fulfilled.



## 5.2 Future works

Although results obtained were promising and satisfactory, improvements to the operation of the device are possible. Future work could include refining the prototype to further enhance reliability, functionality, and accuracy of the monitoring device by incorporating the following:

- Although SWH malfunctioning warnings are already incorporated in the UI, more detailed error reports would be beneficial for both the user and technical people. Future updates shall include more detailed error diagnostics including malfunction pinpointing, error push notifications (to inform users of malfunction), possible fixes highlighting, and date of error occurrence;
- The *surplus hot water fraction* is reliant on the combined efficiency of a single day. Thus, the value is expected to be inaccurate for all other days of the chosen monitoring period. In future updates, the UI shall calculate the *combined efficiency* for all days of the chosen monitoring period and perform calculations accordingly. Additionally, the UI shall include an option to calculate the *surplus hot water fraction* using the maximum attainable efficiency for the SWH technology being used;
- External ADCs could be added for more accurate and stable analogue signal conversions without heavy software dependencies. One example of an external ADC is the *ADS1115*, which is also low-cost and compact;
- Instead of potential dividers, where applicable, the use of logic level converters shall be used to translate 5Vdc signals to 3.3Vdc signals. Logic level converters, such as the *TXS0108E* are high speed and more accurate than the currently implemented potential dividers;
- The project could be miniaturized, mainly by swapping THT (through-hole technologies) with SMT (surface mount technologies) components and switching to more compact microcontrollers. Some modules may also be stripped down to their bare minimum component configuration and added directly to the PCB;
- A firmware featuring OTA (over-the-air) updates would make it possible for centralised and controlled updates on all systems in operation;
- Another relay for circulation pump control could be included. The monitoring device should then include smart functions to automatically control the circulation pump, including enhanced features such as automated speed control and anti-freeze control;

- Proper ambient temperature measurements should be made using an embedded module thermocouple on the PCB. Version 2 of the PCB already allows for an additional thermometer (*DS18B20*) however, the software is not yet configured to utilise this feature;
- In future version of the UI, a security page will be added to prevent unauthorised access to the SWH, particularly on the control of the backup heater and settings. The page will require the user to enter a username and password, after which the user is given full access to the UI;
- Some UI reports and settings can be split into two, one for basic users and the other for more experienced users and technical personnel;
- A more accurate means of measuring CO<sub>2</sub> reductions should be provided, which also caters for the COP (Coefficient of performance) of thermal storage systems.
- A future update to incorporate a proper calibration over the entire range of solar radiation monitoring, together with software compensation can produce more accurate readings, even for lower values of solar irradiance;
- An IP65 case should be designed and manufactured, which will house the PCB and allow it to be installed in an outdoor area close to the SWH.

## References

- [1] NASA, "Climate Change Evidence: How Do We Know?" *Climate Change: Vital Signs of the Planet*, 2018. Available: <https://climate.nasa.gov/evidence>. [Accessed 12 January 2021]
- [2] United Nations / Framework Convention on Climate Change, "Adoption of the Paris Agreement," 2015.
- [3] European Commission, "2030 climate & energy framework," 2019. Available: [https://ec.europa.eu/clima/policies/strategies/2030\\_en](https://ec.europa.eu/clima/policies/strategies/2030_en).
- [4] ClimateWatch, "Greenhouse Gas (GHG) Emissions," *Climate Watch*, Available: <https://www.climatewatchdata.org/ghg-emissions>. [Accessed 3 March 2021]
- [5] EPA and OAR, "Renewable Hot Water Heating," *US EPA*, 2014. Available: <https://www.epa.gov/rhc/renewable-hot-water-heating>. [Accessed 4 March 2021]
- [6] B. Hong and R. W. Howarth, "Greenhouse gas emissions from domestic hot water: heat pumps compared to most commonly used systems," *Energy Science & Engineering*, vol. 4, (2), pp. 123-133, 2016. Available: <https://onlinelibrary.wiley.com/doi/abs/10.1002/ese3.112>. DOI: 10.1002/ese3.112.
- [7] National Statistics Office Malta, "Development of Detailed Statistics on Energy Consumption in Households," Available: [https://ec.europa.eu/eurostat/cros/system/files/SECH\\_Project\\_Malta.pdf](https://ec.europa.eu/eurostat/cros/system/files/SECH_Project_Malta.pdf). [Accessed 18 February 2021]
- [8] The Energy and Water Agency, "The National Renewable Energy Action Plan 2015 - 2020," *Publications Office of the European Union*, 2017. Available: [https://ec.europa.eu/energy/topics/renewable-energy/national-renewable-energy-action-plans-2020\\_en](https://ec.europa.eu/energy/topics/renewable-energy/national-renewable-energy-action-plans-2020_en).
- [9] The Energy and Water Agency, "2030 National Energy and Climate Plan ," 2018. Available: [https://ec.europa.eu/energy/sites/ener/files/documents/mt\\_final\\_necp\\_main\\_en.pdf](https://ec.europa.eu/energy/sites/ener/files/documents/mt_final_necp_main_en.pdf).
- [10] F. Kreith and J. Kreider, *Principles of Solar Engineering*. 2000. DOI: 10.1201/b18119.
- [11] S. A. Kalogirou, "Solar thermal collectors and applications," *Progress in Energy and Combustion Science*, vol. 30, (3), pp. 231-295, 2004. Available: <http://www.sciencedirect.com/science/article/pii/S0360128504000103>. DOI: <https://doi.org/10.1016/j.pecs.2004.02.001>.

- [12] K. Patel, P. Patel and J. Patel, "Review of solar water heating systems," *International Journal of Advanced Engineering Technology*, vol. 3, (4), pp. 146-149, 2012.
- [13] EP and EC, "Directive (EU) 2018/2001 of the European Parliament and of the Council of 11 December 2018 on the promotion of the use of energy from renewable sources." 2018. Available: <http://data.europa.eu/eli/dir/2018/2001/oj/eng>.
- [14] EP and EC, "Directive (EU) 2018/844 of the European Parliament and of the Council of 30 May 2018 amending Directive 2010/31/EU on the energy performance of buildings and Directive 2012/27/EU on energy efficiency." 2018. Available: <http://data.europa.eu/eli/dir/2018/844/oj/eng>.
- [15] Eurostat, "Renewable energy statistics," 2021. Available: [https://ec.europa.eu/eurostat/statistics-explained/index.php/Renewable\\_energy\\_statistics#Share\\_of\\_renewable\\_energy\\_more\\_than\\_doubled\\_between\\_2004\\_and\\_2019](https://ec.europa.eu/eurostat/statistics-explained/index.php/Renewable_energy_statistics#Share_of_renewable_energy_more_than_doubled_between_2004_and_2019).
- [16] P. Hanson, "Geothermal Country Overview: Sweden," *GeoEnergy Marketing*, 2017. Available: <https://www.geoenergymarketing.com/energy-blog/geothermal-country-overview-sweden/>. [Accessed 21 April 2021]
- [17] Carlsson Johan, "Solar Thermal Heating and Cooling: Technology Market report," *Publications Office of the European Union*, 2019. Available: <https://ec.europa.eu/jrc/en/publication/solar-thermal-heating-and-cooling-technology-market-report>. [Accessed 29 March 2021]
- [18] Eurostat, "Solar thermal collectors' surface," 2019. Available: [https://ec.europa.eu/eurostat/databrowser/view/nrg\\_inf\\_stcs/default/table?lang=en](https://ec.europa.eu/eurostat/databrowser/view/nrg_inf_stcs/default/table?lang=en).
- [19] Eurostat, "Electricity production capacities for renewables and wastes," 2019. Available: [https://ec.europa.eu/eurostat/databrowser/view/NRG\\_INF\\_EPCRW\\_custom\\_100266\\_7/default/table?lang=en](https://ec.europa.eu/eurostat/databrowser/view/NRG_INF_EPCRW_custom_100266_7/default/table?lang=en).
- [20] Deutsche Gesellschaft für Internationale Zusammenarbeit, (GIZ), "Summary of the monitoring results of the Solar Water Heating System at Synthokem Labs, Hyderabad under ComSolar project of Indo German energy programme in cooperation with Ministry of New and Renewable Energy," 2016. Available: [https://www.solarthermalworld.org/sites/default/files/news/file/2016-08-15/measuring\\_solar\\_heat\\_generation\\_synthokem\\_result\\_overview\\_final.pdf](https://www.solarthermalworld.org/sites/default/files/news/file/2016-08-15/measuring_solar_heat_generation_synthokem_result_overview_final.pdf).
- [21] Deutsche Gesellschaft für Internationale Zusammenarbeit, (GIZ), "Summary of the monitoring results of the Solar Water Heating System at Himachal Pradesh Dairy, Rampur under ComSolar project of Indo German energy programme in cooperation with Ministry of New and Renewable Energy," 2016. Available: [https://www.solarthermalworld.org/sites/default/files/news/file/2016-08-15/measuring\\_solar\\_heat\\_generation\\_hp\\_dairy\\_result\\_overview\\_final.pdf](https://www.solarthermalworld.org/sites/default/files/news/file/2016-08-15/measuring_solar_heat_generation_hp_dairy_result_overview_final.pdf).

- [22] UNEP, "Technical Study Report on Measuring, Remote Monitoring and Remote Controlling for Solar Thermal Systems," *United Nations Environment Programme*, 2015. Available: <http://solarheateurope.eu/wp-content/uploads/2017/07/Technical-Study-Report-on-Measuring-Remote-Monitoring-and-Remote-controlling-for-Solar-Thermal-Systems.pdf>.
- [23] Baerbel Epp, "App-controlled solar thermal equipment," *Solarthermalworld*, 2019. Available: <https://www.solarthermalworld.org/news/app-controlled-solar-thermal-equipment>. [Accessed 6 January 2021]
- [24] M. Zukowski, "Energy efficiency of a solar domestic hot water system," vol. 22, pp. 1-209, 2017.
- [25] Jiaxing-Passion, "Jiaxing Passion New Energy Technology Co. Ltd." Available: <https://www.thermalsolarwaterheater.com/aboutus.html>. [Accessed 14 February 2021]
- [26] SunReports, "SunReports Inc." Available: <http://www.sunreports.com>. [Accessed 6 January 2021]
- [27] STIEBEL, "Products and Solutions," Available: <https://www.stiebel-eltron.com/en/home/products-solutions/renewables.html>. [Accessed 14 February 2021]
- [28] P. Frey *et al*, "Monitoring results of a solar process heat system installed at a textile company in Southern Germany," *Energy Procedia*, vol. 70, pp. 615-620, 2015.
- [29] Onset, "Solar Thermal Monitoring Case Study: Southern California," 2009. Available: [https://www.onsetcomp.com/files/CS3\\_CaseStudy\\_solar.pdf](https://www.onsetcomp.com/files/CS3_CaseStudy_solar.pdf).
- [30] L. Korcaj, U. J. J. Hahnel and H. Spada, "Intentions to adopt photovoltaic systems depend on homeowners' expected personal gains and behavior of peers," *Renewable Energy*, vol. 75, pp. 407-415, 2015. Available: <http://www.sciencedirect.com/science/article/pii/S0960148114006326>. DOI: <https://doi.org/10.1016/j.renene.2014.10.007>.
- [31] X. Zhang, L. Shen and S. Y. Chan, "The diffusion of solar energy use in HK: What are the barriers?" *Energy Policy*, vol. 41, pp. 241-249, 2012. Available: <http://dx.doi.org/10.1016/j.enpol.2011.10.043>. DOI: 10.1016/j.enpol.2011.10.043.
- [32] A. Masini and E. Menichetti, "The impact of behavioural factors in the renewable energy investment decision making process: Conceptual framework and empirical findings," *Energy Policy*, vol. 40, pp. 28-38, 2012. Available: <http://dx.doi.org/10.1016/j.enpol.2010.06.062>. DOI: 10.1016/j.enpol.2010.06.062.
- [33] W. Jager, "Stimulating the diffusion of photovoltaic systems: A behavioural perspective," *Energy Policy*, vol. 34, (14), pp. 1935-1943, 2006. Available: <http://dx.doi.org/10.1016/j.enpol.2004.12.022>. DOI: 10.1016/j.enpol.2004.12.022.
- [34] M. C. Claudy, M. Peterson and A. O'Driscoll, "Understanding the Attitude-Behavior Gap for Renewable Energy Systems Using Behavioral Reasoning Theory,"

- Journal of Macromarketing*, vol. 33, (4), pp. 273-287, 2013. Available: <https://doi.org/10.1177/0276146713481605>. DOI: 10.1177/0276146713481605.
- [35] J. M. Nolan *et al*, "Normative Social Influence is Underdetected," *Personality & Social Psychology Bulletin*, vol. 34, (7), pp. 913-923, 2008. Available: <https://journals.sagepub.com/doi/full/10.1177/0146167208316691>. DOI: 10.1177/0146167208316691.
- [36] J. Keirstead, "Household behavioural responses to photovoltaic-system monitoring devices," 2005.
- [37] S. Darby, "The Effectiveness of Feedback on Energy Consumption," *A Review for DEFRA of the Literature on Metering, Billing and Direct Displays*, vol. 486, 2006.
- [38] S. Stettler *et al*, "Web-based functionality check for solar heating systems," *Energy Procedia*, vol. 48, pp. 674-680, 2014.
- [39] B. Norton, *Solar Energy Thermal Technology*. London: Springer-Verlag, 1992.
- [40] S. Jaisankar *et al*, "A comprehensive review on solar water heaters," *Renewable and Sustainable Energy Reviews*, vol. 15, (6), pp. 3045-3050, 2011. Available: <http://www.sciencedirect.com/science/article/pii/S1364032111001092>. DOI: <https://doi.org/10.1016/j.rser.2011.03.009>.
- [41] ASHRAE, "Method of testing to determine the thermal performance of solar collectors." 1985. Available: <https://www.osti.gov/biblio/575023>.
- [42] ISO - International Organization for Standardization, "ISO 9806:2017 Solar energy — Solar thermal collectors — Test methods," 2017. Available: <https://www.iso.org/obp/ui/#iso:std:iso:9806:ed-2:v1:en>.
- [43] W. A. Beckman, S. A. Klein and J. A. Duffie, *Solar Heating Design by the F-Chart Method*. Wiley, 1977.
- [44] University of Wisconsin, Madison, USA, "TRNSYS 16 Program Manual," vol. 1, pp. 1-87, 1996.
- [45] M. Chandrashekar *et al*, "WATSUN - A simulation program for solar-assisted heating systems," *Renewable Alternatives, Volume 1*, vol. 1, 1978. Available: <https://ui.adsabs.harvard.edu/abs/1978real....1Q....C>.
- [46] ISO - International Organization for Standardization, "ISO 9459-2:1995 Solar heating - Domestic water heating systems Part 2: Outdoor test methods for system performance characterization and yearly performance prediction of solar-only systems," 1995. Available: <https://www.iso.org/cms/render/live/en/sites/isoorg/contents/data/standard/01/71/17187.html>.
- [47] German Solar Energy Society (DGS), *Planning and Installing Solar Thermal Systems*. Taylor and Francis, 2010.

- [48] C. Yousif, G. Ona and J. Bilbao, "Comparison of solar radiation in Marsaxlokk, Malta and Valladolid, Spain," *Renewable Energy*, vol. 49, pp. 203-206, 2013. . DOI: 10.1016/j.renene.2012.01.031.
- [49] G. Charles, *The Climate of Malta: Statistics, Trends and Analysis 1951-2010*. 2011.
- [50] Heltec-Automation, "Heltec Automation TM," Available: <https://heltec.org/>. [Accessed 17 April 2021]
- [51] Espressif Systems Inc, "ESP32 MCU with integrated Wi-Fi and Bluetooth," 2021. Available: <https://www.espressif.com/en/products/socs/esp32>. [Accessed 20 December 2020]
- [52] AZ-Delivery, "Your expert in microelectronics," Available: <https://www.az-delivery.de/en>. [Accessed 13 January 2021]
- [53] Wayne Storr, "Hall Effect Sensor and How Magnets Make It Work," *Basic Electronics Tutorials*, 2013. Available: <https://www.electronicstutorials.ws/electromagnetism/hall-effect.html>. [Accessed 8 December 2020]
- [54] Hobbytronics, "YF-S201 Hall Effect Waterflow Sensor," Available: <https://www.hobbytronics.co.uk/datasheets/sensors/YF-S201.pdf>. [Accessed 9 December 2020]
- [55] K. Hutter, Y. Wang and I. P. Chubarenko, "Phenomenological coefficients of water," in *Physics of Lakes* Anonymous Berlin, Heidelberg: Springer Berlin Heidelberg, 2010, pp. 389-418.
- [56] Maxim-Integrated, "DS18B20 Programmable Resolution 1-Wire Digital Thermometer," Available: <https://www.maximintegrated.com/en/products/sensors/DS18B20.html>. [Accessed 3 December 2020]
- [57] Qingxian Zeming Langxi Electronic, "ZMPT101B Current-type Voltage Transformer," Available: <https://www.datasheet4u.com/datasheet-pdf/ZemingLangxi/ZMPT101B/pdf.php?id=1381510>. [Accessed 12 February 2021]
- [58] YHDC, "HSTS016L-100A Datasheet - Hall split core current sensor," Available: <https://html.alldatasheet.com/html-pdf/1154730/YHDC/HSTS016L-100A/117/1/HSTS016L-100A.html>. [Accessed 12 February 2021]
- [59] Jean-Pierre Charras *et al*, "Ki-Cad," vol. 5.1.9, 1992. Available: <https://www.kicad.org/>. [Accessed 12 February 2021]
- [60] MuleSoft, "What is an API? (Application Programming Interface)," 2014. Available: <https://www.mulesoft.com/resources/api/what-is-an-api>. [Accessed 11 February 2021]
- [61] Mathworks, "Learn More About ThingSpeak," Available: [https://thingspeak.com/pages/learn\\_more](https://thingspeak.com/pages/learn_more). [Accessed 14 February 2021]

- [62] MDN, "Working with JSON - Learn web development," 2020. Available: <https://developer.mozilla.org/en-US/docs/Learn/JavaScript/Objects/JSON>. [Accessed 14 February 2021]
- [63] Highcharts, "Highcharts Javascript Charting Library," Available: <https://www.highcharts.com/blog/products/highcharts/>. [Accessed 14 February 2021]
- [64] RenSMART, "Carbon Emissions Calculator," Available: <https://www.rensmart.com/Calculators/KWH-to-CO2>. [Accessed 21 February 2021]
- [65] European Environment Information and Observation Network (Eionet), "Air pollution," *European Environment Agency*, Available: <https://www.eea.europa.eu/themes/air>. [Accessed 22 February 2021]
- [66] A. A. Makki *et al*, "Revealing the determinants of shower water end use consumption: enabling better targeted urban water conservation strategies," *J. Clean. Prod.*, vol. 60, pp. 129-146, 2013. Available: <https://www.sciencedirect.com/science/article/pii/S0959652611003076>. DOI: <https://doi.org/10.1016/j.jclepro.2011.08.007>.
- [67] Tadakatsu Ohnaka, Yutaka Tochihara and Yumiko Watanabe, "The effects of variation in body temperature on the preferred water temperature and flow rate during showering," *Ergonomics*, vol. 37, (3), pp. 541-546, 1994. Available: <https://doi.org/10.1080/00140139408963669>. DOI: 10.1080/00140139408963669.
- [68] Q. Jiao *et al*, "Data measurement and analysis of a solar heating system with seasonal storage," *Energy Procedia*, vol. 70, pp. 241-248, 2015.